Appendix

This page is intentionally left blank

Appendix A

Dye sensitized solar cells based on pre-dye treated ZnO nanoparticles

This page is intentionally left blank

1. Introduction

Recent years have seen an increase in demand for efficient solar photovoltaic (PV) cell power generation due to the world's increasing energy needs and the depletion of fossil fuels [1-3]. Effect of substantial use of fossil fuel on the environment is a matter of significant worry as well [4]. Modules made of crystalline silicon and based on bulk wafers make up the majority of the photovoltaic (PV) modules produced today. The high expense of these solar cells' fabrication as well as the use of hazardous ingredients has driven researchers to develop new, less expensive solar cells that are not silicon-based in order to capture solar energy more effectively [5-8].

Due to its high conversion efficiencies and low cost, dye-sensitized solar cells (DSSCs), a novel photovoltaic technology, have garnered much interest. Using nanoporous titanium dioxide (TiO_2) semiconductor electrodes, ruthenium (Ru) metal complex dyes, and iodine electrolyte solutions, O'Regan, B., and Grätzel reported high efficiency cells in Nature in 1991 [9]. Since then, many studies have been actively carried out on DSSCs and revealed their performance comparable to amorphous silicon thin films [10, 11].

Dye-sensitized solar cells (DSSCs) are a non-conventional photovoltaic technology that has attracted significant attention because of their high conversion efficiencies and low cost. O'Regan. B. & Grätzel reported high efficiency cells using nanoporous titanium dioxide (TiO_2) semiconductor electrodes, ruthenium (Ru) metal complex dyes, and iodine electrolyte solutions in the journal of Nature in 1991 [9]. Since then, many studies have been actively carried out on DSSCs and revealed their performance comparable to amorphous silicon thin films [10, 11]. The advantages of these DSSCs are their low cost, light weight, and ease of production; yet, problems with durability and future enhancement of their features exist. Numerous efforts have been undertaken to address these problems, including upgrading materials

and structures and solidifying electrolytes, but major advancements have not yet been accomplished [12, 13]. Two conducting glass electrodes are sandwiched together to form a dye-sensitized solar cell. Each layer plays a particular function in the cell.

The photovoltaic performance of a DSSC highly depends on all of its components and the fabrication methodology. Therefore, the optimization of every component is highly crucial to achieve the best performance. Since its introduction into the science community in 1991, the nanocrystalline photoanode in dye-sensitized solar cells has predominantly been comprised of titanium (TiO_2) nanoparticles as the semiconducting material [9, 14, 15]. Many researchers became very interested in studying the dye-sensitized solar cell performance fabricated using alternative semiconducting nanomaterials [16, 17]. Specifically, Zinc Oxide (ZnO) has been an ideal alternative to TiO_2 because of having a similar conduction band edge that is appropriate for proper electron injection from the excited dyes; moreover, ZnO provides better electron transport due to its higher electronic mobility. Moreover, ZnO is also highly transparent, allowing greater light penetration [18-22].

In this study, ZnO nanoparticles were used to fabricate the photoanode of the DSSCs and Rose Bengal dye was utilized as a sensitizer. To obtain better efficiency, the dye molecules must bind tightly to the mesoporous ZnO photoanode surface with the assistance of their anchoring group to ensure proficient electron injection from the LUMO of the dye molecule to the conduction band (CB) of ZnO. Here, we have studied the effect of the inclusion of rose bengal dye solution during the ZnO nanoparticle paste preparation. This yielded a coloured pre-dye treated paste of ZnO nanoparticles. The performance of pre-dye treated DSSC was compared with the cell prepared without pre-dye treating.

2. Materials and Method

2.1. Materials

Transparent ITO coated glass (10 Ω/ square) was purchased from Techinstro, India. Commercial ZnO nanopowder, Rose Bengal dye, and Triton X-100 were bought from Sigma Aldrich, India. The liquid electrolyte used in our experiment was a Solaronix high performance electrolyte (Iodolyte AN50) with iodide/tri-iodide as redox couple, ionic liquid, and lithium salt and pyridine derivative as additives dissolved in acetonitrile solvent. The liquid platinum paint (Platisol T) purchased from Solaronix, Switzerland was used to prepare the platinum-coated transparent counter electrode. Meltonix 1170-25 (25μm) purchased from Solaronix was used as a spacer between the working and counter electrode to avoid short-circuiting. All the reagents utilized in the fabrication process were of analytical grades. So no further purification was required.

2.2. Preparation of pure ZnO photoanode

To prepare the thin films of the photoanode materials, the ITO coated glass substrates were first cleaned with dilute HCl in an ultrasonic bath for 15 minutes and then thoroughly rinsed with deionized water to remove the HCL residues. Then the substrates were cleaned with acetone and ethanol using an ultrasonic cleaning bath [17, 22].

The working electrode of the DSSC was prepared by following the standard doctor blade method. The paste for doctor blading was prepared by mixing ZnO nanopowder with dilute acetylacetone as a solvent and ethyl cellulose as a binder. One drop of Triton X-100 was added to the mixture to reduce the surface tension of the slurry and to enable even spreading. The mixture was stirred continuously in order to obtain a smooth lump-free slurry. The ZnO paste was then coated on the conductive side of the cleaned ITO glass substrate and subsequently annealed at 450^{o}C on a hot plate for 30 min in order

to burn out the ethyl cellulose contents of the working electrode and strengthens the bonding between the substrate and the ZnO film. In addition to that, the annealing procedure also helps to improve the surface quality of the thin film along with increasing the crystallinity of the sample.

2.3. Preparation of pre-dye treated ZnO photoanode

To prepare the pre-dye treated ZnO photoanode, the above procedure is slightly modified by directly adding 0.3 mM ethanolic solution of Rose Bengal dye during the ZnO nanoparticle paste preparation. This yielded a coloured pre-dye treated paste of ZnO nanoparticles. This paste was also coated using the doctor blade method (Fig. 1) on a previously cleaned ITO glass substrate and annealed following the identical procedure as followed for the pure ZnO electrode to obtain the pre-dye treated ZnO working electrode.

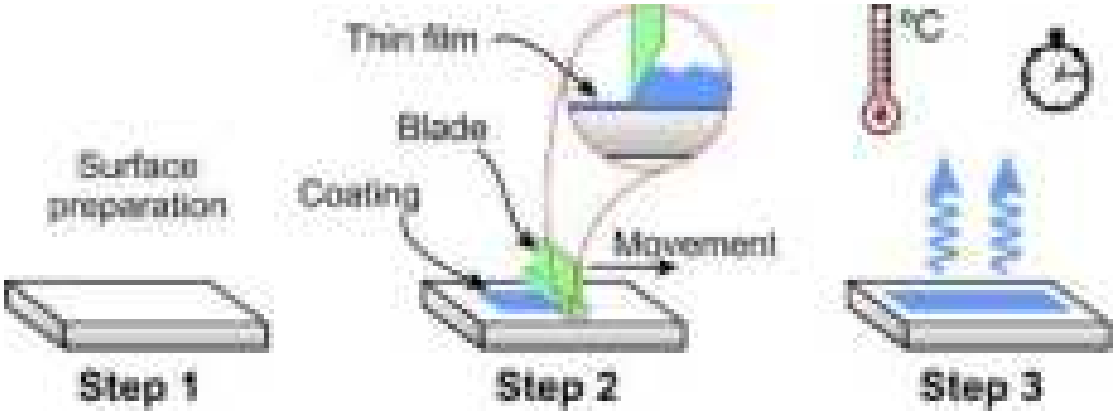

Figure 1. Schematic diagram of doctor blade method.
(https://link.springer.com/article/10.1007/s11356-020-10022-9)

2.4. Fabrication of the cells

Both of the pure and pre-dye treated ZnO electrodes were sensitized by immersing them in a 0.3 mM ethanolic solution of Rose Bengal dye for 12 hours. The working electrodes were then removed from the solution and thoroughly rinsed with deionized water and ethanol to remove any excess dye

from the ZnO nanoparticle film surface and left for air drying at room temperature. The platinum catalyst precursor solution Platisol-T (Solaronix) was spin-coated on the conducting side of the cleaned ITO glasses and heated at 450 ^{o} C for 15 minutes on a hot plate to prepare the counter electrodes for the cells. The dye adsorbed working electrodes and platinum(Pt)-coated counter electrodes were assembled against the coated sides of each other in a sandwich manner using two binder clips with a Surlyn film (Meltonix 1170-25µm, Solaronix) gasket as a spacer in between them. The liquid electrolyte used in the fabrication process was poured inside the cell through fine holes pre-drilled on the counter electrodes. The redox concentration of the electrolyte was 50 mM. The active area of the cells for illumination was 0.16 cm^2.

2.5. Characterization and Measurements

PAN-analytical X'Pert PRO X-ray diffractometer (CuKα radiation, 30 mA, 40 kV, λ= 1.5406 Å) was used to study the crystalline structure of the ZnO nanoparticles. The surface morphology of the prepared ZnO thin films was studied by using scanning electron microscopy (JEOL). The Current-Voltage (I-V) characterization of the cells was done using a Keithley 2400 digital source meter under 100 mW/cm^2 illumination (Xenon lamp 450W).

3. Results and Discussion

3.1. UV-VIS absorption spectral analysis of the dye

UV-VIS absorption spectrum of the Rose Bengal dye is shown in Fig. 2. The Rose Bengal dye absorbs a larger fraction of the solar spectrum in the visible region of 460–600 nm and it shows the highest optical absorption at 549 nm wavelength.

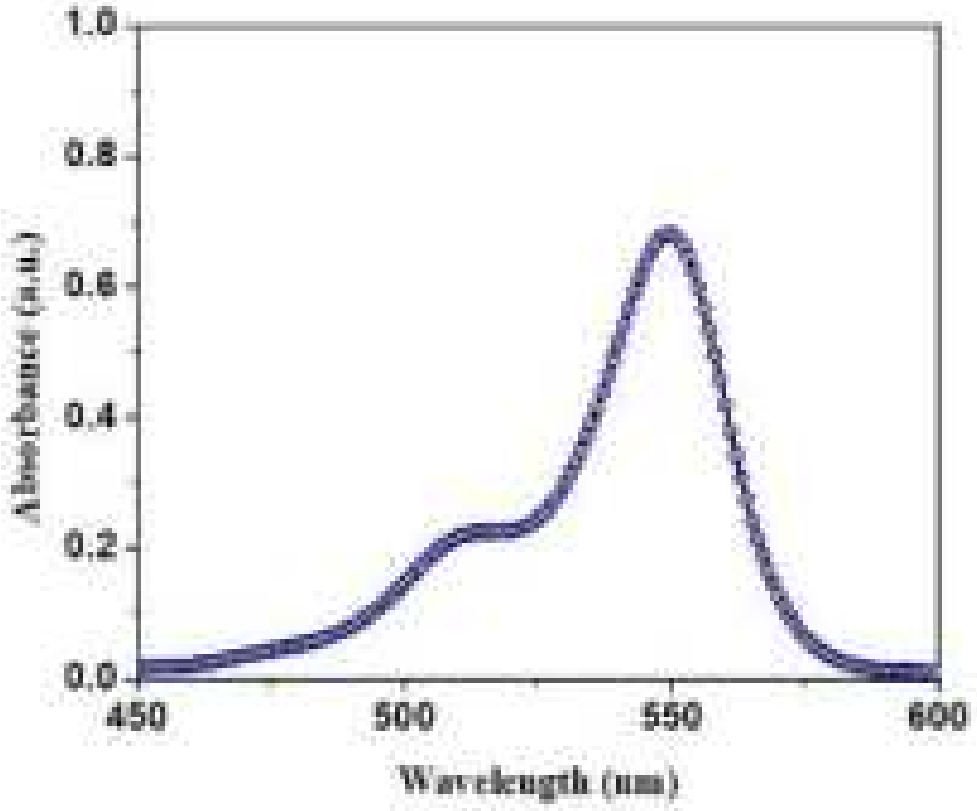

Figure 2. Absorption spectra of Rose Bengal dye.

3.2. Structural and phase characterization ZnO of the photoanode

X-ray diffraction pattern of the as-purchased ZnO nanopowder is shown in Fig. 3. The XRD pattern exhibits the hexagonal wurtzite crystal phase of ZnO and peaks well match the standard JCPDS card no. 36-1451. The diffraction peaks observed at 2θ values of 31.79°, 34.42°, 36.25°, 47.51°, 56.60°, 62.86°, 67.96°, and 69°corresponds to the reflection from the (100), (002), (101), (110), (103), (112), and (201) lattice planes respectively. Sharp and strong peaks indicate the highly crystalline nature of the material [23, 24].

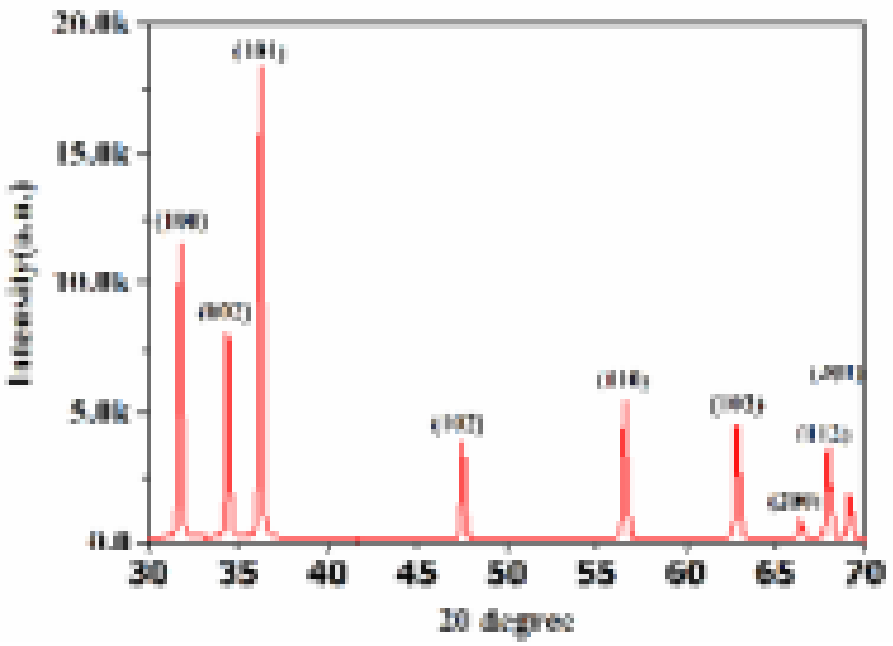

Figure 3. X-ray diffraction pattern of ZnO nanoparticles.

3.3. Surface Morphology study and energy dispersive spectroscopy of the photoanodes

Scanning electron microscopic (SEM) analysis of the ZnO nanopowder film on the ITO substrate was carried out to study the morphological properties and the particle size of the sample. The SEM image of the ZnO nanoparticles on an ITO substrate is shown in Fig.4 (a).

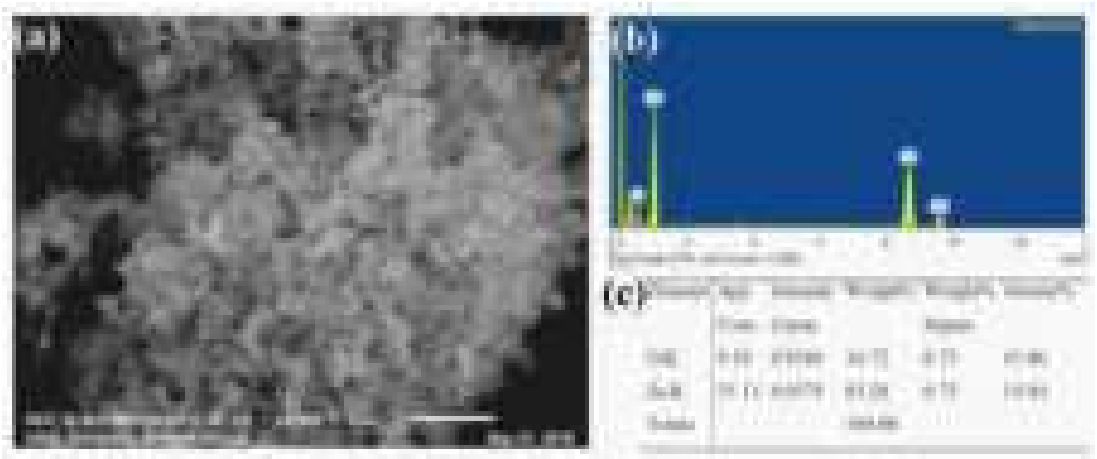

Figure 4. (a) SEM images, (b) EDS and (c) Elemental composition of ZnO Nanoparticles respectively

The SEM observation confirms that the ZnO particle size is in the nanometre range and they have a hexagonal wurtzite structure. Further, the chemical composition and elemental percentage of the film are revealed by the EDS analysis which is shown in Fig. 4 (b) and 4 (c) respectively.

3.4. *Photovoltaic (Current-Voltage) characterization of the cells*

The Current-Voltage characteristic is an essential measurement that reveals the values of the overall photovoltaic performance of a solar cell along with key performance parameters like open circuit voltage and short circuit current density. Fig. 5 depicts the I-V characteristics of the DSSCs based on pure and pre-dye treated ZnO as photoanodes respectively. The overall photoconversion efficiency of the solar cell is calculated by the formula

$$\eta = \frac{P_{out}}{P_{in}} = \frac{I_{sc}V_{oc}FF}{P_{in}} \qquad (1)$$

Where $P_{in,}$ V_{oc}, I_{sc} and FF denote the incident photon power, open-circuit voltage, the short circuit current density and fill factor respectively. The fill factor is calculated using the following formula:

$$FF = \frac{I_{max}V_{max}}{I_{sc}V_{oc}} \qquad (2)$$

Where I_{max} and V_{max}, respectively, represent values of the current and voltage at the maximum output power point of the solar cell.

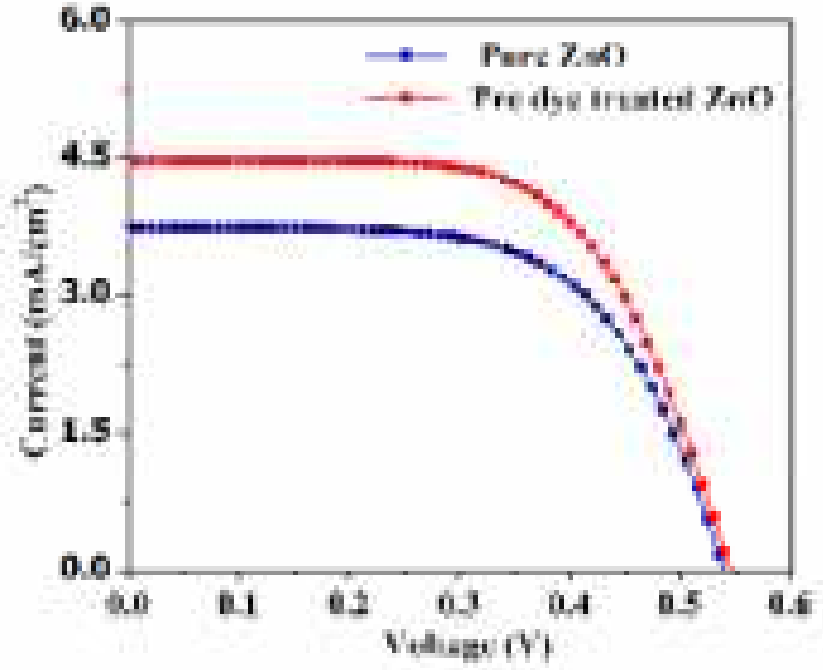

Figure 5. Current-voltage characteristics of different cells under illumination.

The photovoltaic parameters extracted from the I-V characteristics of the fabricated DSSCs are shown in table 1 below.

Table 1.

Photovoltaic performance of uncoated and ZnO coated WO_3 photoanode based DSSC

ZnO precursor concentration	J_{sc} (mA/cm^2)	V_{oc}(V)	FF	Efficiency (η %)
Pure ZnO	3.73	0.53	0.63	1.26
Pre-dye treated ZnO	4.47	0.55	0.62	1.53

A considerable improvement in the values of J_{sc} and η for the pre-dye treated DSSC can be observed compared to the conventionally prepared pure ZnO electrode from Table 1. This demonstrates the positive role of the pre-dye treating process. This may be attributed to the fact that the pre-dye loading method resulted in uniform dye adsorption, reduced agglomeration, the improved surface morphology of photoanode and less dye aggregation [25].

The V_{oc} is also improved slightly. The increased amount of dye molecule adsorption on the pre-dye treated ZnO nanoparticle surface absorbs more photons and thereby injecting more electrons to the conduction band of ZnO. This yielded increased J_{sc} and η.

4. Conclusion

DSSCs using pure and pre-dye treated ZnO nanoparticles as photoanode material were fabricated and their electro-optical performances were compared. The performance of the DSSC was remarkably improved upon pre-dye loading. The pre-dye treated ZnO DSSC showed a 19.84% improvement in Short circuit current density (J_{sc}) and 21.43 % improvement in photoconversion efficiency (η). Therefore, the method of pre-dye loading of ZnO nanoparticles may be used as an effective and novel way to improve the performance of dye sensitized solar cells.

References

[1] Bach W. Global warming: the complete briefing (2nd ed). John Houghton. Cambridge University Press: Cambridge, 1997. Pp. xv + 251. Paperback: ISBN 0521-62932-2, ú12.95; hardback: ISBN 0-321-62089-9, ú35.00. International Journal of Climatology. 1998;18(5):579-80.

[2] Meadows DH, Meadows DL, Randers J, Behrens WW. The limits to growth. New York. 1972;102:27.

[3] Minger TJ, editor Greenhouse glasnost: the crisis of global warming: essays. Greenhouse/Glasnost: the Sundance Symposium on Global Climate Change,(USA), 1989; 1990: Ecco Press.

[4] Barbir F, Veziroğlu TN, Plass Jr HJ. Environmental damage due to fossil fuels use. International journal of hydrogen energy. 1990 Jan 1;15(10):739-49.

[5] Goetzberger A, Hebling C, Schock HW. Photovoltaic materials, history, status and outlook. Materials Science and Engineering: R: Reports. 2003 Jan 1;40(1):1-46.

[6] Alharbi F, Bass JD, Salhi A, Alyamani A, Kim HC, Miller RD. Abundant non-toxic materials for thin film solar cells: Alternative to conventional materials. Renewable Energy. 2011 Oct 1;36(10):2753-8.

[7] Lee TD, Ebong AU. A review of thin film solar cell technologies and challenges. Renewable and Sustainable Energy Reviews. 2017 Apr 1;70:1286-97.

[8] Yamamoto K, Yoshimi M, Tawada Y, Okamoto Y, Nakajima A. Cost effective and high-performance thin film Si solar cell towards the 21st century. Solar energy materials and solar cells. 2001 Feb 1;66(1-4):117-25.

[9] B. O'regan and M. Grätzel, A low-cost, high-efficiency solar cell based on dye-sensitized colloidal TiO2 films, *nature* 353, 737, (**1991**).

[10] Chiba Y, Islam A, Komiya R, Koide N, Han L. Conversion efficiency of 10.8% by a dye-sensitized solar cell using a Ti O 2 electrode with high haze. Applied Physics Letters. 2006 May 29;88(22):223505.

[11] Grätzel M. Solar energy conversion by dye-sensitized photovoltaic cells. Inorganic chemistry. 2005 Oct 3;44(20):6841-51.

[12] Chung,I., Lee,B., Jiaqing, H.,Robert, P. H. C. & Kanatzidis, M. G. (2012). All-solid-state dye-sensitized solar cells with high efficiency.Nature, 485,7399,415-540.

[13] Cai, N., Moon, SJ., Cevey-Ha, L., Moehl, T., Humphry-Baker, R., Wang, P., Zakeeruddin, SM., & Grätzel, M. (2011). An organic D-π-A dye for record efficiency solid-state sensitized heterojunction solar cells. Nano Lett. 11, 11(4), 452–1456.

[14] M. Grätzel, Dye-sensitized solar cells, Journal of Photochemistry and Photobiology C: Photochemistry Reviews 4, 145, (2003).

[15] F. Shao, J. Sun, L. Gao, S. Yang and J. Luo, Growth of various TiO2 nanostructures for dye-sensitized solar cells, The Journal of Physical Chemistry C 115, 1819, (2010).

[16] Tiwana P, Docampo P, Johnston MB, Snaith HJ, Herz LM. Electron mobility and injection dynamics in mesoporous ZnO, SnO2, and TiO2 films used in dye-sensitized solar cells. ACS nano. 2011 Jun 28;5(6):5158-66.

[17] Biswas R, Chatterjee S. Effect of surface modification via sol-gel spin coating of ZnO nanoparticles on the performance of WO3 photoanode based Dye Sensitized Solar Cells. Optik. 2019 Dec 28:164142.

[18] Zhang Q, Dandeneau CS, Zhou X, Cao G. ZnO nanostructures for dye-sensitized solar cells. Advanced Materials. 2009 Nov 6;21(41):4087-108.

[19] Guillén E, Peter LM, Anta JA. Electron transport and recombination in ZnO-based dye-sensitized solar cells. The Journal of Physical Chemistry C. 2011 Nov 17;115(45):22622-32.

[20] Quintana M, Edvinsson T, Hagfeldt A, Boschloo G. Comparison of dye-sensitized ZnO and TiO2 solar cells: studies of charge transport and carrier lifetime. The Journal of Physical Chemistry C. 2007 Jan 18;111(2):1035-41.

[21] Vittal R, Ho KC. Zinc oxide based dye-sensitized solar cells: A review. Renewable and Sustainable energy reviews. 2017 Apr 1;70:920-35.

[22] Biswas R, Roy T, Chatterjee S. Study of Electro-Optical Performance and Interfacial Charge Transfer Dynamics of Dye Sensitized Solar Cells Based on ZnO Nanostructures and Natural Dyes. Journal of Nanoelectronics and Optoelectronics. 2019 Jan 1;14(1):99-108.

[23] Costantino U, Marmottini F, Nocchetti M, Vivani R. New Synthetic Routes to Hydrotalcite-Like Compounds− Characterisation and Properties of the Obtained Materials. European Journal of Inorganic Chemistry. 1998;1998(10):1439-46.

[24] Oh J-M, Hwang S-H, Choy J-H. The effect of synthetic conditions on tailoring the size of hydrotalcite particles. Solid State Ionics. 2002;151(1-4):285-91.

[25] Ananth S, Vivek P, Arumanayagam T, Murugakoothan P. Pre dye treated titanium dioxide nanoparticles synthesized by modified sol–gel method for efficient dye-sensitized solar cells. Applied Physics A. 2015 Jun 1;119(3):989-95.

This page is intentionally left blank

Appendix B

List of Research Journal Publications

1. **Rajat Biswas**, Trinakhi Roy, and Suman Chatterjee, "Study of electro-optical performance and interfacial charge transfer dynamics of dye sensitized solar cells based on ZnO nanostructures and natural dyes", Journal of Nanoelectronics and Optoelectronics, Vol. 14, no. 1 (2019): 99-108.
2. **Rajat Biswas** and Suman Chatterjee, "Effect of surface modification via sol-gel spin coating of ZnO nanoparticles on the performance of WO_3 photoanode based dye sensitized solar cells", Optik, Vol. 212 (2020): 164142.
3. Trinakhi Roy, **Rajat Biswas**, and Suman Chatterjee, "An Investigation on the Stability Enhancement of Dye-Sensitized Solar Cells Fabricated with Ethyl Cellulose Based Gel Electrolyte", Applied Solar Energy, Vol. 57, no. 1 (2021): 23-29.
4. **Rajat Biswas** and Suman Chatterjee. "Effect of chenodeoxycholic acid as dye co-adsorbent and ZnO blocking layer in improving the performance of Rose Bengal dye based dye sensitized solar cells", Optical and Quantum Electronics, Vol. 54, no. 6 (2022): 1-20.
5. **Rajat Biswas**, Joy Sarkar, and Suman Chatterjee, "Improvement of Photovoltaic Performance of Dye Sensitized Solar Cells by Pre-Dye Treating of Zno Nanoparticles." Journal of Physics Research and Education, Vol. 1, no. 1 (2021), pp. 17-29.

6. Joy Sarkar, **Rajat Biswas**, and Suman Chatterjee, "Electronic Band Structure and Density of States Analysis of Electron Transport Materials for Perovskite Solar Cells", Journal of Physics Research and Education , Vol. 1, no. 1 (2021), pp. 46-58.

7. **Rajat Biswas** and Suman Chatterjee, "Optimizing the concentration of ethyle cellulose to improve stability and photovoltaic performance of gel electrolyte based dye-sensitized solar cells". (Communicated)

Appendix C

List of Conference Presentations

1. **Rajat Biswas** and Suman Chatterjee,"ZnO naonorod based dye sensitized solar cells sensitized using natural dyes extracted from pomegranate and curcumin", Modern Trends in Material Science, Dept. of Physics, University of North Bengal, Siliguri (2015).
2. **Rajat Biswas** and Suman Chatterjee, "Fabrication and characterization of ZnO naonorod based dye sensitized solar cells using some natural photosensitizers", National Seminar on Condensed Matter, Laser and Communication, Dept. of Physics, University of Burdwan, Burdwan (2015).
3. **Rajat Biswas** and Suman Chatterjee, "Electrochemical impedance spectroscopy study of dye sensitized solar cells with gold, graphite and carbon black as counter electrode material", Recent Innovations in Renewable Energy, Centre for renewable Energy Studies, Dept. of Physics, B.N. Mandal University, Madhepura (2018).

This Page is intentionally left blank

Reprint of Selected Papers

Optical and Quantum Electronics (2022) 54:391
https://doi.org/10.1007/s11082-022-03775-9

Effect of chenodeoxycholic acid as dye co-adsorbent and ZnO blocking layer in improving the performance of Rose Bengal dye based dye sensitized solar cells

Rajat Biswas[1] · **Suman Chatterjee**[1]

Received: 23 May 2021 / Accepted: 26 April 2022

Abstract

Effective suppression of dye aggregation on the photoanode surface of dye sensitized solar cells plays a key role in improving solar cell efficiency. Chenodeoxycholic acid (CDCA) is a very popular anti dye aggregation material used in dye sensitized solar cells (DSSC). However, the selection of an improper concentration of CDCA may lead to decreased solar cell efficiency by lowering the open circuit voltage and short circuit current as a consequence of reduced dye loading. The influence of CDCA as a dye co-adsorbent on the performance of DSSCs fabricated using Rose Bengal dye was studied in this paper. The concentration of the CDCA solution was varied to identify the optimum value for the best device performance. Aside from this, the effect of a very thin and compact ZnO blocking layer was also investigated to reduce the charge recombination. With photovoltaic parameters such as short circuit current density (J_{sc}) = 1.98 mA/cm^2, open circuit voltage (V_{oc}) = 0.58 V, and fill factor (FF) = 0.43, the traditional cell displayed an overall conversion efficiency of 0.49%, while the power conversion efficiency was found to be increased to 1.00% (Jsc = 2.80 mA/cm^2, V_{oc} = 0.64, FF = 0.58) when CDCA was added at optimised concentration of 8 mM. Reduced dye aggregation and increased electron injection in the presence of CDCA may be accounted for the DSSC's remarkable improvement in the efficiency. Moreover, the combined effect of 8 mM CDCA and the compact ZnO blocking layer dramatically enhanced the efficiency further to 1.22% (J_{sc} = 3.09 mA/cm^2, V_{oc} = 0.66, FF = 60). Electrochemical impedance spectroscopic (EIS) analysis revealed that the addition of CDCA as a co-adsorbent in the dye solution and addition of ZnO blocking layer resulted in significantly improved electron lifetime and reduced electron recombination yielding improved J_{sc}, V_{oc} and η.

Keywords Dye sensitized solar cell · Dye co-adsorbent · Chenodeoxycholic acid · ZnO blocking layer · Rose bengal dye · Electrochemical impedance spectroscopy

✉ Suman Chatterjee
suman@nbu.ac.in

Rajat Biswas
rajat_biswas@nbu.ac.in

[1] Department of Physics, University of North Bengal, Raja Rammohunpur, Darjeeling, Siliguri 734013, India

Published online: 05 June 2022

1 Introduction

Ever growing global energy requirement and depleting level of fossil fuels have accelerated the demand for efficient power generation from solar photovoltaic (PV) cells in recent years (Bach 1997; Meadows et al. 1972; Hosenuzzaman et al. 2015). The environmental impact of the use of fossil fuels is another major concern (Barbir et al. 1990). The current production of photovoltaic (PV) modules is dominated by crystalline silicon modules based on bulk wafers. However, the use of toxic materials and the high production cost of these solar cells have motivated the researchers to find new kinds of less expensive and non silicon-based solar cells to harvest solar energy efficiently (Goetzberger et al. 2003; Alharbi et al. 2011; Lee and Ebong 2017; Yamamoto et al. 2001).

Dye-sensitized solar cells (DSSCs) are a non-conventional photovoltaic technology that has attracted significant attention because of their high conversion efficiencies and low cost. O'Regan. B. and Grätzel reported high efficiency cells using nanoporous titanium dioxide (TiO_2) semiconductor electrodes, ruthenium (Ru) metal complex dyes, and iodine electrolyte solutions in the journal of Nature in 1991 (O'Regan and Grätzel 1991). Since then, many studies have been actively carried out on DSSCs and revealed their performance comparable to amorphous silicon thin films (Chiba et al. 2006; Grätzel 2005). These DSSCs have the advantages of low cost, lightweight and easy fabrication, but issues include durability and further improvement of their properties. To respond to these issues, many attempts have been made, such as solidifying electrolytes and improving materials and structures, but there have been no great breakthroughs yet (Chung et al. 2012; Cai et al. 2011).

A dye-sensitized solar cell consists of two conducting glass electrodes in a sandwich arrangement. Each layer has a specific role in the cell. The transparent glass electrodes allow the light to pass through the cell. The titanium dioxide serves as a holding place for the dye and participates in electron transfer. The dye molecules collect light and produce excited electrons which cause a current in the cell. The iodide electrolyte layer acts as a source for electron replacement. The bottom conductive layer is coated with platinum which plays the role of the counter electrode. A schematic structure of a liquid electrolyte DSSC and its working principle is shown in Fig. 1. When light passes through the conductive glass electrode, the dye molecules absorb the photons and the electrons in the dye go from the ground state (HOMO) to an empty excited state (LUMO). This is referred to as photoexcitation. The excited electrons jump to the conduction band of the semiconducting dioxide and diffuse across this layer reaching the conductive electrode. Then they travel through the outer circuit and reach the counter electrode. The dye molecules become oxidized after losing an electron to the semiconductor oxide material. The red-ox iodide electrolyte donates electrons to the oxidized dye molecules thereby regenerating them. When the originally lost electron reaches the counter electrode, it gives the electron back to the electrolyte (O'Regan and Grätzel 1991; Grätzel 2003).

The photovoltaic performance of a DSSC highly depends on all of its components and the fabrication methodology. Therefore, the optimization of every component is extremely crucial to achieve the best performance. Since its introduction into the science community in 1991, the nanocrystalline photoanode in dye-sensitized solar cells has predominantly been comprised of titanium (TiO_2) nanoparticles as the semiconducting material (O'Regan and Grätzel 1991; Grätzel 2003; Shao et al. 2011). Many researchers became very interested in studying the dye-sensitized solar cell performance fabricated using alternative semiconducting nanomaterials (Tiwana et al. 2011; Biswas and Chatterjee 2020).

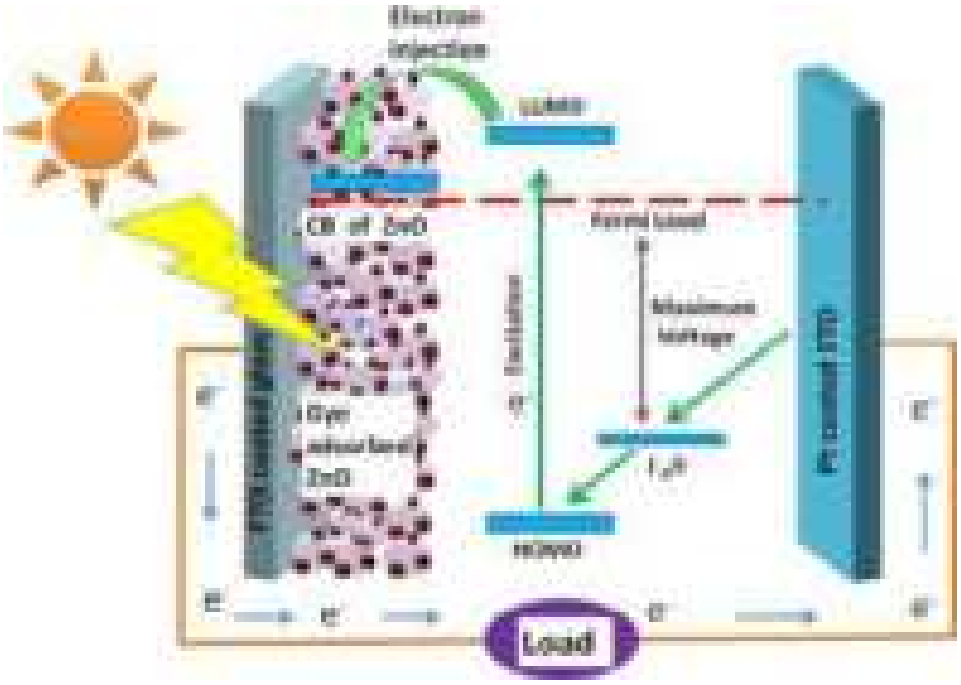

Fig. 1 Schematic diagram and working principle of a conventional DSSC

Specifically, Zinc Oxide (ZnO) has been an ideal alternative to TiO_2 because of having a similar conduction band edge that is appropriate for proper electron injection from the excited dyes; moreover, ZnO provides better electron transport due to its higher electronic mobility. Along with that, ZnO is also highly transparent, which allows greater light penetration (Zhang et al. 2009; Guillén et al. 2011; Quintana et al. 2007; Vittal and Ho 2017; Biswas et al. 2019).

In this study, ZnO nanoparticles were implemented to fabricate the photoanode of the DSSCs and rose bengal dye was utilized as a sensitizer. To obtain better efficiency, the dye molecules must bind tightly to the mesoporous ZnO photoanode surface with the assistance of their anchoring group to ensure proficient electron injection from the LUMO of the dye molecule to the conduction band (CB) of ZnO.

Ruthenium dyes have long been used as quite efficient sensitizers for the photoanodes of the DSSCs (Ito et al. 2006, Aghazada et al. 2018, Nazeeruddin et al. 2011). However, these dyes are expensive, difficult to synthesis, requires high production cost, toxic, rare and easily pollute the environment (Sayyed et al. 2016). Owing to these facts, the organic photosensitizer Rose Bengal (RB), emerges as a promising and alternative candidate. It is a xanthenes class photosensitizer having high absorbtion coefficient and absorbs a wide spectrum of solar radiation. It energetically matches the conduction band edge of ZnO and iodine/iodide redox couple for DSSC application (Pradhan et al. 2007, Duffy et al. 2000). Accordingly, ZnO based DSSC performes specifically well when sensitized with Rose Bengal. Although the efficiency of these type of organic sensitizer based DSSCs is less, production cost per watt will be less compared to the ruthenium based DSSCs even if we achieve moderate efficiency. As the RB dye is an organic dye and does not contain any toxic noble metal such as ruthenium, there are no environmental pollution related issues with it. It is widely used because of its high absorption coefficient in the visible region of solar spectrum and its molecular structure (Fig. 2) comprises of anchoring groups that can be adsorbed onto the semiconductor oxide surface. For the particular case of ZnO–RB combination, the interaction between the unfilled valance shell of the ZnO and the carboxyl

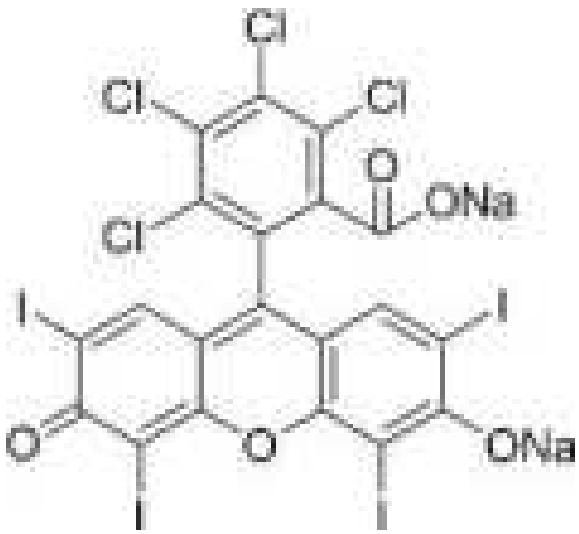

Fig. 2 Chemical structure of Rose Bengal dye

groups present in the dye molecules leads to easy adsorption of the dye molecules on the ZnO surface. Such kind of bonding between the dye molecule and ZnO not only increases adsorptivity of dye but also facilitates electron injection because of the substantial overlap between the electron molecular orbitals of the dye and those of the semiconductor's conduction band (Rani et al. 2010).

However, in case of ZnO photoanode based DSSCs, the dye aggregation on the ZnO surface affects the photoelectron injection by increasing charge recombination and hence limits the overall device performance (Kim et al. 2014; Patwari et al. 2017; Zhang and Cole 2017). The use of additives such as Chenodeoxycholic acid (CDCA) is a very useful and widely used strategy in lowering the self-aggregation of dye molecules by suppressing unfavourable dye-dye interactions as shown in Fig. 3 and thereby enhances the photoconversion efficiency (Buene et al. 2020; Kumar et al. 2020; Ismail et al. 2018). However, the strong binding of CDCA molecules to the ZnO surface partially displaces dye molecules and consequently reduces photon harvesting. Therefore, to maximize the positive effect of the co-adsorbent, it is very crucial to carefully optimize the amount of CDCA (Li et al. 2011). Few researchers have studied the role of CDCA as an anti-aggregation agent in ruthenium and organic dye based DSSCs and found it to be very effective in reducing the aggregation of dye molecules over the semiconductor surface (Inoue et al. 2010; Lee et al. 2007; Yum et al. 2008; Lu et al. 2009). But there is no report available related to the application of CDCA on Rose Bengal dye. Herein, we report the investigation on the effect of CDCA as co-adsorbent in the performance of Rose Bengal (RB) dye based DSSCs. Different concentrations of CDCA were studied to identify the optimum value for achieving the best device performance.

On the other hand, the mesoporous nature of the ZnO film is very essential to tender high surface area offering more dye loading and thereby generating more photoelectrons. However, small pores present in the nanocrystalline ZnO layer of the photoanode may provide a path for the direct contact between the liquid electrolyte and the FTO substrate. This may allow the electrons of FTO to recombine with the I^-_3 ion present in the electrolyte resulting in high recombination current and hence decreased cell performance (Yang et al. 2014; Yeoh and Chan 2019). Therefore, to inhibit the electron back transfer, a promising approach is to modify the FTO/electrolyte interface by adding a compact metal oxide blocking layer. A thin blocking layer (BL) of ZnO was deposited by a facile and cost-effective sol–gel spin coating process before depositing the mesoporous active ZnO layer. In this

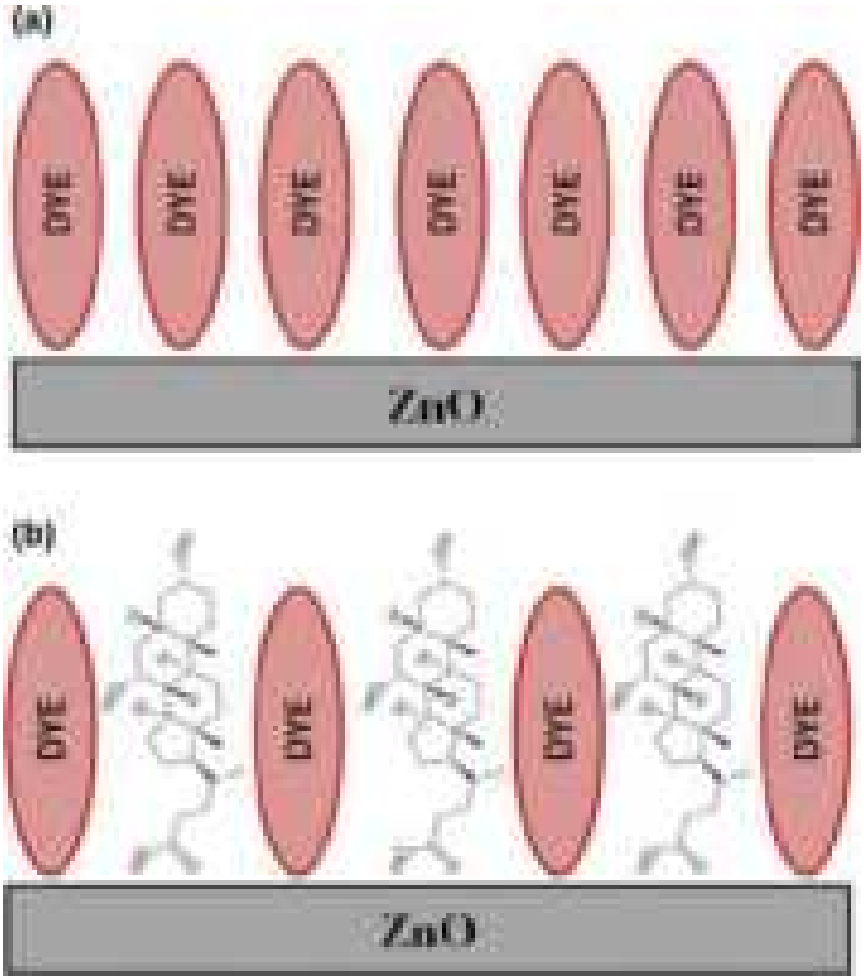

Fig. 3 **a** Unfavourable dye-dye interaction in absence of CDCA **b** reduced self-aggregation of dye molecules in presence of CDCA

work, we reported the fabrication and characterization of DSSCs based on ZnO nanoparticles and Rose Bengal dye. The effect of CDCA concentration and the compact ZnO blocking layer in boosting the photovoltaic performance of the device was investigated in terms of photocurrent–voltage (J–V) characteristics and dark current measurement. In addition to that, electrochemical impedance spectroscopy (EIS) analysis was employed to investigate the charge transfer kinetics and electron back reaction of the fabricated cells.

2 Materials and methods

2.1 Materials

ZnO nanopowder, Zinc acetate dehydrate $(CH_3COO)_2Zn$, $2H_2O$) and Monoethanolamine (MEA) were bought from Sigma Aldrich, India. ethylcellulose and terpineol were bought from TCI Chemicals, India. Transparent FTO coated glass (10 Ω/square), the high-performance liquid electrolyte (Iodolyte AN50), chenodeoxycholic acid (CDCA) as a dye co-adsorbent and liquid platinum paint (Platisol T) to prepare the platinum-coated counter electrode were purchased from Solaronix, Switzerland. Meltonix 1170–25 (25 μm) (Solaronix) was used as a spacer between the working and counter electrode to avoid

short-circuiting. All the reagents utilized in the fabrication process were of analytical grades. So no further purification was required.

2.2 Preparation of conventional ZnO photoanode

To prepare the thin films of the photoanode materials, the FTO coated glass substrates were first cleaned with dilute HCl in an ultrasonic bath for 15 min and then thoroughly rinsed with deionized water to remove the HCL residues. The substrates were then cleaned with acetone and ethanol using an ultrasonic cleaning bath (Biswas and Chatterjee 2020; Biswas et al. 2019). The mesoporous ZnO photoelectrode of the DSSC was prepared by following the standard doctor blade method. The paste for doctor blading was prepared by mixing 0.5 g of ZnO nanopowder with α-terpineol as a solvent and 0.45 g of ethyl cellulose as a binder (Wong et al. 2012). The mixture was stirred continuously to obtain a smooth lump-free slurry. The ZnO paste was then coated on the conductive side of the cleaned FTO glass substrate and subsequently annealed at 400 °C on a hot plate for 30 min to burn out the ethyl cellulose and other organic contents of the working electrode and to strengthening the bonding between the substrate and the ZnO film. In addition to that, the annealing procedure also helps to improve the surface quality of the thin film along with increasing the crystallinity of the sample (Elilarassi and Chandrasekaran 2010; Shivaraj et al. 2015; Al-Kahlout 2015; Pandey et al. 2017).

2.3 Preparation of photoanode with compact ZnO layer

In order to improve the photovoltaic performance of the cells further by preventing the direct contact between FTO and liquid electrolyte, a thin and compact ZnO layer was deposited on FTO coated glass substrate by employing a simple sol–gel spin coating method prior to deposition of mesoporous active ZnO nanoparticle layer. The precursor solution was prepared by mixing Zinc acetate dehydrate $(CH_3COO)_2Zn$, $2H_2O$) in 50 ml isopropanol as solvent and monoethanolamine (MEA) was used as a stabilizer. The precursor solution concentration was maintained at 0.05 M. The mixture was vigorously stirred at 60° C by a magnetic stirrer for 1 h. MEA was added dropwise under stirring, yielding a clear homogenous solution. The solution was left for 24 h at room temperature for aging before it could be used for film deposition. The aged solution was then spin-coated on a cleaned FTO glass substrate with a programmable spin coater (Apex Instruments Co. Pvt. Ltd, Model SpinNXG-P1)at 3000 rpm for 30 s and annealed at 200 °C for 20 min to form the ZnO blocking layer. Over this compact blocking layer, the mesoporous active layer was coated using the same doctor blade method and then annealed at 400 °C as done earlier.

2.4 Assembling the devices

One set of ZnO photoanodes were sensitized by immersing them in a 0.5 mM ethanolic solution of pure Rose Bengal dye for 12 h. Another set of photoanodes (both with and without ZnO blocking layer) were sensitized with the RB dye solution containing various concentrations (0–10 mM) of CDCA at room temperature for 12 h. The working electrodes were then removed from the solution and rinsed thoroughly with deionized water and ethanol to get rid of any excess dye from the thin film surface and left for air drying at room temperature. The platinum catalyst precursor solution (Platisol-T) was spin-coated

on the conducting side of the cleaned FTO glasses and heated at 450 °C for 15 min on a hot plate to prepare the counter electrodes for the cells. The dye adsorbed working electrodes and platinum(Pt)-coated counter electrodes were assembled against the coated sides of each other in a sandwich manner using two binder clips with a Surlyn film (Meltonix 1170–25 µm, Solaronix) gasket as a spacer in between them. The liquid electrolyte used in the fabrication process was poured inside the cell through fine holes pre-drilled on the counter electrodes. The red-ox concentration of the electrolyte was 50 mM. The active area of the cells for illumination was adjusted to 0.16 cm^2.

2.5 Characterization and measurements

X-ray diffraction (XRD) analysis is a technique used for the determination of the crystal structure of materials in the nanomaterial, thin-film, or bulk material form. In the XRD experiment, a monochromatic X-ray beam is allowed to incident on the sample and the diffraction occurs. Constructive interference is obtained for the glancing angles (θ) corresponding to those (hkl) planes only for which the path difference is equal to integral multiple (n) of wavelength (λ) of the X-ray used. This condition is given by Bragg's equation

$$2\,d\,\mathrm{Sin}(\theta) = n\,\lambda$$

where d is the interplanar spacing. The schematic of the experimental arrangement is shown in Fig. 4. The reflected X-rays make an angle 2θ with the material surface. A typical XRD pattern consists of these reflection peaks along the y-axis with the diffraction angles 2θ along the x-axis (Epp 2016, Zhang et al. 2004). In our study, the X-ray diffraction analysis was employed using PAN-analytical X'Pert PRO X-ray diffractometer (CuKα radiation, 30 mA, 40 kV, λ = 1.5406 Å) to determine the crystalline structure of ZnO nanoparticles used in making the photoanode of the DSSC.

Absorbance spectrum measurement of the dye was carried out using a Perkin-Elmer Lambda-35 UV–VIS spectrophotometer. In this measurement, the sample is exposed to light within a selected range of wavelengths. Absorption occurs when the incident photon energy surpasses the energy gap between the lower energy orbital (highest occupied molecular orbital-HOMO) and the higher energy unoccupied orbital (lowest unoccupied molecular orbital-LUMO) of the materials, and then the spectrometer records the signal.

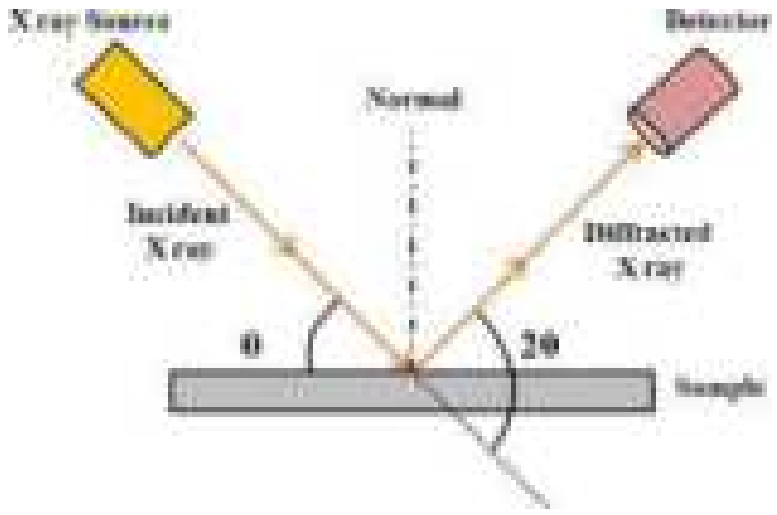

Fig. 4 X-ray diffraction at the sample film surface

The block diagram of the UV–VIS spectrophotometer is shown in Fig. 5. (Rocha et al. 2018).

Scanning electron microscopy (JEOL) was used to examine the surface morphology of the prepared ZnO thin films. The current–voltage (J–V) characterization of the cells was measured under 100 mW/cm.^{2} illumination using a Keithley 2400 digital source meter which was controlled by Keithley LabTracer computer software. The overall photoconversion efficiency of the solar cell was calculated using the formula

$$\eta = \frac{P_{out}}{P_{in}} = \frac{I_{sc} V_{oc} FF}{P_{in}} \tag{1}$$

where $P_{in,}$ V_{oc}, I_{sc} and FF denote the incident photon power, open-circuit voltage, the short circuit current density and fill factor respectively. The fill factor was estimated using the following formula:

$$FF = \frac{I_{max} V_{max}}{I_{sc} V_{oc}} \tag{2}$$

where I_{max} and V_{max}, respectively, represent values of current and voltage at the maximum output power point of the solar cell. The area of the fabricated cells that was exposed to light was 1 cm^2. The electrochemical impedance spectroscopy (EIS) of the cells was done in the frequency range of 0.1–190 kHz under open circuit conditions.

3 Results and discussion

3.1 UV–VIS absorption spectral analysis of the dye

0.5 mM ethanolic solution of Rose Bengal dye was prepared and its absorption property was studied using Perkin Elmer Lambda–35 UV–VIS spectrophotometer. UV–VIS absorption spectrum of the RB dye is shown in Fig. 7a. The value of λ_{max} obtained from the absorption spectrum is a very important parameter as it demonstrates the potential of the molecular systems for significant usage as a functional material in DSSC. It can observed that the Rose Bengal dye absorbs a larger fraction of the solar spectrum in the visible

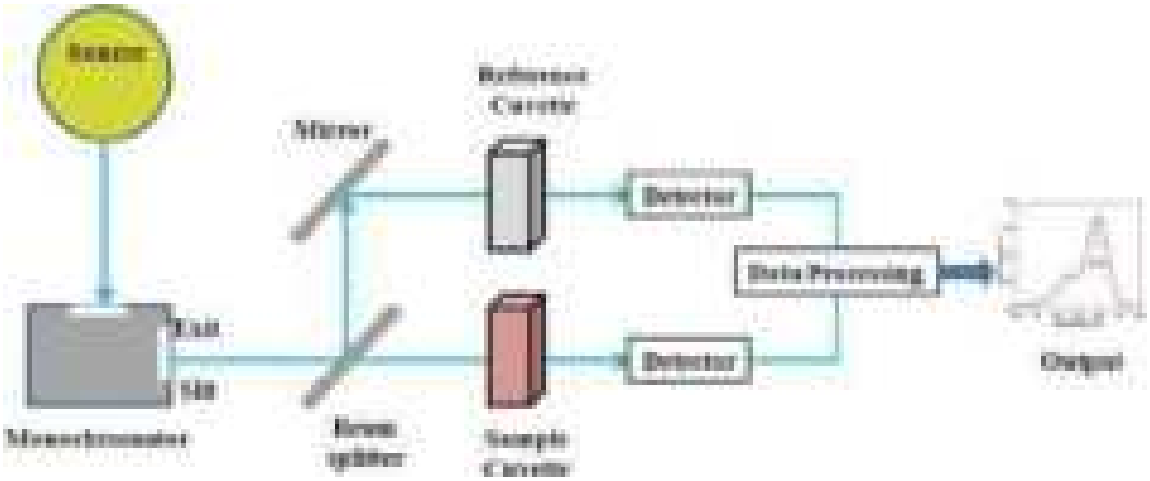

Fig. 5 Schematic of UV–VIS spectrophotometer

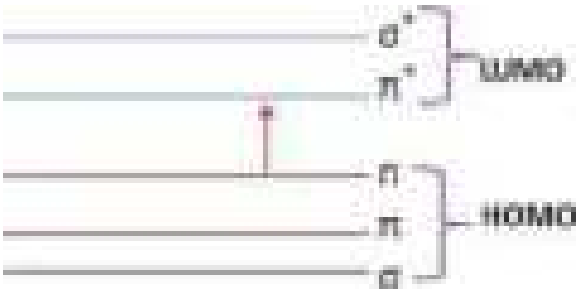

Fig. 6 Possible transition mechanism in the Rose Bengal molecular system

region of 460–600 nm and it shows the highest optical absorption at 549 nm wavelength. The strong absorption peak may be assigned to the intra-molecular charge transfer (ICT) transitions from the donor to acceptor level within HOMO (Highest Occupied Molecular Orbital)- (Lowest Unoccupied Molecular Orbital)LUMO energy levels as shown in Fig. 6 (Sayyed et al. 2016, Singh et al. 2012).

The optical energy gap of the dye was calculated using Tauc's relation (Eq. 3) (Shamsuddin et al. 2017, Ghobadi 2013, Uyanga et al. 2020)

$$\alpha h\nu = B(h\nu - \mathrm{E}_g)^m \tag{3}$$

where α is the absorption coefficient, $h\nu$ is the photon energy, E_g is the optical energy gap of the material and value of m depends on type of transition. The value of m is 2 or $\frac{1}{2}$ for indirect and direct transition respectively. The direct band gap of the Rose Bengal dye was found to be $2.19eV$ by extrapolating the linear part of the $(\alpha h\nu)^2$ versus $h\nu$ plot as shown in Fig. 7b. The indirect band gap of the dye was calculated through extrapolation of the linear portion of the $(\alpha h\nu)^{1/2}$ versus $h\nu$ plot as shown in Fig. 7c (Patni et al. 2020) which indicates indirect transition at $\mathrm{E}_g = 2.13eV$.

The HOMO–LUMO direct band gap of the dye affects the electron transfer from the LUMO of the dye molecule to the conduction band of the ZnO particles. It facilitates the vertical electron transition through the dye excitation (Henson et al. 2013). On the other hand, indirect transition is a phonon assited transition where change in momentum must be taken into account. When the photons having energy fairly above the indirect band gap of dye molecule is absorbed by the dye electron, phonons get emitted (Seo and Hoffmann 1999). As a result the direct band gap is utilized to determine the vertical transition during the course of photosesitization (Nguyen et al. 2013, Prima et al. 2016). Hence, the lowest electronic transition, which corresponds to the onset of absorption in the UV–visible absorption spectrum, was used to calculate the optical bandgap. It is the energy difference between HOMO and LUMO which is caused by the excitation of electrons from HOMO to LUMO.

3.2 Structural and phase characterization ZnO compact layer

The X-ray diffraction pattern of the ZnO compact blocking layer, shown in Fig. 8a, exhibits the hexagonal wurtzite crystal phase of ZnO and the peaks well match with the standard JCPDS card no. 36–1451. The diffraction peaks observed at 2θ values of 31.79°, 34.42°, 36.25°, 47.51°, 56.60°, 62.86°, 67.96°, and 69°corresponds to the reflection from the (100), (002), (101), (110), (103), (112), and (201) lattice planes respectively. Sharp and strong peaks indicate the highly crystalline nature of the material

Fig. 7 **a** UV–VIS absorption spectra of Rose Bengal dye **b** Tauc's plot for direct transition and **c** Tauc's plot for indirect transition

(Costantino et al. 1998; Oh et al. 2002). The XRD pattern for the commercial ZnO nanopowder is shown in Fig. 8b. It can be clearly seen that both the commercial ZnO nanopowder and synthesized ZnO blocking layer showed similar XRD patterns. The XRD pattern of sample with both the blocking and active layer is shown in Fig. 8c. This is very similar to the XRD pattern of the blocking layer. This is because the blocking layer is more crystalline in nature, which is evident from its XRD pattern with its sharper peaks.

3.3 Surface morphology study and energy dispersive spectroscopy of the photoanodes

Scanning electron microscopic (SEM) analysis of the ZnO active layer and the compact blocking layer on the FTO substrate was carried out to study the surface morphology and the particle size of the sample. The SEM images of the ZnO active and blocking layers on the FTO substrate are depicted in Fig. 9. It can be seen from Fig. 9a that the ZnO nanoparticles have a hexagonal structure. Figure 9b and c represent the SEM images of compact blocking layer at low and high magnifications respectively. The diameter of the spin-coated nanoparticles ranges from 150 to 180 nm. Further, the chemical composition and elemental percentage of the compact ZnO film are revealed by the Energy Dispersive X-Ray Spectroscopy (EDS) analysis which is shown in Fig. 9d. Predominating peaks of Zn and O_2 unveil that the synthesized blocking layer contains pure ZnO.

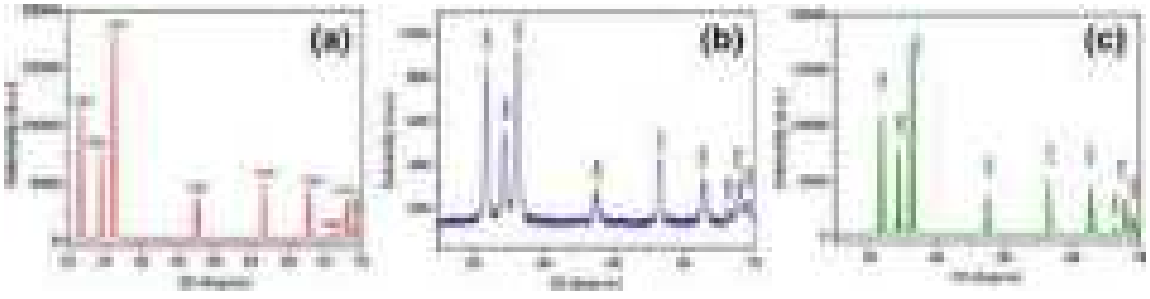

Fig. 8 X-ray diffraction pattern of **a** ZnO compact blocking layer **b** ZnO nanoparticles as active layer **c** ZnO blocking/active layer

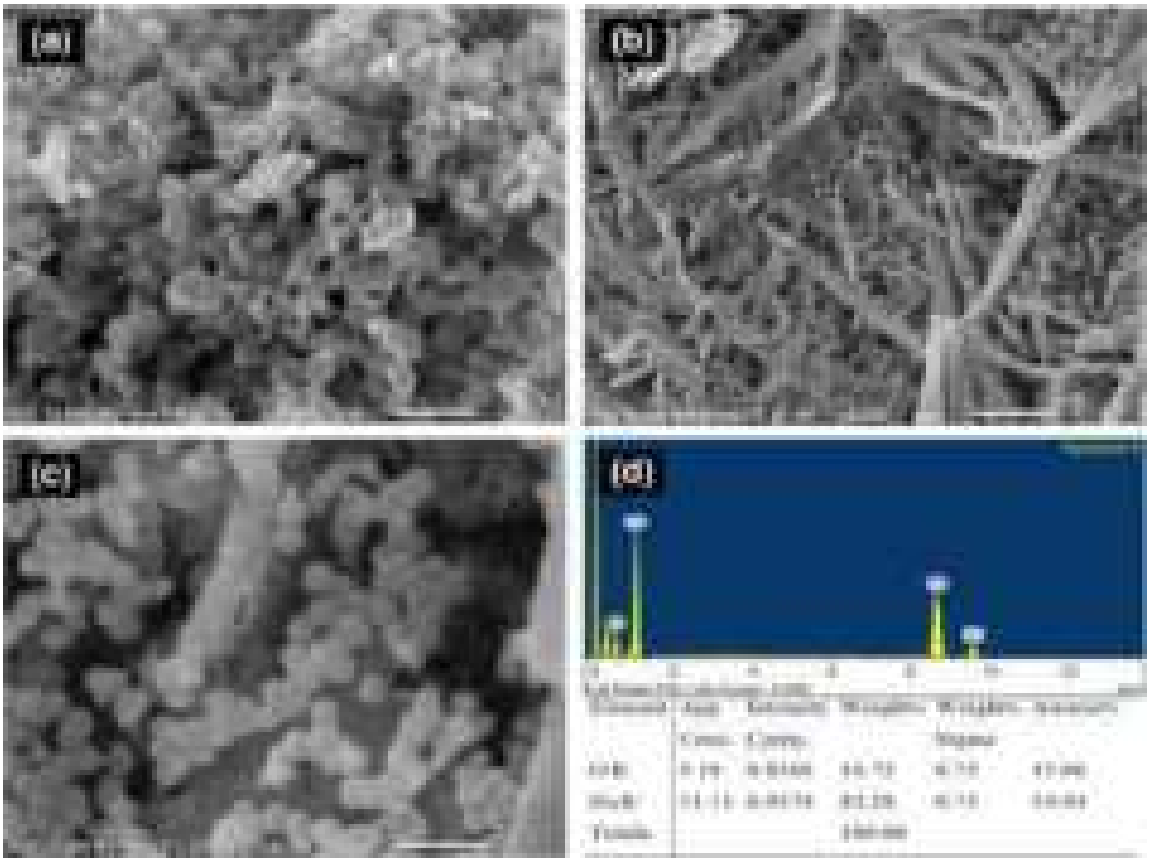

Fig. 9 SEM images of **a** ZnO NP active layer, **b** ZnO blocking layer at lower magnification, **c** ZnO blocking layer at higher magnification and **d** EDS and Elemental composition of ZnO blocking layer

3.4 Photovoltaic characterization of the cells

The Current–Voltage (J–V) characteristic is a crucial measurement that reveals the value of the overall photovoltaic performance of a solar cell along with the key performance parameters like open circuit voltage and short circuit current density. Figure 10a depicts the J–V characteristics of the DSSCs based on different types of photoanodes used in this study and the obtained photovoltaic parameters for each of the cells are summarized in Table 1.

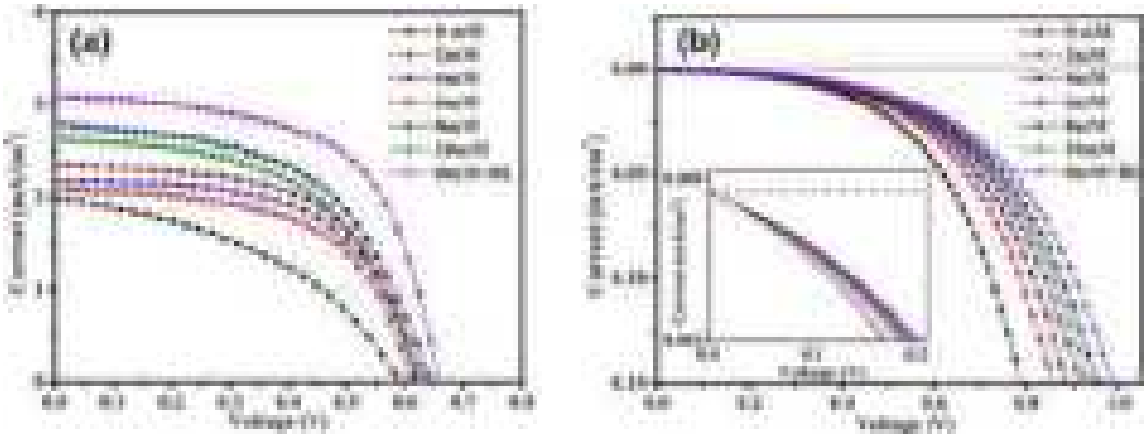

Fig. 10 Current–voltage characteristics of different cells under **a** illumination **b** dark

Table 1 Photovoltaic parameters of DSSCs fabricated with various ZnO photoanodes

Cell name	CDCA concentration	J_{sc} (mA/cm.^{2})	V_{oc}(V)	FF	Efficiency (η %)
DSSC1	0 mM	1.98	0.58	0.43	0.49
DSSC2	2 mM	2.08	0.61	0.58	0.74
DSSC3	4 mM	2.18	0.62	0.60	0.81
DSSC4	6 mM	2.36	0.63	0.58	0.86
DSSC5	8 mM	2.80	0.64	0.56	1.00
DSSC6	10 mM	2.63	0.64	0.54	0.91
DSSC7	8 mM + BL	3.09	0.66	0.60	1.22

3.4.1 Effect of CDCA

The conventionally prepared DSSC with ZnO nanoparticles and Rose Bengal dye displayed a short circuit current density (J_{sc}) of 1.98 mA/cm^2, an open circuit voltage (V_{oc}) of 0.58 V, and a fill factor (FF) of 0.43, resulting in a photoconversion efficiency(η) of 0.49%. However, under the same working conditions, the device performance was found to be highly influenced when CDCA solution was incorporated into the dye solution at various concentrations. From Table 1, it can be noted that the value of V_{oc}, as well as J_{sc}, increases with an increase in the concentration of CDCA. Optimum concentration (8 mM) provides the finest dye attachment to the ZnO surface. The best device performance was achieved for the optimized CDCA concentration of 8 mM when added with 0.5 mM RB dye solution. This improvement in the performance may be attributed to reduced dye aggregation along with uniform dye adsorption yielding better electron injection into the conduction band of ZnO.

3.4.2 Effect of compact ZnO blocking layer

To avoid the direct contact between the FTO and the liquid electrolyte through the pores present in the nanocrystalline ZnO film in a conventionally prepared DSSC, a thin and compact layer of ZnO was employed as shown in Fig. 11. From Table 1 it can be observed that the addition of a compact ZnO blocking layer in DSSC7 with 8 mM CDCA additive shows a remarkable enhancement in J_{sc} (3.09 mA/cm^2) and V_{oc} (0.66 V) and consequently the highest value of photoconversion efficiency η (1.22%) was obtained among all the fabricated cells. Such type of performance enhancement may be accredited to the consolidated effect of improved dye loading due to the addition of CDCA with proper concentration and increased charge collection along with decreased electron recombination at the FTO/ZnO/electrolyte interface hindering the direct contact between FTO and electrolyte by the blocking layer.

3.4.3 Dark current measurement

To explore the effect of CDCA concentration and ZnO blocking layer in the process of electron back transfer, the J-V characteristics were also measured in the dark which is shown in Fig. 10b. It is regarded as a qualitative method to assess the degree of electron back transfer in DSSCs. The dark current generation is known to be partly due to the

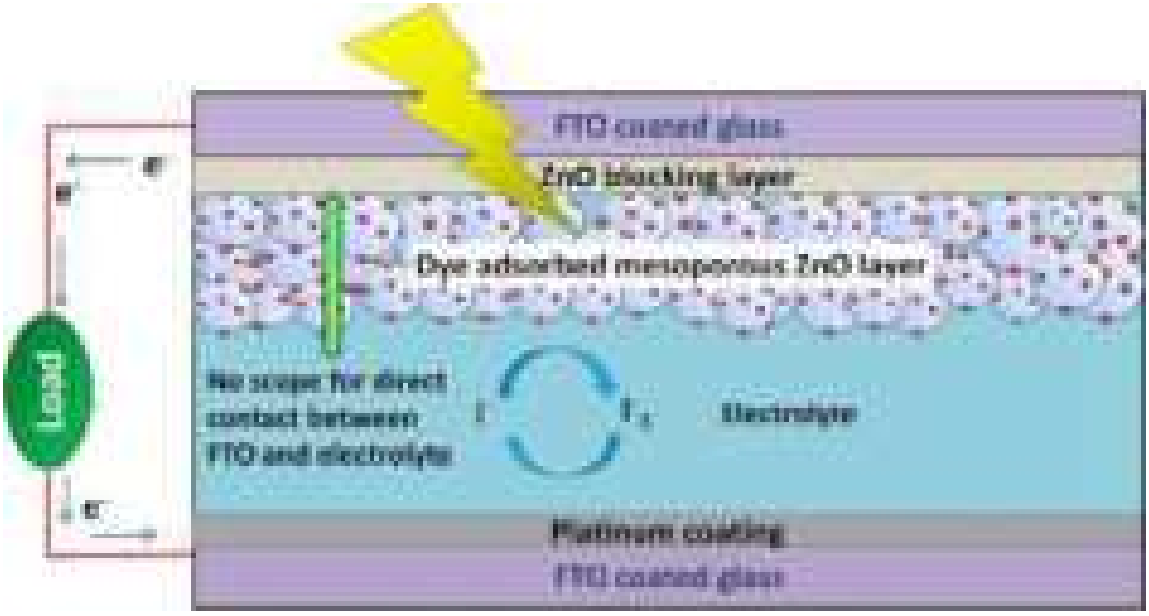

Fig. 11 Schematic diagram of a DSSC with compact ZnO blocking layer

presence of exposed FTO sites having direct contact with the liquid electrolyte and the pores left between the ZnO nanoparticles and the FTO surface (Yang et al. 2014; Yeoh and Chan 2019). These exposed FTO sites and the pores of ZnO nanoparticle film would allow the liquid electrolyte to penetrate through ZnO film and directly come in contact with bare FTO sites resulting in recombination losses as shown in the energy band diagram for conventional ZnO NP based DSSC in Fig. 12a. It can be observed from Fig. 10b that for a particular value of the voltage on the X-axis (i.e. voltage axis) of the dark current characteristics, the corresponding Y-axis value (i.e. value of dark current) is lowest for DSSC7 for that particular voltage. It can also be seen that the dark current has the highest value for conventionally prepared cell (DSSC1) with bare FTO and decreases with an increase in CDCA concentration up to 8 mM. An enlarged plot of the dark current characteristics is provided as an inset in Fig. 10b so that a clear scenario is observed. For the cell (DSSC7) with compact ZnO BL and 8 mM CDCA solution as dye co-adsorbent, the dark current is reduced significantly for the same bias potential in comparison to all other cells. This

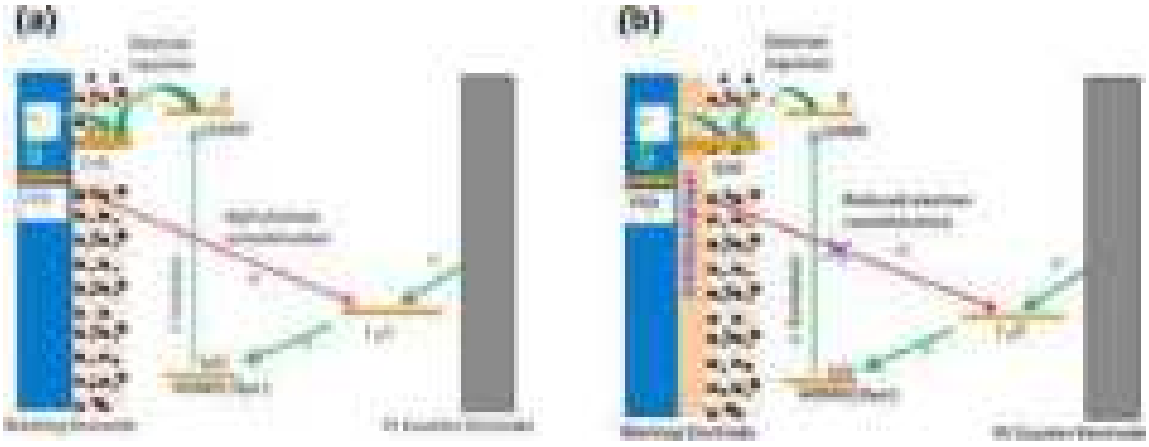

Fig. 12 Schematic diagram showing interfacial charge transfer and recombination in case of DSSCs **a** without ZnO BL **b** with compact ZnO BL

demonstrates that the compact ZnO BL reduces the bare FTO site and thereby successfully suppresses the dark current by lowering the electron back transfer. It was also observed that the DSSC7 has the slowest rate of increase of dark current with an increase in bias voltage confirming excellent suppression of electron recombination and consequently reduced current loss.

The variations of different cell parameters with the concentration of CDCA solution for the fabricated DSSCs are depicted in Fig. 13. It can be observed that CDCA concentration highly influences the value of J_{sc}. ZnO BL improves the current further. A small increase in the values of V_{oc} and FF can also be noted from Fig. 10 due to these processes. The highest values of cell parameters were obtained for the cell DSSC7.

3.5 Electrochemical impedance spectroscopy study

To further gain an insight into the influence of CDCA concentration and the coating of compact ZnO blocking layer on the charge transfer and recombination kinetics of the prepared devices, the DSSCs were further investigated by electrochemical impedance spectroscopic (EIS) measurement in dark under V_{oc} bias voltage with 10 mV AC perturbation amplitude. This gives a more precise understanding of the limiting factors for the cell performance parameters. In the EIS measurement done under the dark condition and with an applied bias voltage, electrons from FTO are injected into the conduction band of ZnO and then transported through the ZnO network. Some of the injected electrons recombine with the I_3^- ion present in the electrolyte giving rise to the recombination phenomenon (Liu et al. 2018). Figure 14a shows the Nyquist plot of all the prepared cells exhibiting two obvious semicircles. The curves are fitted using the equivalent circuit shown in the inset of Fig. 14a and the EIS measurement results obtained in terms of resistances and capacitances are summarized in Table 2. The charge transfer resistance (R_{pt}) and double layer capacitance (C_{pt}) at the Pt counter electrode/electrolyte interface is responsible for the first semicircle in the high-frequency range, while the second semicircle in the mid-frequency range may be assigned to the charge transfer and recombination resistance (R_{rec})

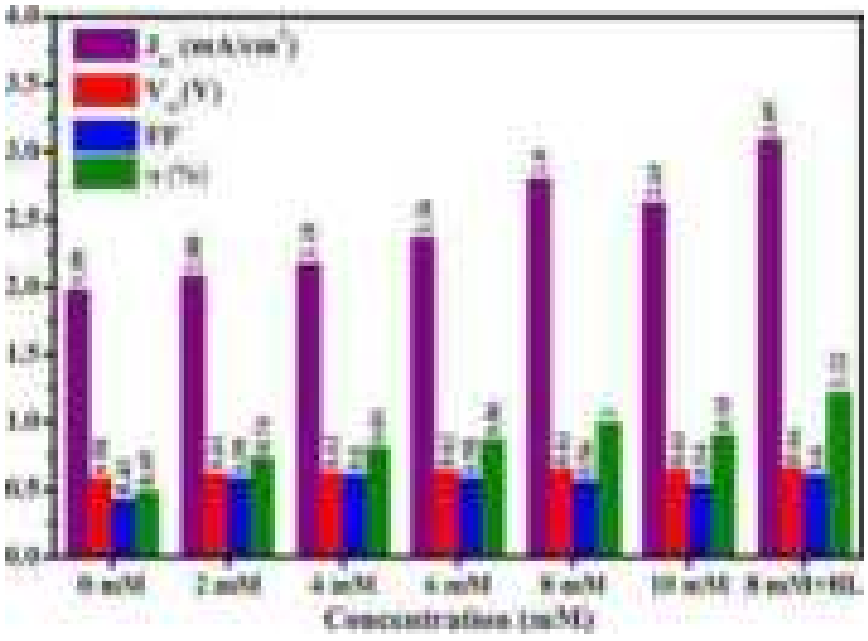

Fig. 13 Effect of CDCA concentration and ZnO blocking layer (BL) on different cell parameters

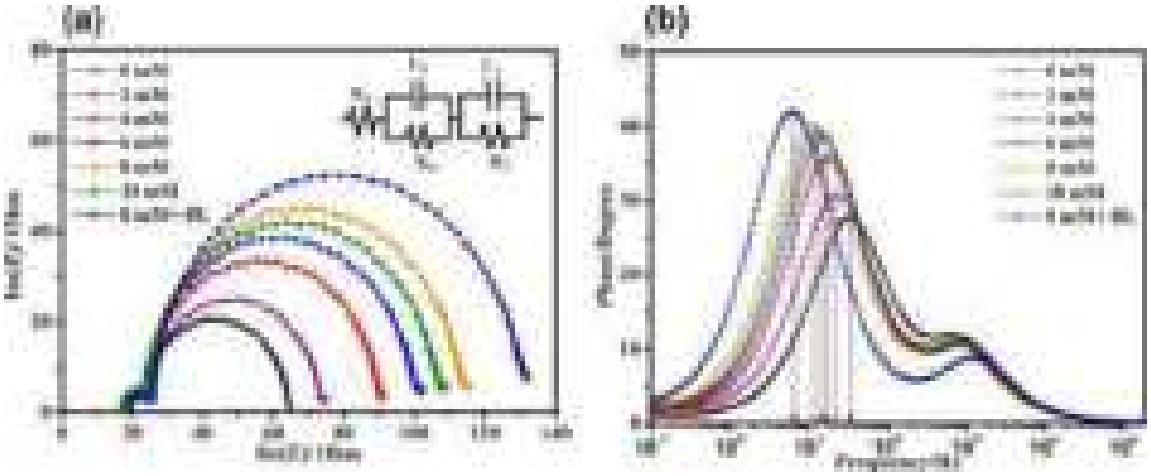

Fig. 14 EIS of the DSSCs representing **a** Nyquist plot along with equivalent circuit (inset) and **b** Bode plot

Table 2 Parameters obtained from EIS measurement

Cell name	CDCA concentration	R_s (Ω)	R_{pt} (Ω)	R_{rec} (Ω)	Peak freq. f(Hz)	Electron lifetime (τ_e) (ms)
DSSC1	0 mM	17.15	6.51	40.2	34.21	4.65
DSSC2	2 mM	17.23	6.55	48.8	22.13	7.19
DSSC3	4 mM	17.05	6.46	65.4	17.05	9.34
DSSC4	6 mM	17.12	6.23	75.2	15.62	10.94
DSSC5	8 mM	17.36	6.65	87.6	11.03	14.45
DSSC6	10 mM	17.29	6.37	81.4	13.13	12.13
DSSC7	8 mM + BL	19.23	6.39	102.7	6.54	24.35

and chemical capacitance (C) at the ZnO/dye/electrolyte interface (Li et al. 2011, Mazloum et al. 2019, Zhao et al. 2017). The intercept at the real axis of the Nyquist plot represents the series resistance (R_s) of FTO and other ohmic contacts like connecting cables, clamps and clips used to connect the cells for measurement. (Ondersma and Hamann 2010; Chou et al. 2019).

The small semicircles in the high-frequency range are almost identical indicating nearly similar values of R_{pt} for all four kinds of cells as all of them have similar Pt counter electrodes and the same electrolyte. On the contrary, a substantial dissimilarity can be observed in large semicircles in the mid-frequency range. This indicates that the charge transport and recombination behaviour at the ZnO/dye/electrolyte interface was extensively affected due to working electrode modification by the addition of CDCA and incorporation of the blocking layer. The middle arc of the Nyquist plot for the conventionally prepared DSSC has the lowest diameter indicating the lowest recombination resistance (R_{rec}) and thus representing the highest recombination process among all the cells. The diameter is evidently larger for the CDCA treated cells indicating its positive role in increasing the recombination resistance and hence lowering the recombination phenomena. It can be observed from Table 2 that the recombination resistance increases in the order of DSSC1 < DSSC2 < DSSC3 < DSSC4 < DSSC6 < DSSC5 < DSSC7 indicating that the recombination resistance increases with an increase in CDCA concentration from 0 to 8 mM and decreases at 10 mM

concentration. The larger R_{rec} value indicates it is more difficult to transfer the injected electrons from the ZnO back to the electrolyte, and thus the back recombination can be suppressed in the cell, thus giving a higher J_{sc} and V_{oc}. The highest value of recombination resistance is obtained when the optimum CDCA concentration (8 mM) is combined with the ZnO blocking layer in DSSC7 leading to the highest J_{sc} and V_{oc} of 3.09 mA/cm^2 and 0.66 V respectively and consequently best device performance. The highest recombination resistance is obtained for the cell with the blocking layer as the blocking layer prevents the injected electrons to come in direct contact with the electrolyte and consequently reduces the direct capture of electrons by the I_3^- ions of the electrolyte. Furthermore, the CDCA addition with optimum concentration and blocking layer increases the number of electrons accumulated in the conduction band of ZnO which led to increased electron density. This creates a small shift of Fermi level for the electrons present in the ZnO. This rise in Fermi level slightly improves V_{oc} which can also be observed from Table 1 (Li et al. 2011; Wei et al. 2015).

Apart from recombination resistance, the second semicircle also provides information about the electron lifetime in the conduction band of ZnO which gives the measure of the rate at which the recombination reaction occurs. This lifetime is inversely proportional to the oscillation frequency at which the peak on the second arc is obtained. But, since, the frequency information is missing in the Nyquist plot; the electron lifetime can be calculated from the phase bode plot using the formula

$$\tau_e = \frac{1}{2\pi f_{peak}} \tag{3}$$

where f_{peak} represents the peak frequency of phase Bode plot in the mid-frequency range as shown in Fig. 14b. A shift in the peaks may be observed in the Bode plots of the DSSCs prepared following different procedures. Shifting of peak frequency towards lower frequency represents longer electron lifetime (τ_e) and slower recombination process. The calculated electron lifetimes for all the cells are summarised in Table 2. The highest electron lifetime of 24.35 ms is obtained for the cell fabricated with 8 mM CDCA concentration along with ZnO compact blocking layer (DSSC 7). The increased electron lifetime due to CDCA and blocking layer effectively enhances the photoconversion efficiency (PCE) which is in good agreement with the results obtained from J-V measurement. The reduced dye aggregation in presence of CDCA and inhibition of electron recombination by the blocking layer may be accounted for this.

4 Conclusion

Effects of co-adsorption of CDCA and ZnO blocking layer were investigated in Rose Bengal dye based DSSCs. The surface, photovoltaic and electrochemical properties of all the cells were extensively studied. The strong binding of CDCA molecules to the ZnO surface partially displaces dye molecules and consequently reduces photon harvesting. Excessive CDCA concentration implies significantly reduced dye attachment to the ZnO surface leading to decreased amount of light energy absorption. Therefore, to maximize the positive effect of the co-adsorbent, it is very crucial to carefully optimize the amount of CDCA. The amount of CDCA has been optimized by adjusting its concentration in the dye solution and found that the best device performance was obtained for 8 mM concentration. At optimized co-adsorbent concentration, the reduced dye loading due to the presence of CDCA

and consequently decreased light-harvesting was compensated by the increased electron injection efficiency leading to maximum device efficiency of 0.97%. The performance was further increased from 1.00 to 1.22% when a compact ZnO blocking layer was added to the FTO before depositing the mesoporous ZnO active layer. This was due to the suppression of electron back transfer from the FTO to the liquid electrolyte. These results indicate that the addition of CDCA as a dye co-adsorbent and the introduction of ZnO blocking layer is an effective way to boost the performance of Rose Bengal dye based DSSCs. The efficiency of the fabricated cells is low as the dye used in this study is rose bengal. Though the efficiency is low here compared to the ruthenium based cells, it lies in the range of efficiency of rose bengal dye based DSSCs obtained by other researchers. Higher efficiencies can be obtained by using high performance ruthenium dye.

Funding The project was funded by the Department of Physics, University of North Bengal.

Data availability Datasets generated during the current study are available and shall be provided on reasonable request.

Declarations

Conflict of interest There is no financial and non-financial conflict of interest in this research work.

Consent for publication All the authors of this manuscript agree with the final version of the manuscript and give their consent for it to be published, accepting all the ethical standards of the Journal of Optical and Quantum Electronics. The authors also certify that this manuscript has not been published elsewhere and that it is not under consideration for publication in any other journal.

References

Aghazada, S., Nazeeruddin, M.K.: Ruthenium complexes as sensitizers in dye-sensitized solar cells. Inorganics **6**(2), 52 (2018). https://doi.org/10.3390/inorganics6020052

Alharbi, F., Bass, J.D., Salhi, A., Alyamani, A., Kim, H.C., Miller, R.D.: Abundant non-toxic materials for thin film solar cells: alternative to conventional materials. Renew. Energy **36**, 2753–2758 (2011). https://doi.org/10.1016/j.renene.2011.03.010

Al-Kahlout, A.: Thermal treatment optimization of ZnO nanoparticles-photoelectrodes for high photovoltaic performance of dye-sensitized solar cells. J. Assoc. Arab Univ. Basic Appl. Sci. **17**(1), 66–72 (2015). https://doi.org/10.1016/j.jaubas.2014.02.004

Bach, W.: Global warming: the complete briefing (2nd ed). John Houghton. Cambridge University Press: Cambridge, 1997. Pp. xv + 251. Paperback: ISBN 0521–62932–2, ??12.95; hardback: ISBN 0–321–62089–9, ??35.00. Int. J. Climatol. (1998). https://doi.org/10.1002/(sici)1097-0088(199804)18:5<579::aid-joc278>3.3.co;2-0

Barbir, F., Veziroğlu, T.N., Plass, H.J.: Environmental damage due to fossil fuels use. Int. J. Hydrogen Energy **15**(10), 739–749 (1990). https://doi.org/10.1016/0360-3199(90)90005-J

Biswas, R., Roy, T., Chatterjee, S.: Study of electro-optical performance and interfacial charge transfer dynamics of dye sensitized solar cells based on ZnO nanostructures and natural dyes. J. Nanoelectron. Optoelectron. **14**(1), 99–108 (2019). https://doi.org/10.1166/jno.2019.2445

Biswas, R., Chatterjee, S.: Effect of surface modification via sol-gel spin coating of ZnO nanoparticles on the performance of WO3 photoanode based dye sensitized solar cells. Optik **212**, 164142 (2020). https://doi.org/10.1016/j.ijleo.2019.164142

Buene, A.F., Almenningen, D.M., Hagfeldt, A., Gautun, O.R., Hoff, B.H.: First report of chenodeoxycholic acid-substituted dyes improving the dye monolayer quality in dye-sensitized solar cells. Sol. RRL **4**(4), 1900569 (2020). https://doi.org/10.1002/solr.201900569

Cai, N., Moon, S.J., Cevey-Ha, L., Moehl, T., Humphry-Baker, R., Wang, P., Zakeeruddin, S.M., Grätzel, M.: An organic D-π-A dye for record efficiency solid-state sensitized heterojunction solar cells. Nano Lett. **11**(4), 1452–1456 (2011). https://doi.org/10.1021/nl104034e

Chiba, Y., Islam, A., Komiya, R., Koide, N., Han, L.: Conversion efficiency of 10.8% by a dye-sensitized solar cell using a TiO2 electrode with high haze. Appl. Phys. Lett. **88**(22), 223505 (2006). https://doi.org/10.1063/1.2208920

Chou, J.C., Lu, C.C., Liao, Y.H., Lai, C.H., Nien, Y.H., Kuo, C.H., Ko, C.C.: Fabrication and electrochemical impedance analysis of dye-sensitized solar cells with titanium dioxide compact layer and graphene oxide dye absorption layer. IEEE Trans. Nanotechnol. **18**, 461–466 (2019). https://doi.org/10.1109/TNANO.2019.2913537

Chung, I., Lee, B., He, J., Chang, R.P.H., Kanatzidis, M.G.: All-solid-state dye-sensitized solar cells with high efficiency. Nature **485**(7399), 486–489 (2012). https://doi.org/10.1038/nature11067

Costantino, U., Marmottini, F., Nocchetti, M., Vivani, R.: New synthetic routes to hydrotalcite-like compounds: characterisation and properties of the obtained materials. Eur. J. Inorg. Chem. **1998**(10), 1439–1446 (1998). https://doi.org/10.1002/(sici)1099-0682(199810)1998:10%3c1439::aid-ejic1439%3e3.0.co;2-1

Duffy, N.W., Peter, L.M., Rajapakse, R.M.G., Wijayantha, K.G.U.: Investigation of the kinetics of the back reaction of electrons with tri-iodide in dye-sensitized nanocrystalline photovoltaic cells. J. Phys. Chem. B **104**(38), 8916–8919 (2000). https://doi.org/10.1021/jp001185z

Elilarassi, R., Chandrasekaran, G.: Effect of annealing on structural and optical properties of zinc oxide films. Mater. Chem. Phys. **121**(1–2), 378–384 (2010). https://doi.org/10.1016/j.matchemphys.2010.01.053

Epp, J.: X-ray diffraction (XRD) techniques for materials characterization. In: Materials characterization using nondestructive evaluation (NDE) methods, pp. 81–124. Elsevier (2016). https://doi.org/10.1016/B978-0-08-100040-3.00004-3

Ghobadi, N.: Band gap determination using absorption spectrum fitting procedure. Int. Nano Lett. **3**(1), 1–4 (2013). https://doi.org/10.1186/2228-5326-3-2

Goetzberger, A., Hebling, C., Schock, H.W.: Photovoltaic materials, history, status and outlook. Mater. Sci. Eng. R. Rep. **40**(1), 1–46 (2003). https://doi.org/10.1016/S0927-796X(02)00092-X

Grätzel, M.: Dye-sensitized solar cells. J. Photochem. Photobiol. C Photochem. Rev. **4**(2), 145–153 (2003). https://doi.org/10.1016/S1389-5567(03)00026-1

Grätzel, M.: Solar energy conversion by dye-sensitized photovoltaic cells. Inorg. Chem. **44**(20), 6841–6851 (2005). https://doi.org/10.1021/ic0508371

Guillén, E., Peter, L.M., Anta, J.A.: Electron transport and recombination in ZnO-based dye-sensitized solar cells. J. Phys. Chem. C. **115**(45), 22622–22632 (2011). https://doi.org/10.1021/jp206698t

Henson, Z.B., Zhang, Y., Nguyen, T.Q., Seo, J.H., Bazan, G.C.: Synthesis and properties of two cationic narrow band gap conjugated polyelectrolytes. J. Am. Chem. Soc. **135**(11), 4163–4166 (2013). https://doi.org/10.1021/ja400140d

Hosenuzzaman, M., Rahim, N.A., Selvaraj, J., Hasanuzzaman, M., Malek, A.B.M.A., Nahar, A.: Global prospects, progress, policies, and environmental impact of solar photovoltaic power generation. Renew. Sustain. Energy Rev. **41**, 284–297 (2015). https://doi.org/10.1016/j.rser.2014.08.046

Inoue, T., Pandey, S.S., Fujikawa, N., Yamaguchi, Y., Hayase, S.: Synthesis and characterization of squaric acid based NIR dyes for their application towards dye-sensitized solar cells. J. Photochem. Photobiol. A **213**(1), 23–29 (2010). https://doi.org/10.1016/j.jphotochem.2010.04.015

Ismail, M., Ahmad Ludin, N., Hisham Hamid, N., Adib Ibrahim, M., Sopian, K.: The Effect of Chenodeoxycholic Acid (CDCA) in Mangosteen (Garcinia mangostana) Pericarps Sensitizer for Dye-Sensitized Solar Cell (DSSC). In: Journal of Physics: Conference Series. Vol. 1083, No. 1, p. 012018 (2018). doi :https://doi.org/10.1088/1742-6596/1083/1/012018

Ito, S., Nazeeruddin, M.K., Liska, P., Comte, P., Charvet, R., Péchy, P., Jirousek, M., Kay, A., Zakeeruddin, S.M., Grätzel, M.: Photovoltaic characterization of dye-sensitized solar cells: effect of device masking on conversion efficiency. Prog. Photovolt. Res. Appl. **14**(7), 589–601 (2006). https://doi.org/10.1002/pip.683

Kim, H., Veerappan, G., Park, J.H.: Conducting polymer coated non-woven graphite fiber film for dye-sensitized solar cells: superior Pt-and FTO-free counter electrodes. Electrochim. Acta **137**, 164–168 (2014). https://doi.org/10.1016/j.electacta.2014.06.012

Kumar, V., Gupta, R., Bansal, A.: Role of chenodeoxycholic acid as co-additive in improving the efficiency of DSSCs. Sol. Energy **196**, 589–596 (2020). https://doi.org/10.1016/j.solener.2019.12.034

Lee, T.D., Ebong, A.U.: A review of thin film solar cell technologies and challenges. Renew. Sustain. Energy Rev. **70**, 1286–1297 (2017). https://doi.org/10.1016/j.rser.2016.12.028

Lee, K.M., Suryanarayanan, V., Ho, K.C., Thomas, K.J., Lin, J.T.: Effects of co-adsorbate and additive on the performance of dye-sensitized solar cells: A photophysical study. Sol. Energy Mater. Sol. Cells **91**(15–16), 1426–1431 (2007). https://doi.org/10.1016/j.solmat.2007.03.009

Li, J., Wu, W., Yang, J., Tang, J., Long, Y., Hua, J.: Effect of chenodeoxycholic acid (CDCA) additive on phenothiazine dyes sensitized photovoltaic performance. Sci. China Chem. **54**(4), 699–706 (2011). https://doi.org/10.1007/s11426-011-4227-9

Liu, X., Zhang, Q., Li, J., Valanoor, N., Tang, X., Cao, G.: Increase of power conversion efficiency in dye-sensitized solar cells through ferroelectric substrate induced charge transport enhancement. Sci. Rep. **8**(1), 1–8 (2018). https://doi.org/10.1038/s41598-018-35764-y

Lu, H.P., Tsai, C.Y., Yen, W.N., Hsieh, C.P., Lee, C.W., Yeh, C.Y., Diau, E.W.G.: Control of dye aggregation and electron injection for highly efficient porphyrin sensitizers adsorbed on semiconductor films with varying ratios of coadsorbate. J. Phys. Chem. C **113**(49), 20990–20997 (2009). https://doi.org/10.1021/jp908100v

Mazloum-Ardakani, M., Arazi, R.: Improving the effective photovoltaic performance in dye-sensitized solar cells using an azobenzenecarboxylic acid-based system. Heliyon **5**(3), e01444 (2019). https://doi.org/10.1016/j.heliyon.2019.e01444

Meadows, D.H., Meadows, D.L., Randers, J., Behrens, W.: The Limits to Growth - Club of Rome. (1972). http://www.donellameadows.org/wp-content/userfiles/Limits-to-Growth-digital-scan-version.pdf

Nazeeruddin, M.K., Baranoff, E., Grätzel, M.: Dye-sensitized solar cells: a brief overview. Sol. Energy **85**(6), 1172–1178 (2011). https://doi.org/10.1016/j.solener.2011.01.018

Nguyen, W.H., Bailie, C.D., Burschka, J., Moehl, T., Grätzel, M., McGehee, M.D., Sellinger, A.: Molecular engineering of organic dyes for improved recombination lifetime in solid-state dye-sensitized solar cells. Chem. Mater. **25**(9), 1519–1525 (2013). https://doi.org/10.1021/cm3036357

O'Regan, B., Grätzel, M.: A low-cost, high-efficiency solar cell based on dye-sensitized colloidal TiO_2 films. Nature **353**(6346), 737–740 (1991). https://doi.org/10.1038/353737a0

Oh, J.M.: The effect of synthetic conditions on tailoring the size of hydrotalcite particles. Solid State Ionics **151**(1–4), 285–291 (2002). https://doi.org/10.1016/S0167-2738(02)00725-7

Ondersma, J.W., Hamann, T.W.: Impedance investigation of dye-sensitized solar cells employing outer-sphere redox shuttles. J. Phys. Chem. C. **114**(1), 638–645 (2010). https://doi.org/10.1021/jp908442p

Pandey, P., Parra, M.R., Haque, F.Z., Kurchania, R.: Effects of annealing temperature optimization on the efficiency of ZnO nanoparticles photoanode based dye sensitized solar cells. J. Mater. Sci. Mater. Electron. **28**(2), 1537–1545 (2017). https://doi.org/10.1007/s10854-016-5693-9

Patni, N., Pillai, S.G., Sharma, P.: Effect of using betalain, anthocyanin and chlorophyll dyes together as a sensitizer on enhancing the efficiency of dye-sensitized solar cell. Int. J. Energy Res. **44**(13), 10846–10859 (2020). https://doi.org/10.1002/er.5752

Patwari, J., Sardar, S., Liu, B., Lemmens, P., Pal, S.K.: Three-in-one approach towards efficient organic dye-sensitized solar cells: aggregation suppression, panchromatic absorption and resonance energy transfer. Beilstein J. Nanotechnol. **8**(1), 1705–1713 (2017). https://doi.org/10.3762/bjnano.8.171

Pradhan, B., Batabyal, S.K., Pal, A.J.: Vertically aligned ZnO nanowire arrays in Rose Bengal-based dye-sensitized solar cells. Sol. Energy Mater. Sol. Cells **91**(9), 769–773 (2007). https://doi.org/10.1016/j.solmat.2007.01.006

Prima, E.C., Al Qibtiya, M., Yuliarto, B., Dipojono, H.K.: Influence of anthocyanin co-pigment on electron transport and performance in black rice dye-sensitized solar cell. Ionics **22**(9), 1687–1697 (2016). https://doi.org/10.1007/s11581-016-1673-6

Quintana, M., Edvinsson, T., Hagfeldt, A., Boschloo, G.: Comparison of dye-sensitized ZnO and TiO_2 solar cells: studies of charge transport and carrier lifetime. J. Phys. Chem. C. **111**(2), 1035–1041 (2007). https://doi.org/10.1021/jp065948f

Rani, S., Shishodia, P.K., Mehra, R.M.: Enhancement of photovoltaic performance of quasi-solid state dye sensitized solar cell with dispersion of a hole conducting agent. Mater. Sci. Pol. **28**(1), 281 (2010)

Rocha, F.S., Gomes, A.J., Lunardi, C.N., Kaliaguine, S., Patience, G.S.: Experimental methods in chemical engineering: ultraviolet visible spectroscopy: UV–Vis. Can. J. Chem. Eng. **96**(12), 2512–2517 (2018). https://doi.org/10.1002/cjce.23344

Sayyed, S.A., Beedri, N.I., Kadam, V.S., Pathan, H.M.: Rose Bengal sensitized bilayered photoanode of nano-crystalline TiO_2–CeO_2 for dye-sensitized solar cell application. Appl. Nanosci. **6**(6), 875–881 (2016). https://doi.org/10.1007/s13204-015-0495-6

Sayyed, A.R.S.A., Beedri, N.I., Kadam, V.S., Pathan, H.M.: Rose bengal-sensitized nanocrystalline ceria photoanode for dye-sensitized solar cell application. Bull. Mater. Sci. **39**(6), 1381–1387 (2016). https://doi.org/10.1007/s12034-016-1279-7

Seo, D.K., Hoffmann, R.: Direct and indirect band gap types in one-dimensional conjugated or stacked organic materials. Theoret. Chem. Acc. **102**(1), 23–32 (1999). https://doi.org/10.1007/s002140050469

Shamsuddin, L., Noor, I.M., Albinsson, I., Mellander, B.E., Arof, A.K.: Perovskite solar cells using polymer electrolytes. Mol. Cryst. Liq. Cryst. **655**(1), 181–194 (2017). https://doi.org/10.1080/15421406.2017.1362889

Shao, F., Sun, J., Gao, L., Yang, S., Luo, J.: Growth of various TiO_2 nanostructures for dye-sensitized solar cells. J. Phys. Chem. C. **115**(5), 1819–1823 (2011). https://doi.org/10.1021/jp110743m

Shivaraj, B.W., Murthy, H.N.N., Krishna, M., Satyanarayana, B.S.: Effect of annealing temperature on structural and optical properties of dip and spin coated zno thin films. Procedia Mater. Sci. **10**, 292–300 (2015). https://doi.org/10.1016/j.mspro.2015.06.053

Singh, S.P., Roy, M.S., Thomas, K.J., Balaiah, S., Bhanuprakash, K., Sharma, G.D.: New triphenylamine-based organic dyes with different numbers of anchoring groups for dye-sensitized solar cells. J. Phys. Chem. C **116**(9), 5941–5950 (2012). https://doi.org/10.1021/jp210971u

Tiwana, P., Docampo, P., Johnston, M.B., Snaith, H.J., Herz, L.M.: Electron mobility and injection dynamics in mesoporous ZnO, SnO_2, and TiO_2 films used in dye-sensitized solar cells. ACS Nano **5**(6), 5158–5166 (2011). https://doi.org/10.1021/nn201243y

Uyanga, K.A., Ezike, S.C., Onyedika, A.T., Kareem, A.B., Chiroma, T.M.: Effect of acetic acid concentration on optical properties of lead acetate based methylammonium lead iodide perovskite thin film. Opt. Mater. **109**, 110456 (2020). https://doi.org/10.1016/j.optmat.2020.110456

Vittal, R., Ho, K.C.: Zinc oxide based dye-sensitized solar cells: a review. Renew. Sustain. Energy Rev. **70**, 920–935 (2017). https://doi.org/10.1016/j.rser.2016.11.273

Wei, L., Yang, Y., Zhu, Z., Fan, R., Wang, P., Dong, Y., Chen, S.: Effect of different donor groups in bis(6-methoxylpyridin-2-yl) substituted co-sensitizer on the performance of N719 sensitized solar cells. RSC Adv. **5**(117), 96934–96944 (2015). https://doi.org/10.1039/c5ra19417b

Wong, K.K., Ng, A., Chen, X.Y., Ng, Y.H., Leung, Y.H., Ho, K.H., Djurišić, A.B., Ng, A.M.C., Chan, W.K., Yu, L., Phillips, D.L.: Effect of ZnO nanoparticle properties on dye-sensitized solar cell performance. ACS Appl. Mater. Interfaces. **4**(3), 1254–1261 (2012). https://doi.org/10.1021/am201424d

Yamamoto, K., Yoshimi, M., Tawada, Y., Okamoto, Y., Nakajima, A.: Cost effective and high-performance thin film Si solar cell towards the 21st century. Sol. Energy Mater. Sol. Cells. **66**, 117–125 (2001). https://doi.org/10.1016/S0927-0248(00)00164-1

Yang, Y., Peng, X., Chen, S., Lin, L., Zhang, B., Feng, Y.: Performance improvement of dye-sensitized solar cells by introducing a hierarchical compact layer involving ZnO and TiO_2 blocking films. Ceram. Int. **40**(9), 15199–15206 (2014). https://doi.org/10.1016/j.ceramint.2014.07.001

Yeoh, M.E., Chan, K.Y.: Efficiency enhancement in dye-sensitized solar cells with ZnO and TiO_2 blocking layers. J. Electron. Mater. **48**(7), 4342–4350 (2019). https://doi.org/10.1007/s11664-019-07207-5

Yum, J.H., Jang, S.R., Humphry-Baker, R., Grätzel, M., Cid, J.J., Torres, T., Nazeeruddin, M.K.: Effect of coadsorbent on the photovoltaic performance of zinc pthalocyanine-sensitized solar cells. Langmuir **24**(10), 5636–5640 (2008). https://doi.org/10.1021/la800087q

Zhang, L., Cole, J.M.: Dye aggregation in dye-sensitized solar cells. J. Mater. Chem. A. **5**(37), 19541–19559 (2017). https://doi.org/10.1039/c7ta05632j

Zhang, L.Z., Tang, G.Q.: Preparation, characterization and optical properties of nanostructured ZnO thin films. Opt. Mater. **27**(2), 217–220 (2004). https://doi.org/10.1016/j.optmat.2004.03.002

Zhang, Q., Dandeneau, C.S., Zhou, X., Cao, C.: ZnO nanostructures for dye-sensitized solar cells. Adv. Mater. **21**(41), 4087–4108 (2009). https://doi.org/10.1002/adma.200803827

Zhao, Y., Lu, F., Zhang, J., Dong, Y., Zhang, B., Feng, Y.: Stepwise co-sensitization of two metal-based sensitizers: probing their competitive adsorption for improving the photovoltaic performance of dye-sensitized solar cells. RSC Adv. **7**(17), 10494–10502 (2017). https://doi.org/10.1039/C6RA28473F

Optik - International Journal for Light and Electron Optics 212 (2020) 164142

Contents lists available at ScienceDirect

Optik

journal homepage: www.elsevier.com/locate/ijleo

Original research article

Effect of surface modification via sol-gel spin coating of ZnO nanoparticles on the performance of WO_3 photoanode based dye sensitized solar cells

Rajat Biswas, Suman Chatterjee*

Department of Physics, University of North Bengal, Raja Rammohunpur, Darjeeling, Siliguri 734013, India

ARTICLE INFO

Keywords:
DSSC
Surface modification
WO_3 nanoparticle
Alternate photoanode
Electron back recombination

ABSTRACT

In this paper, we have reported the improvement of electro-optical performance of dye sensitized solar cells based on highly porous WO_3 nanoparticles as photoanode by an ultrathin coating of ZnO nanoparticles with varying precursor solution concentration over WO_3 surface and the results were compared with the performance of a Dye Sensitized Solar Cell (DSSC) fabricated with bare WO_3 photoanode. The semiconducting material WO_3 was chosen in search of a photoanode material for DSSC alternative to TiO_2. But the performance of pure WO_3 based DSSC was found to be extremely poor in spite of having several advantageous properties. To improve the photovoltaic performance, we have coated the WO_3 surface with varying concentrations of the ZnO precursor solution. It was observed that the concentration of the precursor solution of ZnO highly controls the performance of the DSSC. From the electrochemical measurements, it was found that the bare WO_3 cell suffers high electron recombination. But the coating of an ultrathin layer of ZnO over the WO_3 surface introduces an energy barrier and reduces the electron recombination and thereby enhances the cell performance. The solar cell energy conversion efficiency was found to be highest for 5 mM ZnO precursor solution concentration and it decreases with the increase in concentration further and becomes very low at a concentration of 25 mM. This may be attributed to the poor dye adsorption on the WO_3 surface due to complete screening by the thicker ZnO layer.

1. Introduction

Increasing energy demand and environmental contamination are the two major problems faced by the society in recent years. The major energy requirements of the world are fulfilled by fossil fuels (i.e., coal, petroleum and natural gas), which may not be sufficient to overcome the energy crisis in the future due to fast depletion, the rapid development of industrialization and environmental pollution [1–4]. To address these issues, scientists have focused on renewable and environment-friendly energy sources. As Sun represents an immense source of renewable energy, expected to provide an appreciable amount of power in the future, it is the most widespread type of alternative energy source among all the renewable energy sources [5–7]. Dye-sensitized solar cells, an unconventional photoelectrochemical device that directly converts photo-energy into electrical energy, have drawn much more attention than conventional silicon solar cells due to their easy fabrication technique, the low-level requirement of the high-temperature process, cost-effectiveness and environment-friendly nature [8,9]. But until now, DSSCs are not commercially viable as the reason for their comparatively low conversion efficiency and stability issues compared to the silicon-based solar cells [10].

* Corresponding author.
E-mail addresses: rajat_biswas@nbu.ac.in (R. Biswas), suman_chatterjee@hotmail.com (S. Chatterjee).

https://doi.org/10.1016/j.ijleo.2019.164142
Received 27 November 2019; Accepted 27 December 2019

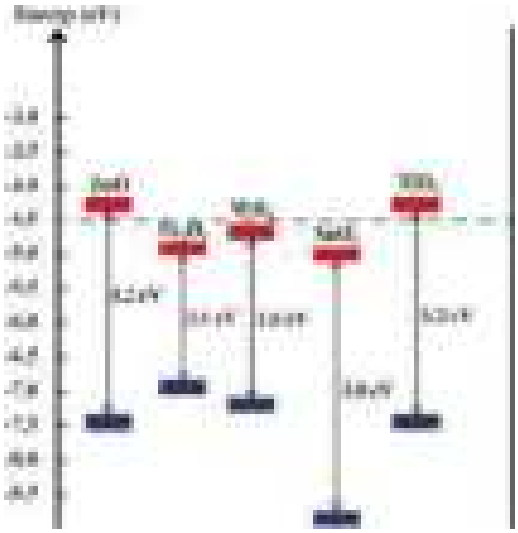

Fig. 1. Band positions of several semiconductors.

Photo anode, the heart of a DSSC system plays a key role in enhancing the overall performance of the DSSC by transferring electrons and supporting the Dye molecules [11]. It consists of a nanostructured mesoporous semiconductor film deposited on a conducting glass or a flexible substrate [12,13]. An ideal photoanode material should have some properties of high charge carrier mobility, significantly high surface areas, environmental friendliness, cost-effectiveness, and comparatively less electron-hole recombination rate. The band edge positions and corresponding band gap values of several commonly used wide bandgap metal oxide semiconductors are shown in Fig. 1 [14,15]. The semiconducting oxide material TiO_2 is mostly used as a photoanode because of its excellent optical, electrical and chemical properties [16–19]. Although appreciably high conversion efficiency is achieved with TiO_2, its low electron mobility leads many scientists to think about new alternative photoanode materials for better performance of Dye sensitized solar cells [20]. On the other hand, WO_3, a wide bandgap semiconductor having bandgap in the range of 2.6 eV–3.1 eV has been used extensively in the fabrication of gas sensors, water splitting and photocatalyst [21]. Owing to the favorable bandgap, high electron mobility and extreme stability in harsh environments, it has attracted the attention of researchers as an alternative photoanode material for DSSC fabrication. Moreover, the nonreactive nature of WO_3 in acidic environments may provide the solution of long-term stability issues in DSSCs with more acidic electrolytes. However, DSSCs based on pure WO_3 photoanode have been proven to be inefficient. On the other hand, DSSCs based on surface modified WO_3 photoanode by ultrathin layer of TiO_2 exhibited significant increase in power conversion efficiency [22]. ZnO can be used as a substitute for TiO_2 due to its agreeable properties in the view of high electron mobility and abundant nanostructure morphologies [23–25]. To the best of our knowledge, however, there are no detailed reports found in which surface modification of WO_3 is done by an ultrathin layer of ZnO in the fabrication of DSSCs. In this work, we have prepared the WO_3 photoanode and a facile sol-gel spin coating technique was utilized to alter the surface property of it by a thin layer of ZnO. Very careful control of the thickness of the ZnO layer is necessary to get the optimum performance out of the solar cell and for this purpose different concentration of ZnO precursor solution was used.

2. Materials and method

2.1. Preparation of working electrodes

All the reagents used in the fabrication process were of analytical grades. So no further purification was required. To prepare the thin films of the photoanode materials, the ITO coated glass substrates were first cleaned with dilute HCl in an ultrasonic bath for 15 min and then thoroughly rinsed with deionized water to remove the HCL residues. Then the substrates were cleaned with acetone and ethanol using an ultrasonic cleaning bath [26].

The working electrode of the DSSC was prepared by following the standard doctor blade method. The WO_3 paste for doctor blading was prepared by mixing WO_3 nanopowder with terpineol as solvent and ethyl cellulose as a binder and stirred continuously in order to obtain a smooth lump-free slurry. The WO_3 paste was then coated on the conductive side of the cleaned ITO glass substrate and subsequently annealed at 500 °C for 2 h in order to burn out the terpineol and ethyl cellulose contents of the working electrode

and strengthens the bonding between the substrate and the WO_3 film. In addition to this, the annealing procedure also helps to improve the surface quality of the thin film along with increasing the crystallinity of the sample [22].

The Sol-Gel spin-coating technique was employed to deposit thin layers of ZnO onto the surface of the as-prepared WO_3 photoanode. Zinc acetate dihydrate $(CH_3COO)_2 Zn, 2H_2O$, (98 % Merck) was mixed with acetone at different molar ratios to obtain desired concentrations of ZnO precursor solution. The prepared solutions were then mixed extensively in an ultrasonic bath for 2 h and then spin-coated on the WO_3 coated substrate using a programmable spin coater (Apex Instruments Co. Pvt. Ltd, Model SpinNXG-P1) at 2000 rpm for 30 s. The thickness of the ZnO film can be controlled by varying the precursor solution concentration. In our experiment we have prepared 1 mM, 5 mM, 10 mM, 15 mM, 20 mM, and 25 mM solutions of ZnO precursor and spin-coated them over WO_3 film keeping the number of sol drops unchanged in order to obtain various ZnO film thickness and study the effect on the solar cell performance. The ZnO coated WO_3 electrode was annealed at 450 °C for 1 h. All the electrodes were sensitized by immersing them in a 0.3 mM ethanolic solution of Ruthenium based dye ($C_{26}H_{20}O_{10}N_6S_2Ru$) known as N_3 (Solaronix) for 48 h. The working electrodes were then removed from the solution and thoroughly rinsed with deionized water and ethanol to remove any excess dye from the semiconductor film surface and air-dried at room temperature.

The counter electrodes of the cells were prepared by spin coating the platinum catalyst precursor solution Platisol-T (Solaronix) on the conducting side of the cleaned ITO coated glasses and heating on a hot plate at 450 °C for 15 min.

The dye adsorbed working electrode and Pt- coated counter electrode was assembled against the coated sides of each other in a sandwich manner using two binder clips with a Surlyn film (Meltonix 1170−25 μm, Solaronix) gasket as a spacer in between them. The liquid electrolyte used in our experiment was a Solaronix high-performance electrolyte (Iodolyte AN50) with iodide/tri-iodide as redox couple, ionic liquid, lithium salt and pyridine derivative as additives dissolved in acetonitrile solvent. The redox concentration of the electrolyte was 50 mM. The active area of the cells for illumination was determined by employing a black mask of aperture size 0.25 cm^2.

2.2. Characterization and measurements

The crystalline structure of the WO_3 and ZnO were analyzed with the help of X-ray diffraction analysis using the PAN-analytical X'Pert PRO X-ray diffractometer (CuKα radiation, 30 mA, 40 kV, λ = 1.5406 Å). Scanning electron microscopy (JEOL) was done to reveal the surface morphology of the prepared thin films. More detailed structural information of the samples was obtained from Raman Spectroscopy. The Photocurrent-Voltage (I–V) characteristics data of the cells were recorded using Keithley 2400 digital source meter with the help of a computer under 100 mW/cm^2 illumination (Xenon lamp 450 W). HIOKI Impedance Analyzer in the frequency range of 0.1 Hz to 190 kHz was used to study the electrochemical impedance spectra of the cells.

3. Results and discussion

3.1. Structural and phase characterization WO_3 of the photoanode

Fig. 2 shows the X-ray diffraction pattern of the as-purchased WO_3 nanopowder. The XRD pattern exhibits the coexistence of both the monoclinic and orthorhombic crystal phases. The peaks corresponding to the monoclinic phase well matches with the standard JCPDS card no. 43-1035 and the orthorhombic phase matches with JCPDS card no. 20-1324. Sharp and strong peaks signify the high crystalline nature of the sample [27,28].

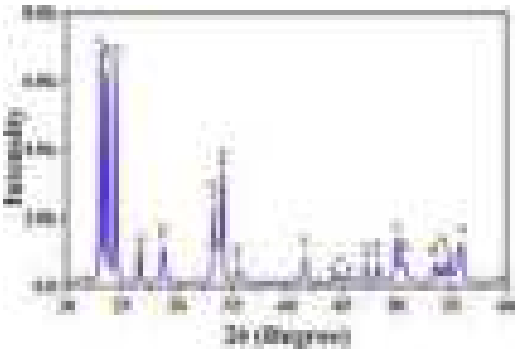

Fig. 2. X-ray diffraction pattern of WO_3 nanoparticles. The peaks correspond to Monoclinic (*) and orthorhombic (■) phases of WO_3 respectively.

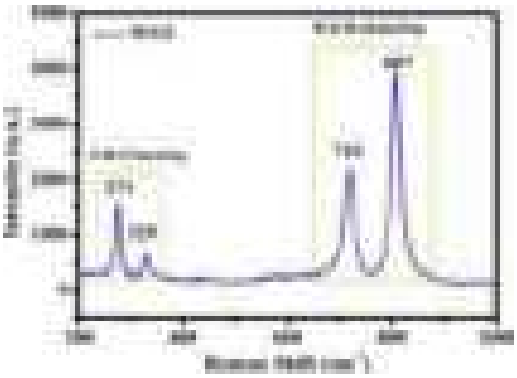

Fig. 3. Raman spectra of WO_3 nanoparticle.

The crystal phases are further confirmed by Raman spectra of the pure WO_3 powder, which is shown in Fig. 3 and it consists of well-resolved four sharp Raman peaks at 274, 329, 719 and 807 cm^{-1}. The lower peaks centered at 274 cm^{-1} and 329 cm^{-1} attributed to OWO−− bending vibrations and the higher peaks at 719 cm^{-1} and 807 cm^{-1} are due to WOW−− stretching mode vibration [29]. Sharp peaks suggest profoundly crystalline nature of the sample. All four Raman peaks attribute to the monoclinic phase [30]. However, the Raman peaks corresponding to the orthorhombic phase lie neighboring to the peaks mentioned above. Consequently, both phases are believed to be present in the sample. No impurity was found in the Raman spectra of the pure WO_3 sample.

3.2. Surface Morphology study and energy dispersive spectroscopy of the photoanodes

Scanning Electron Microscopy was employed to investigate the surface morphology of the pure and ZnO coated WO_3 photoanodes. Fig. 4(a) shows the SEM image of pure WO_3 photoanode on the FTO substrate whereas Fig. 4(b–g) show the SEM images of WO_3 photoanodes coated with 1 mM, 5 mM, 10 mM, 15 mM, 20 mM and 25 mM concentrations of ZnO precursor solution concentrations respectively. Highly porous films with nearly spherical shape WO_3 nanoparticle having a diameter in the range of 140 nm–150 nm can be clearly seen from the SEM images. High porosity the film enhances the surface to volume ratio, consequently increasing the dye loading amount resulting in high photocurrent [31–34]. It can also be observed from the SEM images that the surface morphology of uncoated and ZnO coated WO_3 substrate are not so visually different for low ZnO precursor concentrations, but for higher concentrations like 20 mM and 25 mM, the screening of WO_3 surface by ZnO nanoparticles may be evidently observed in Fig. 4(f) and 4 (g).

The EDS spectrum, which reveals the elementary analysis are shown in Fig. 4(h) and (i) for bare WO_3 and the WO_3 surface coated with 5 mM ZnO precursor solution concentration respectively. Predominating peaks of W and O_2 in Fig. 4(h) unveil that the sample contains only WO_3 whereas in Fig. 4(i) additional strong peak of Zn confirms the presence of ZnO coating over WO_3.

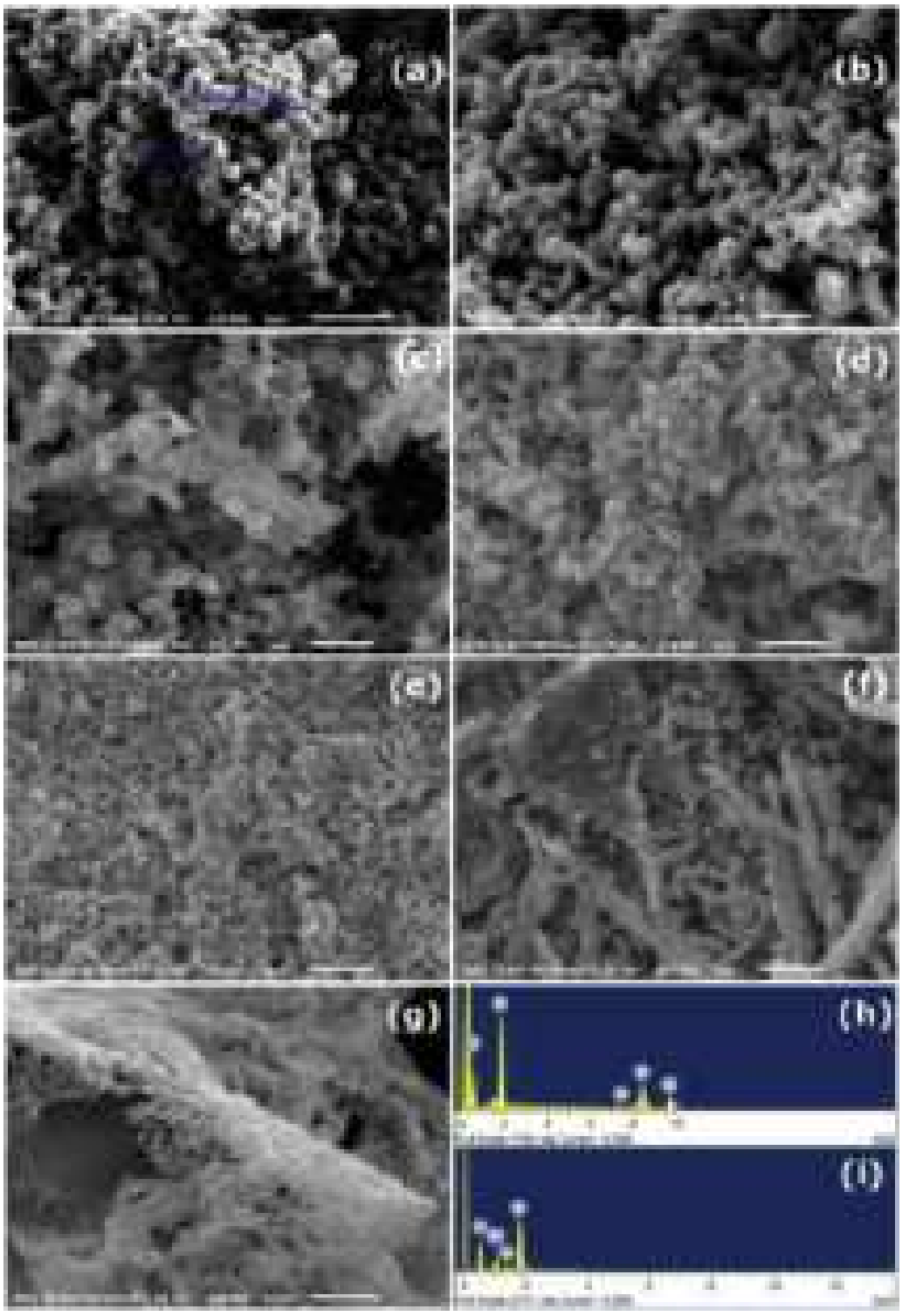

Fig. 4. SEM images of (a) Bare WO_3 photoelectrode; photoelectrodes having WO_3 coated with (b) 1 mM (c) 5 mM (d) 10 mM (e) 15 mM (f) 20 mM and (g) 25 mM ZnO precursor solution respectively. (h) EDS of Bare WO_3 and (i) EDS of WO_3 coated with 5 mM ZnO.

3.3. Photovoltaic (Current-Voltage) characterization of the cells

The Current-Voltage characteristic is a crucial characterization to investigate the overall photovoltaic performance of a solar cell. Fig. 5(a) illustrates the I–V characteristics of the seven DSSCs based on pure and coated WO_3 as photoanodes with different precursor solution concentrations. The overall photoconversion efficiency of the solar cell is given by

$$\eta = \frac{P_{out}}{P_{in}} = \frac{I_{sc} V_{oc} FF}{P_{in}} \quad (1)$$

Where V_{oc}, I_{sc}, P_{in}, and FF represent open-circuit voltage, the short circuit current density, Fill factor and incident light power respectively. The fill factor is calculated by the formula

$$FF = \frac{I_{max} V_{max}}{I_{sc} V_{oc}} \quad (2)$$

Where V_{max} and I_{max} are the voltage and current corresponding to the maximum output power point of the solar cell respectively. The photovoltaic parameters like Short circuit current density, Open circuit voltage, Fill factor and the efficiency obtained from the I–V curve are summarized in Table 1.

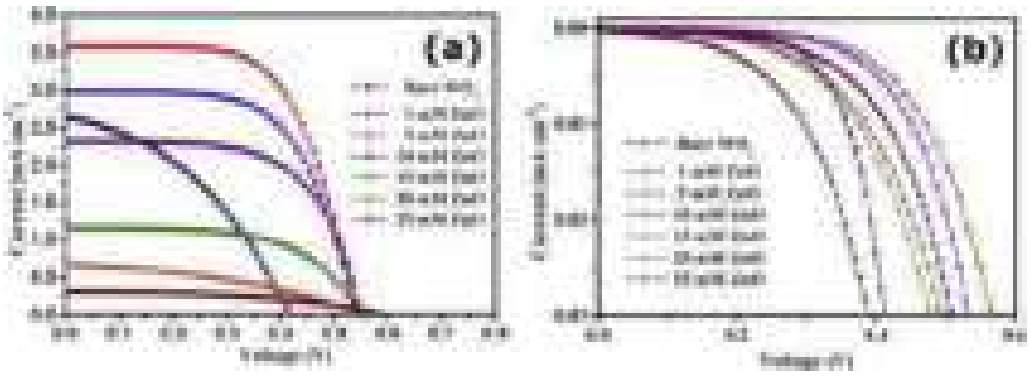

Fig. 5. Current-voltage characteristics of different cells under (a) Illumination and (b) Dark.

A clear enhancement in the efficiency and fill factor due to the presence of ZnO on the WO_3 surface compared to the bare WO_3 electrode can be observed from Table 1. The fill factor, which represents the squareness of the I–V curve [35], is very low for bare WO_3 which in turn decreases cell efficiency. The low fill factor may be attributed to the high recombination rate of electrons for bare WO_3 photoelectrode DSSC. However, a significant improvement in the value of J_{sc} can be noted from Table 1 upon ZnO coating over the WO_3 surface which demonstrates the positive role of the ZnO layer in reducing the recombination process. The DSSC with 5 mM ZnO precursor solution concentration yielded the highest short circuit photocurrent J_{SC} and efficiency η. But the photocurrent and the efficiency start falling sharply with a further increase in the precursor solution concentration.

The maximum value of open-circuit voltage is determined by the difference between the Fermi level of the photoanode (metal oxide) material and the red-ox potential of the liquid electrolyte [36]. WO_3 is known to possess a lower conduction band edge (E_{cb}) i.e. more positive E_{cb} thereby reducing the open-circuit voltage (V_{oc}). However, employing an ultrathin layer of more E_{cb} negative metal oxides like ZnO onto WO_3 surface may increase the value of V_{oc} as the photogenerated electrons from LUMO of dye molecules are now injected to the more negative conduction band of ZnO and then step down to the conduction band of WO_3 which is illustrated in Fig. 6(b).

Table 1
Photovoltaic performance of uncoated and ZnO coated WO_3 photoanode based DSSC.

ZnO precursor solution concentration	J_{sc} (mA/cm^2)	V_{oc}(V)	FF	Efficiency (η %)
Pure WO3	2.65	0.42	0.39	0.44
1 mM ZnO	2.98	0.53	0.63	1.07
5 mM ZnO	3.58	0.55	0.62	1.21
10 mM ZnO	2.32	0.56	0.62	0.80
15 mM ZnO	1.15	0.56	0.60	0.38
20 mM ZnO	0.68	0.57	0.38	0.15
25 mM ZnO	0.32	0.58	0.47	0.09

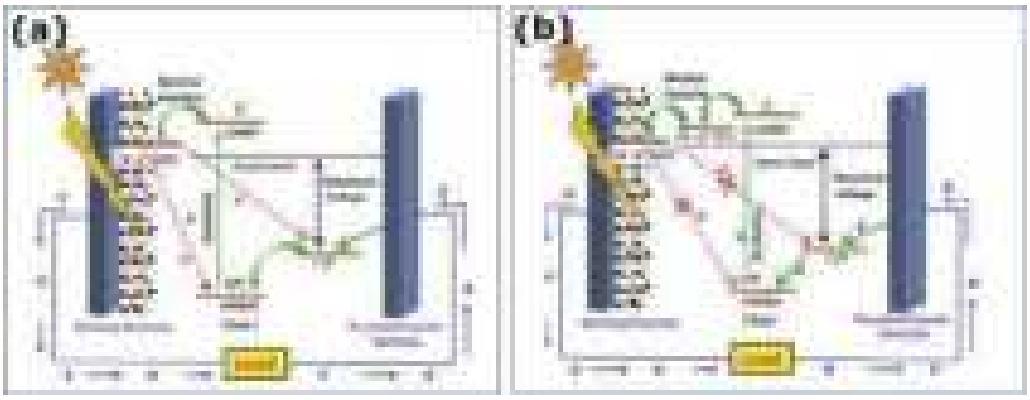

Fig. 6. Schematic energy level diagram and mechanism of the (a) Conventional DSSC and (b) DSSC with the ZnO barrier.

Furthermore, the energy barrier created due to the incorporation of ZnO onto the WO_3 film surface may prevent the charge carrier recombination and as well as decreasing back transfer of electrons to the HOMO of the dye molecule. Aside from this, the ultrathin layer of ZnO incorporation on the WO_3 surface facilitates the amount of dye adsorption and hence increasing the amount of photon absorption resulting in higher J_{sc}.

The dark current measurement was done in order to interpret the variation of charge recombination reaction of the photo-generated electrons with I_3^- ions at the Pt coated counter electrode/red-ox electrolyte interface. Fig. 5(b) shows the dark J–V characteristics of the DSSCs fabricated with uncoated and coated with different concentrations of the ZnO precursor solution. The photoelectron injection from LUMO of dye to the CB of the working electrode is completely absent in the dark condition and hence the dark current is mainly due to the diffusion of electrons from semiconductor to the redox electrolyte [37]. Ultrathin coating of ZnO layer on the WO_3 surface decreases the dark current which can be observed in dark current characteristics in Fig. 5(b). On the other hand, the uncoated WO_3 possesses a higher dark current for a particular bias voltage. This may be due to the fact that poor dye

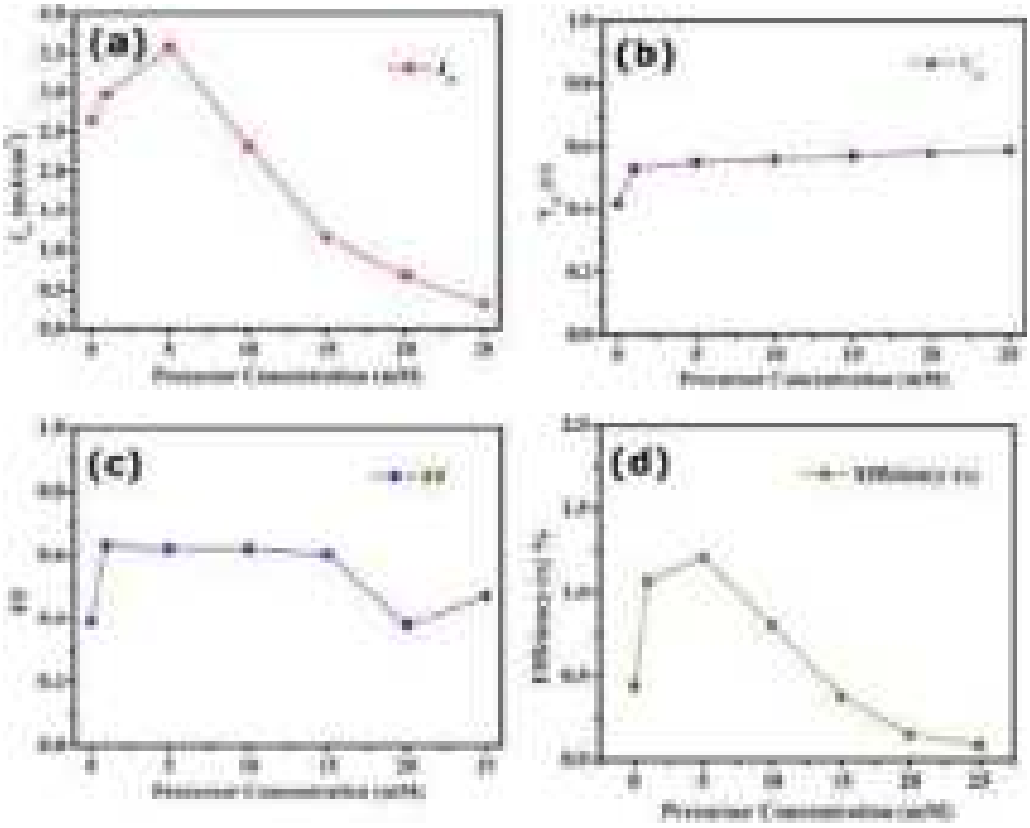

Fig. 7. Effect of ZnO precursor solution concentration on the values of photovoltaic parameters (a) J_{SC} (b) FF (c) V_{oc} and (d) η.

loading capacity of WO_3 allows more direct contact between WO_3 surface and liquid electrolyte. This facilitates the back transfer of electrons from WO_3 to electrolyte via reduction of I_3- into I- which led to increased dark current [22]. But the coating of ZnO creates an energy barrier that effectively reduces the rate of electron recombination thereby decreasing the dark current, consequently suppressed recombination of charge carriers due to ZnO coating increases cell FF. In addition to that, a very thin coating of ZnO also improves the dye loading which enables the ZnO treated WO_3 DSSC to harvest more light energy compared to ordinary WO_3 DSSC and significantly enhances current density. However, with the increase in the ZnO precursor concentration of more than 5 mM, the values of FF and J_{sc} start decreasing. This decrease in J_{sc} and FF might be due to the fact that thicker ZnO layer completely screens WO_3 from dye molecules. Moreover, a higher amount of ZnO content act as recombination sites [38]. Apart from this, an increased amount of ZnO deposition via increasing the ZnO precursor solution concentration promotes aggregation of Zn^{+2} ions and N3 dye which may decrease the photocurrent due to light loss due to absorption and scattering of light by these aggregates [39–41].

Fig. 7 shows the variation of DSSC performance parameters as a function of ZnO precursor solution concentration. The values of J_{sc}, FF, and η enhanced significantly for the cells with ultrathin ZnO nanoparticles coating as compared to the cell with bare WO_3 nanoparticle thin film. The best performance was obtained with 5 mM ZnO solution concentration with values of cell parameters like J_{sc}, V_{oc}, FF, and η as 3.56 mA/cm^2, 0.55 V, 0.62 and 1.21 % respectively.

3.4. Electrochemical impedance spectroscopy

Electrochemical impedance spectroscopy was performed to further explore the interfacial charge transport properties and recombination resistances for a better understanding of the cell parameters. The EIS measurement was carried out at V_{oc} bias voltage and applying an AC voltage of 10 mV amplitude to the DSSC under 1 sun illumination in the frequency range 0.1 Hz to 190 kHz. The Nyquist plot of the different DSSCs fabricated using bare WO_3 and with a coating of different concentrations of ZnO onto it are depicted in Fig. 8(a). Usually, a typical Nyquist plot consists of three semi-circles. The first semicircle in the high-frequency range is attributed to the charge transport resistance at the Pt counter electrode/ electrolyte interface, while the second semicircle in the mid-frequency range represents the recombination resistance at the semiconductor/dye/electrolyte interface. The third semicircle is associated with Nernst diffusion (Warburg diffusion impedance Z_w) which is the impedance faced by the electrons during diffusion through the electrolyte [39]. However, in our case only two semicircles are present as the third semicircle is usually observed at frequencies below 0.1 Hz [42]. The intercept of the 1st semicircle on the real axis of the Nyquist plot in the high-frequency range represents the sheet resistance of FTO and other ohmic contact resistances (R_s) of the assembled cells. The capacitive components C_1 & C_2 in the equivalent circuit are due to the formation of charge double layer between the counter electrode/electrolyte and semiconductor/dye/electrolyte interfaces respectively [43]. The equivalent circuit, shown in the inset of Fig. 8(a) is used to fit the experimental Nyquist plot and the obtained EIS parameters are represented in Table 2. The value of contact resistance (R_s) is almost the same for all the coated cells except the bare WO_3 cell. The increase in the value of R_s in ZnO coated cells may be due to the increase in the number of layers. The value of recombination resistance (R_2) is very low for bare WO_3. But a gradual increase in R_2 with an increase in ZnO precursor concentration may be observed in Fig. 8(a) and Table 2. The highest value of R_2 is observed for 5 mM ZnO concentration as this much concentration provided the highest amount of dye adsorption without affecting the carrier transport through WO_3 thereby generating the highest number of charge carriers and also reducing the charge carrier recombination at the semiconductor/due/electrolyte interface.

Further increase in ZnO concentration starts decreasing R_2 due to poor dye loading on the WO_3 surface. Along with that presence of recombination sites for the free charge carriers in the thick layer of ZnO (38). Thick ZnO layer also makes the thickness of the film such a high that it becomes greater than the diffusion length of the electrons. This decreases the net photocurrent reaching the FTO and lowers the cell performance. The highest value of chemical capacitance C_2 also reflects the transformation of a higher amount of photon energy into chemical energy [44,45]. To estimate the charge carrier lifetime, the Bode plot representing variation in phase angle (θ) with frequency (f) for varying amounts of ZnO concentration is depicted in Fig. 8(b). The electron lifetime is calculated

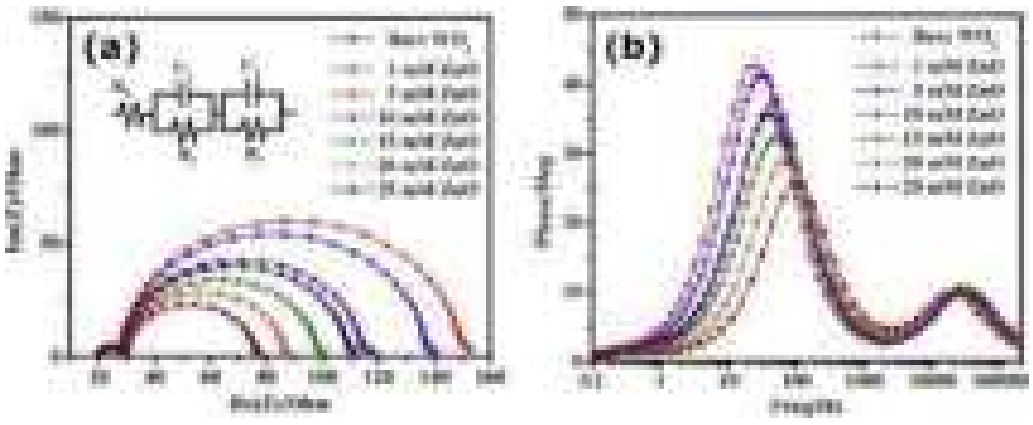

Fig. 8. Electrochemical Impedance Spectra of the DSSCs (a) Nyquist plot along with equivalent circuit (inset) (b) Bode plot.

Table 2
Summary of EIS measurements of DSSCs.

ZnO precursor solution concentration	R_S (Ω)	R_2 (Ω)	R_1 (Ω)	C_2 (μF)	Peak freq. f(Hz)	Electron lifetime (τ_e) (ms)
Pure WO3	19.3	85.2	8.67	84.3	37.18	4.28
1 mM ZnO	19.5	108.3	8.4	103.7	31.36	5.08
5 mM ZnO	19.6	119.7	8.62	125.4	24.15	6.59
10 mM ZnO	20.1	79.57	8.36	98.35	40.72	3.91
15 mM ZnO	20.8	67.57	8.79	87.35	48.47	3.29
20 mM ZnO	21.1	56.23	8.41	68.3	68.67	2.32
25 mM ZnO	21.3	45.76	8.52	55.57	97.29	1.64

using formula [46–49],

$$\tau_n = \frac{1}{2\pi f_{max}} \tag{3}$$

Where f_{max} represents the characteristic peak frequency of the Bode plot in the mid-frequency range. The lower value of f_{max} is associated with a higher electron lifetime. The DSSC with 5 mM ZnO coating has the lowest value of f_{max} leading to the highest lifetime of photogenerated electrons. This enhancement in electron lifetime reduces the recombination process leading to the highest photocurrent among the seven fabricated cells in our study. These results are in accordance with the results obtained from J–V characteristics under illumination and dark.

4. Conclusion

In this study, we have fabricated DSSCs based on WO_3 as an alternative photoanode material. The DSSC showed an efficiency of 0.44 % with a low FF of 0.39. This was due to very high recombination rates of photoexcited electrons along with poor dye loading due to the highly acidic surface of WO_3. Apart from that, the lower conduction band edge position of WO_3 limits the open-circuit voltage of the DSSC. In order to improve the performance of WO_3 based DSSC, the effect of inclusion of the ZnO thin layer on the surface of WO_3 was studied. The current density (J) – voltage (V) characteristics of the prepared cells were compared and a clear enhancement of cell efficiency was recorded upon ZnO coating and the highest efficiency was achieved for 5 mM concentration. Although the incorporation of a thin layer of ZnO onto WO_3 enhances the power conversion efficiency by creating an energy barrier and limiting the electron back-recombination, the thicker layer of ZnO degrades the cell performance by forming an aggregation of Zn^{+2} ions and N3 dye and reducing the dye adsorption quantity of WO_3 film. This suggests an optimum concentration for ZnO to be deposited over WO_3 film to achieve the highest efficiency. The improvement of the value of V_{oc} due to ZnO coating was attributed to the upward shift in CB of WO_3. Apart from J–V characteristics study under illumination and dark, EIS measurement was also performed. It was found that the cell with 5 mM of ZnO over WO_3 film has the highest recombination resistance which efficiently suppresses the electron recombination rate and as result, the lifetime of photogenerated electrons is also highest. The decrease in the photoconversion efficiency with further increase in ZnO concentration above optimum value is due to the complete screening of WO_3 film by a thicker layer of ZnO. Therefore, the novel method used here to modify the surface property of the WO_3 photoelectrode of DSSC is found to be promising to enhance the cell performance and thereby develop an efficient WO_3 based Dye sensitized Solar cell.

Declaration of Competing Interest

The authors declare that they have no known competing financial interests or personal relationships that could have appeared to influence the work reported in this paper.

Acknowledgment

Authors gratefully acknowledge the Dept. of Physics, the University of North Bengal for providing financial support and laboratory facilities for carrying out the research work.

References

[1] W. Bach, Global warming: the complete briefing (2nd ed). John Houghton. Cambridge University Press: Cambridge, 1997. Pp. xv + 251. Paperback: ISBN 0521-62932-2, ú12.95; hardback: ISBN 0-321-62089-9, ú35.00, Int. J. Climatol. 18 (5) (1998) 579–580.
[2] D.H. Meadows, D.L. Meadows, J. Randers, W.W. Behrens, The Limits to Growth 102 (1972), p. 27 New York.
[3] Greenhouse glasnost: the crisis of global warming: essays, in: T.J. Minger (Ed.), Greenhouse/Glasnost: The Sundance Symposium on Global Climate Change (USA), 1989, Ecco Press, 1990.
[4] J. Peet, Energy and the Ecological Economics of Sustainability, Island Press, 1992.
[5] A. Rose, A global view of solar energy in rational units, Physica Status Solidi A 56 (1) (1979) 11–26.
[6] A. Shah, P. Torres, R. Tscharner, N. Wyrsch, H. Keppner, Photovoltaic technology: the case for thin-film solar cells, Science 285 (5428) (1999) 692–698.
[7] J.A. Turner, A realizable renewable energy future, Science 285 (5428) (1999) 687–689.
[8] J. Gong, J. Liang, K. Sumathy, Review on dye-sensitized solar cells (DSSCs): fundamental concepts and novel materials, Renew. Sustain. Energy Rev. 16 (8)

(2012) 5848–5860.
[9] H.M. Upadhyaya, S. Senthilarasu, M.-H. Hsu, D.K. Kumar, Recent progress and the status of dye-sensitised solar cell (DSSC) technology with state-of-the-art conversion efficiencies, Sol. Energy Mater. Sol. Cells 119 (2013) 291–295.
[10] K. Sharma, V. Sharma, S. Sharma, Dye-sensitized solar cells: fundamentals and current status, Nanoscale Res. Lett. 13 (1) (2018) 381.
[11] B. O'regan, M. Grätzel, A low-cost, high-efficiency solar cell based on dye-sensitized colloidal TiO2 films, Nature 353 (6346) (1991) 737.
[12] S. Ito, G. Rothenberger, P. Liska, P. Comte, S.M. Zakeeruddin, P. Péchy, et al., High-efficiency (7.2%) flexible dye-sensitized solar cells with Ti-metal substrate for nanocrystalline-TiO 2 photoanode, Chem. Commun. (38) (2006) 4004–4006.
[13] T. Yamaguchi, N. Tobe, D. Matsumoto, T. Nagai, H. Arakawa, Highly efficient plastic-substrate dye-sensitized solar cells with validated conversion efficiency of 7.6%, Sol. Energy Mater. Sol. Cells 94 (5) (2010) 812–816.
[14] C. Cavallo, F. Di Pascasio, A. Latini, M. Bonomo, D. Dini, Nanostructured semiconductor materials for dye-sensitized solar cells, J. Nanomater. 2017 (2017).
[15] M. Grätzel, Photoelectrochemical cells, Nature 414 (6861) (2001) 338.
[16] D.Y. Leung, X. Fu, C. Wang, M. Ni, M.K. Leung, X. Wang, et al., Hydrogen production over titania-based photocatalysts, ChemSusChem 3 (6) (2010) 681–694.
[17] G. Liu, J. Gong, L. Kong, R.D. Schaller, Q. Hu, Z. Liu, et al., Isothermal pressure-derived metastable states in 2D hybrid perovskites showing enduring bandgap narrowing, Proc. Natl. Acad. Sci. 115 (32) (2018) 8076–8081.
[18] G. Liu, L. Kong, P. Guo, C.C. Stoumpos, Q. Hu, Z. Liu, et al., Two regimes of bandgap red shift and partial ambient retention in pressure-treated two-dimensional perovskites, ACS Energy Lett. 2 (11) (2017) 2518–2524.
[19] X. Wang, Z. Li, J. Shi, Y. Yu, One-dimensional titanium dioxide nanomaterials: nanowires, nanorods, and nanobelts, Chem. Rev. 114 (19) (2014) 9346–9384.
[20] A.K. Chandiran, M. Abdi-Jalebi, M.K. Nazeeruddin, M. Grätzel, Analysis of electron transfer properties of ZnO and TiO2 photoanodes for dye-sensitized solar cells, ACS Nano 8 (3) (2014) 2261–2268.
[21] M. Gillet, K. Aguir, C. Lemire, E. Gillet, K. Schierbaum, The structure and electrical conductivity of vacuum-annealed WO3 thin films, Thin Solid Films 467 (1–2) (2004) 239–246.
[22] H. Zheng, Y. Tachibana, K. Kalantar-zadeh, Dye-sensitized solar cells based on WO3, Langmuir 26 (24) (2010) 19148–19152.
[23] H. Bae, M. Yoon, J. Kim, S. Im, Photodetecting properties of ZnO-based thin-film transistors, Appl. Phys. Lett. 83 (25) (2003) 5313–5315.
[24] Ü. Özgür, Y.I. Alivov, C. Liu, A. Teke, M. Reshchikov, S. Doğan, et al., A comprehensive review of ZnO materials and devices, J. Appl. Phys. 98 (4) (2005) 11.
[25] Q. Zhang, C.S. Dandeneau, X. Zhou, G. Cao, ZnO nanostructures for dye-sensitized solar cells, Adv. Mater. 21 (41) (2009) 4087–4108.
[26] R. Biswas, T. Roy, S. Chatterjee, Study of electro-optical performance and interfacial charge transfer dynamics of dye sensitized solar cells based on ZnO nanostructures and natural dyes, J. Nanoelectron. Optoelectron. 14 (1) (2019) 99–108.
[27] U. Costantino, F. Marmottini, M. Nocchetti, R. Vivani, New synthetic routes to hydrotalcite-like compounds− characterisation and properties of the obtained materials, Eur. J. Inorg. Chem. 1998 (10) (1998) 1439–1446.
[28] J.-M. Oh, S.-H. Hwang, J.-H. Choy, The effect of synthetic conditions on tailoring the size of hydrotalcite particles, Solid State Ion. 151 (1–4) (2002) 285–291.
[29] M. Daniel, B. Desbat, J. Lassegues, B. Gerand, M. Figlarz, Infrared and Raman study of WO3 tungsten trioxides and WO3, xH2O tungsten trioxide tydrates, J. Solid State Chem. 67 (2) (1987) 235–247.
[30] A.Z. Sadek, H. Zheng, M. Breedon, V. Bansal, S.K. Bhargava, K. Latham, et al., High-temperature anodized WO3 nanoplatelet films for photosensitive devices, Langmuir 25 (16) (2009) 9545–9551.
[31] S. Hore, C. Vetter, R. Kern, H. Smit, A. Hinsch, Influence of scattering layers on efficiency of dye-sensitized solar cells, Sol. Energy Mater. Sol. Cells 90 (9) (2006) 1176–1188.
[32] E.M. Jin, K.-H. Park, J.-J. Yun, C.K. Hong, M.-J. Hwang, B.-K. Park, et al., Photovoltaic properties of TiO 2 photoelectrode prepared by using liquid PEG-EEM binder, Surf. Rev. Lett. 17 (1) (2010) 15–20.
[33] K.H. Ko, Y.C. Lee, Y.J. Jung, Enhanced efficiency of dye-sensitized TiO2 solar cells (DSSC) by doping of metal ions, J. Colloid Interface Sci. 283 (2) (2005) 482–487.
[34] K.-H. Park, E.M. Jin, H.B. Gu, S.E. Shim, C.K. Hong, Effects of HNO3 treatment of TiO2 nanoparticles on the photovoltaic properties of dye-sensitized solar cells, Mater. Lett. 63 (26) (2009) 2208–2211.
[35] B. Qi, J. Wang, Fill factor in organic solar cells, J. Chem. Soc. Faraday Trans. 15 (23) (2013) 8972–8982.
[36] M. Grätzel, Dye-sensitized solar cells, J. Photochem. Photobiol. C Photochem. Rev. 4 (2) (2003) 145–153.
[37] S. Ito, P. Liska, P. Comte, R. Charvet, P. Péchy, U. Bach, et al., Control of dark current in photoelectrochemical (TiO 2/I−−I 3−) and dye-sensitized solar cells, Chem. Commun. (34) (2005) 4351–4353.
[38] S. Noor, S. Sajjad, S.A.K. Leghari, S. Shaheen, A. Iqbal, ZnO/TiO2 nanocomposite photoanode as an effective UV-vis responsive dye sensitized solar cell, Mater. Res. Express 5 (9) (2018) 095905.
[39] M. Adachi, M. Sakamoto, J. Jiu, Y. Ogata, S. Isoda, Determination of parameters of electron transport in dye-sensitized solar cells using electrochemical impedance spectroscopy, J. Phys. Chem. B 110 (28) (2006) 13872–13880.
[40] F. Al-juaid, A. Merazga, A. Al-Baradi, F. Abdel-wahab, Effect of sol–gel ZnO spin-coating on the performance of TiO2-based dye-sensitized solar cell, Solid-State Electronics. 87 (2013) 98–103.
[41] I. Bedja, P.V. Kamat, X. Hua, A. Lappin, S. Hotchandani, Photosensitization of Nanocrystalline ZnO Films by Bis (2, 2 '-bipyridine)(2, 2 '-bipyridine-4, 4 '-dicarboxylic acid) ruthenium (II), Langmuir 13 (8) (1997) 2398–2403.
[42] S. Sarker, A. Ahammad, H.W. Seo, D.M. Kim, Electrochemical impedance spectra of dye-sensitized solar cells: fundamentals and spreadsheet calculation, Int. J. Photoenergy 2014 (2014).
[43] M. Younas, M. Gondal, M. Dastageer, U. Baig, Fabrication of cost effective and efficient dye sensitized solar cells with WO3-TiO2 nanocomposites as photoanode and MWCNT as Pt-free counter electrode, Ceram. Int. 45 (1) (2019) 936–947.
[44] Q. Wang, J.-E. Moser, M. Grätzel, Electrochemical impedance spectroscopic analysis of dye-sensitized solar cells, J. Phys. Chem. B 109 (31) (2005) 14945–14953.
[45] J. Bisquert, Chemical capacitance of nanostructured semiconductors: its origin and significance for nanocomposite solar cells, J. Chem. Soc. Faraday Trans. 5 (24) (2003) 5360–5364.
[46] S.P. Lim, A. Pandikumar, N.M. Huang, H.N. Lim, Silver/titania nanocomposite-modified photoelectrodes for photoelectrocatalytic methanol oxidation, Int. J. Hydrogen Energy 39 (27) (2014) 14720–14729.
[47] S. Buda, S. Shafie, S.A. Rashid, H. Jaafar, N. Sharif, Enhanced visible light absorption and reduced charge recombination in AgNP plasmonic photoelectrochemical cell, Results Phys. 7 (2017) 2311–2316.
[48] S.G. Kim, M.J. Ju, I.T. Choi, W.S. Choi, H.-J. Choi, J.-B. Baek, et al., Nb-doped TiO 2 nanoparticles for organic dye-sensitized solar cells, RSC Adv. 3 (37) (2013) 16380–16386.
[49] P. Archana, A. Gupta, M.M. Yusoff, R. Jose, Tungsten doped titanium dioxide nanowires for high efficiency dye-sensitized solar cells, J. Chem. Soc. Faraday Trans. 16 (16) (2014) 7448–7454.

ISSN 0003-701X, Applied Solar Energy, 2021, Vol. 57, No. 1, pp. 23–29. © Allerton Press, Inc., 2021.
Russian Text © The Author(s), 2021, published in Geliotekhnika, 2021, No. 1, pp. 37–44.

SOLAR ENGINEERING
MATERIALS SCIENCE

An Investigation on the Stability Enhancement of Dye-Sensitized Solar Cells Fabricated with Ethyl Cellulose Based Gel Electrolyte

Trinakhi Roy[a], Rajat Biswas[a], and Suman Chatterjee[a, *]

[a] *Department of Physics, University of North Bengal, Raja Rammohunpur, Darjeeling, Siliguri-734013 India*
**e-mail: suman_chatterjee@hotmail.com*

Received December 11, 2019; revised January 10, 2020; accepted June 17, 2020

Abstract—Liquid electrolyte based Dye-Sentisized Solar Cells (DSSC) often suffers stability problems which limit its durability. The stability of the dye-sensitized solar cell is enhanced with the use of gel electrolyte instead of liquid electrolyte in this paper. A detailed effective fabrication method of the DSSC based on gel electrolyte has been presented here. In this approach, the gel-state electrolyte solution was prepared by mixing the traditional liquid-state electrolyte with ethyl cellulose as a gelator and was placed into the DSSC in its quasi-solid state. The prepared gel state electrolyte showed appreciable conductivity, which is comparable to those of traditional liquid electrolytes by Electrochemical impedance analysis. The gel electrolyte based DSSCs exhibited a considerable power-conversion efficiency of 1.29% and enhanced stability compared to the traditional liquid electrolyte based DSSC.

Keywords: dye-sensitized solar cells, electrochemical impedance spectroscopy, gel electrolyte, I–V characteristics, liquid electrolyte, stability

DOI: 10.3103/S0003701X21010084

INTRODUCTION

Due to increasing energy demand, polluting environment, and the rising price of non-renewable fuel sources, scientists are constantly thinking of new ways to find pollution-free renewable energy [1]. The natural resources that can renew itself over time are called renewable energy sources [2]. It is believed that solar energy would be the main source of alternative energy [3]. Conventional Crystalline and polycrystalline silicon solar cells have attained energy conversion efficiency of over 20%, but due to their complicated and difficult fabrication process and high cost [4], people have started to think about its alternative. Grätzel and co-workers first reported Dye-Sentisized Solar Cells (DSSC)s as a useful substitute for conventional solar cells [1], and subsequently, a huge interest has been developed for DSSCs because of its easy fabrication technique and low cost [5].

The various components of a DSSC are fluorine-doped tin oxide (FTO) electrode coated with porous TiO_2 nanoparticles, dye sensitizer, a platinum-coated counter electrode, and an electrolyte containing redox mediator [6]. A schematic diagram of the construction and operating principle of a dye-sensitized solar cell is shown in Fig. 1a,b, respectively. The photons are absorbed by the dye sensitizer molecules and the electrons are excited from the HOMO to LUMO state. Then photogenerated electrons from the sensitizer are injected into the TiO_2 nanostructures and transported through the external circuit. Subsequently, electrons from the electrolyte are transferred to the dye sensitizer and the oxidized dye is restored. The transported electrons are accepted by the electrolyte through the platinum-coated counter electrode, and the electrolyte gets regenerated [7].

Photo anode of a DSSC performs a vital role in determining the overall performance of the DSSC by transporting electrons and supporting the Dye molecules [8]. The semiconducting oxide material TiO_2 is mostly used as a photoanode because of its excellent optical, electrical, and chemical properties [9–12]. Although appreciably high conversion efficiency is achieved with TiO_2, its low electron mobility results in low electron mobility has led renewed investigations in new alternative about new alternative wide-bandgap photoanode materials like ZnO, WO_3, SnO_2 for better performance of Dye-sensitized solar cells [13–15]. Researchers are also using natural dyes extracted from different fruits, vegetables, and flowers in search of low-cost DSSC fabricated with environment-friendly and non-toxic material [16–20].

But the electrolyte has a close interaction with all the components of DSSC and it determines the time stability of the cell. Due to this, scientists have been paying more attention to electrolytes these days [21, 22]. Though the theoretically estimated maximum photoelectric conversion efficiency of a DSSC is 29% [23] has been recorded with liquid electrolytes, the

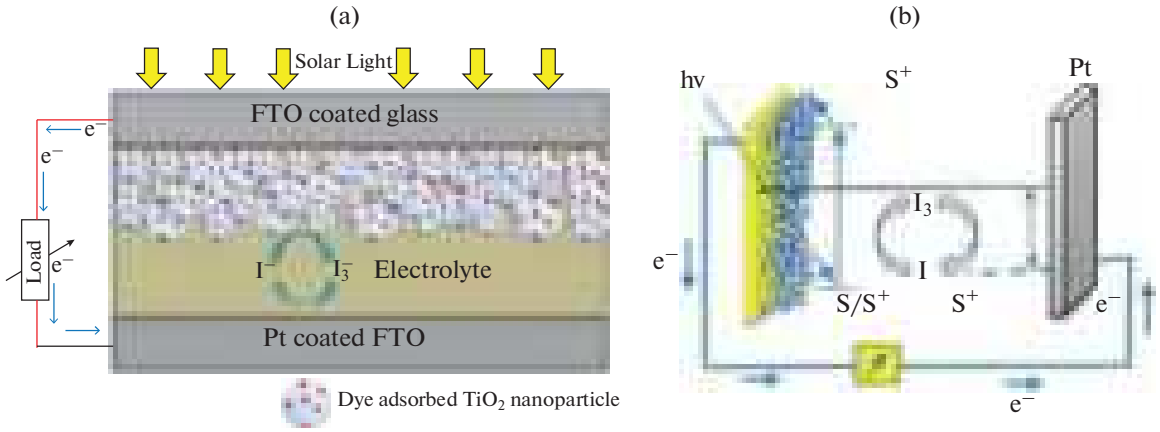

Fig. 1. Schematic diagram of (a) construction and (b) working principle of dye-sensitized solar cell.

actual efficiency of 14.3% could be achieved. This is due to leakage problems, photodegradation of attached dyes, and solvents volatility restrict the long-term performance of DSSCs [24]. To overcome these limitations gel electrolytes have been used instead of liquid electrolytes as the please provide the atmosphere for the sintering process (inert, activated, etc?) [25]. Gel electrolytes are usually prepared by adding materials of high molecular weights with organic solvents and iodides. Polyvinyl carbonate (PC), Acetonitrile (ACN), ethylene carbonate (EC) are an example of some of the popularly used solvents and Lithium iodide (LiI), potassium iodide (KI), Sodium iodide are some of the commonly utilized iodides with iodine (I_2). For gelation of liquid electrolyte, many materials are used namely polyethylene glycol, polyvinylidene fluoride-co-hexafluoropropylene (PVDF-HFP), polyethylene oxide, etc. [26].

In this study, we prepared gel electrolytes using ethyl cellulose (EC) as gelator in the liquid electrolyte, and fabricated DSSCs with both liquid and gel electrolytes to study were fabricated with both liquid and gel electrolytes to study their overall photovoltaic performance including their performance stability over a certain period. Gel electrolyte was also studied in earlier investigation [22], reporting higherstability. A detailed comparison of Photoelectric properties is presented in the investigation.

MATERIALS AND METHODS

All the chemicals used in this study were purchased from commercial sources and used as received. Fluorine-doped tin oxide (FTO) glass slides (10 Ω/square; thickness 2.2 mm), ruthenium dye (N719), Surlyn spacer, and Platinum Precursors solution (Plastisol T) for counter electrode preparation, all were purchased from Solaronix, Switzerland. Titanium dioxide nanopowder (TiO_2), Lithium Iodide (LiI), and Iodine (I_2) were purchased from Sigma-Aldrich, India. The chemicals, used in gel preparation are Acetonitrile (Merck, India), 4-tert-butylpyridine (TCI CHEMICALS, Japan), Tetrabutylammonium iodide (Merck), Ethyl Cellulose (Sigma-Aldrich, India), acetone (C_3H_6O), ethanol (C_2H_5OH), and acetic acid (CH_3CO_2H) (Sigma-Aldrich). All the reagents purchased were used without further purification.

The working electrode of the DSSC was prepared by following the standard available procedure [27]. At first, 10 gm of the TiO_2 nanopowder was mixed with diluted acetic (1 in 50 ml deionized water) acid in a mortar and pastel and adding few drops of Triton X100 (Merck) as surfactant and ground continuously until a homogenous smooth suspension was obtained. The lump-free slurry was then applied on the conductive side of an FTO coated glass using the doctor blade method to make a homogeneous layer. To strengthen the bonding between the FTO glass and the semiconductor paste, the TiO_2 coated glass plate was sintered in normal atmospheric condition at 450°C for 45 min. In the sintering process, at first, after introducing the sample in furnace, the temperature was raised with a rate of 10°C/5 min until the temperature had reached 350°C and after that, it was increased with a rate of 10°C/10 min until 450°C. When it cooled down to room temperature, the sintered glass substrate was immersed in the ruthenium dye (N719) solution for dye adsorption on the surface of the TiO_2 nanoparticles for 24 hours. FTO glass coated with a platinum catalyst (Plastisol-T) and heated at 400°C was used as a counter electrode and a sealed sandwich-type cell was fabricated by assembling dye adsorbed TiO_2 electrode and the platinum (Pt) coated counter electrode with Surlyn film as a spacer between them. Then electrolyte was introduced into the assembled cell through the drilled hole of the counter with a syringe. Glass glue was used to seal the hole and finally the cell was connected to the external circuit with the help of crocodile clips.

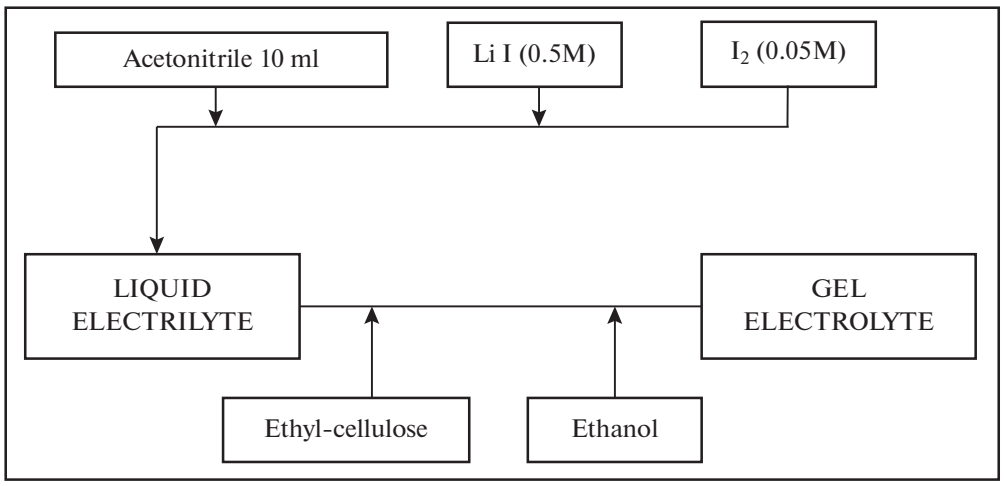

Fig. 2. The fabrication procedure of DSSC's with Liquid and Gel electrolytes.

The liquid electrolyte, which we used here, was prepared by mixing LiI (0.5M) and I_2 (0.05M) in 10 ml acetonitrile. To prepare gel electrolyte, ethyl-cellulose powder mixed with ethanol was added to the prepared liquid electrolyte. For our investigation, two cells were fabricated; one was filled with liquid type electrolyte and another one with gel-type electrolyte (Fig. 2).

After completion of the fabrication of two different cells with liquid and gel type electrolytes, the cells were placed under artificial solar illumination of 100 mW/cm^2 and connected with the J-V measurement system to calculate the photoelectric conversion efficiencies [28]. The photo-current voltage (I-V) characteristics were recorded using a Keithley 2400 source meter. Simulated sunlight was supplied using a xenon lamp (450W). This process had been repeated every alternate day and accordingly, the photovoltaic performances were recorded to investigate the long-term stability of the DSSCs. The ethyl cellulose gelator was selected for its easy availability and low cost.

RESULTS AND DISCUSSIONS

Scanning Electron Microscope (SEM) Analysis

The scanning electron microscope (SEM) was used to examine the surface morphology of TiO_2 film over the FTO glass substrate [29]. The highly porous morphology of the TiO_2 nanostructure deposited on a glass substrate can be observed from the SEM image shown in Fig. 3.

The particle size of the TiO_2 nanoparticles was about 60 nm. The higher porous structure resulted in greater dye molecules adsorption on the surface of the TiO_2 nanoparticles. Also, smaller the particle size of the TiO_2 particles, the higher the overall surface area for dye molecules attachment for a particular volume of the photoanode. More dye adsorption causes a greater number of electron excitation from HOMO to LUMO of dye molecules after photon absorption [29].

Photovoltaic Performance of the DSSCs

The I–V characteristics of the fabricated DSSCs based on liquid and gel electrolyte and pure TiO_2 photoanode is shown in Fig. 3. The energy conversion efficiency of each DSSC was calculated using the formula:

$$\eta = \frac{P_{out}}{P_{in}} = \frac{I_{sc}V_{oc}FF}{P_{in}}, \quad (1)$$

where, I_{sc} is the short circuit current density, V_{oc} the open-circuit voltage, P_{in} is the total incident power density, and is *FF* the fill factor. The fill factor (*FF*) determines the quality of the solar cell, and it was calculated by

$$FF = \frac{I_{max}V_{max}}{I_{sc}V_{oc}}, \quad (2)$$

where I_{max} and V_{max} represent the current density and the voltage at maximum power output.

The Current-Voltage (I–V) characteristics of the DSSCs fabricated using liquid and gel-based electrolytes are shown in Fig. 4. The different electrical parameters of the cells obtained from the I–V characteristics are listed in Table 1 below.

The energy conversion efficiency of gel electrolyte based DSSC was lower than liquid electrolyte based DSSC. The photovoltaic efficiency of DSSCs using liquid and gel type electrolytes is 1.90 and 1.29% respectively. Tab. 1 represents the various photovoltaic parameters extracted from the I–V curves of the cells with liquid and gel electrolytes. The solar cell fabricated using liquid electrolyte exhibits higher short-circuit photocurrent density (J_{SC}), open-circuit voltage (V_{OC}), and fill factor (*FF*) compared to the DSSC fab-

Fig. 3. Scanning electron microscope (SEM) image of TiO_2 nanoparticles on FTO substrate.

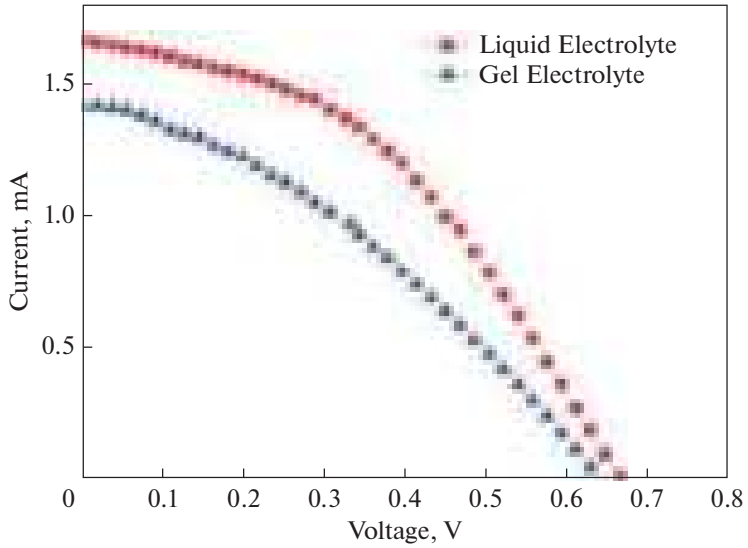

Fig. 4. Current-Voltage characteristics of the cells under illumination.

ricated using gel electrolyte as a dye. The efficiency of the gel-based DSSC may be low compared to the liquid electrolyte based DSSC, but the values of cell parameters obtained are found to be comparable to the efficiencies obtained for gel electrolyte based DSSCs [29].

Electrochemical behavior Analysis of the DSSCs

Electrochemical Impedance Spectroscopy (EIS) is a very useful technique for the interpretation of the kinetics of charge transport processes in different lay-

Table 1. Photovoltaic parameters of the fabricated cells

Cell	Electrolyte used	J_{sc} (mA/cm^2)	V_{oc}(V)	R_s (Ω cm^2)	R_{sh} (Ωcm^2)	*FF*	Efficiency (η %)
Cell-1	Liquid	1.67	0.662	309.5	1793	0.43	1.90
Cell-2	Gel	1.42	0.646	253.7	1547	0.35	1.29

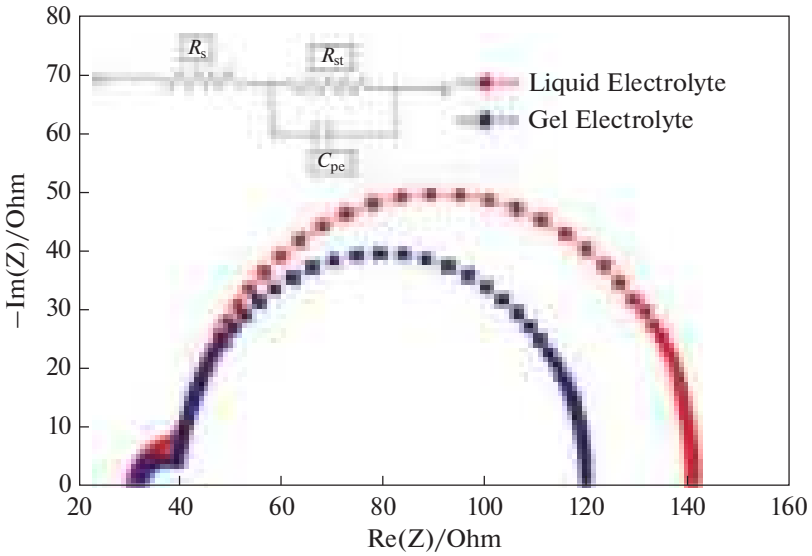

Fig. 5. Nyquist plot of DSSCs.

ers of DSSCs [30]. Generally, EIS data are represented by Nyquist and Bode plots. In the Nyquist plot, the imaginary part of impedance Im(Z) is plotted against the real part of impedance Re(Z) by varying frequencies of the applied signal [31].

An equivalent circuit is incorporated to analyze the EIS data, shown in the inset of Fig. 5. In the Nyquist plot, two semicircles are exhibited. The first semicircle in the low-frequency region represents the electron transfer resistance (R_{ct}) in the electrolyte and the second semicircle in the mid-frequency region indicates the charge transfer resistance (R_s) at photoanode/dye/electrolyte interface [32] and C_{PE} is the equivalent parallel capacitance. In the Nyquist plot, it is obvious that the second semicircle is more prominent than the other one. From the Fig. 4, it was seen that the diameter of the second semicircle for liquid electrolyte (cell 1) is less than the diameter of the semicircle for gel electrolyte (cell-2). This indicates that the charge transfer resistance at the TiO_2/electrolyte interface for liquid electrolyte is lower than the same for gel electrolyte which justifies the slightly greater open circuit voltage, short circuit current, and overall cell efficiency of liquid electrolyte based DSSCs (Table 1). It is also suggested that the more viscous gel electrolyte does not affect the charge transfer process very much in the photoanode/electrolyte interface of the cell, but it affects the charge transfer resistance at the TiO_2/electrolyte interface.

Stability Study of the Cells

The effect of electrolyte on the durability of DSSCs was characterized by calculating the photoelectric conversion efficiency over time [33], as shown in Fig. 6. The photoelectric conversion efficiency of DSSC based on liquid electrolyte was recorded 1.90% immediately after fabrication and was changed to 0.89% after 120 hours. The photoelectric conversion efficiency of DSSC developed with gel electrolyte was recorded at 1.29% immediately after fabrication and 1.13% after some time. From here it is clear that however there is a small decrease in the efficiency for the gel electrolytes, the cell developed with gel electrolyte shows better stability than that with liquid electrolyte. The improvement in long term stability is probably due to the higher viscosity of gel inhibits the ionic migration to stabilize the system over a longer time and also by control of evaporation of liquid electrolyte. Also, higher stability of gel electrolyte gives it a better cost effectiveness than that of liquid electrolyte.

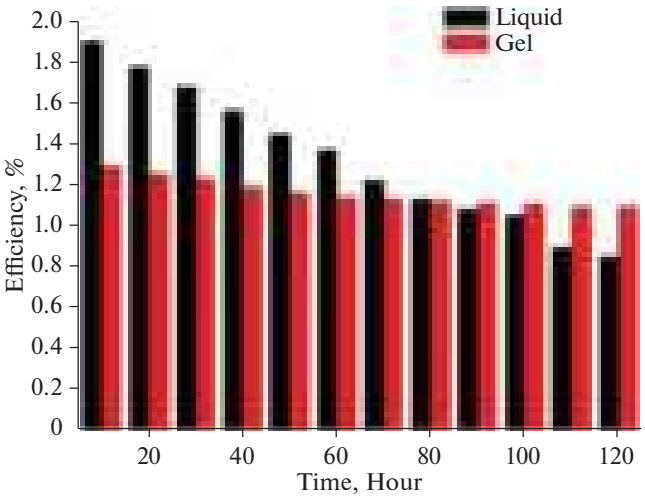

Fig. 6. Stability behavior of the fabricated DSSCs over time.

CONCLUSIONS

DSSCs were fabricated with pure TiO_2 photoanode with liquid and gel-type electrolyte, and cell performances were recorded. The liquid electrolyte cells exhibited higher short-circuit photocurrent density, open-circuit voltage, fill factor, and efficiency compared to the gel electrolyte DSSC. Though the efficiency of the gel-based DSSC is lower than the liquid electrolyte DSSC, the cell parameters obtained were comparable to the parameters obtained for gel electrolyte DSSC. Comparing these two types of DSSCs, it is clear that though the photovoltaic performance of gel electrolyte DSSC is slightly lower than liquid electrolyte DSSC, the performance of gel-based DSSC remains noticeably stable while for the liquid electrolyte the stability decreases remarkably over time.

FUNDING

The financial support to carry out this research was provided by the University of North Bengal. One of the authors' availed Ph.D. Inspire fellowship from the Department of Science and Technology (DST), Govt. of India.

ACKNOWLEDGMENTS

Authors gratefully acknowledge the Dept. of Physics, the University of North Bengal, for providing financial support and laboratory facilities for carrying out the research work. We also acknowledge the financial support from DST for providing a DST Inspire fellowship to one of our coworkers for carrying out the research work.

REFERENCES

1. Grätzel, M., Dye-sensitized solar cells, *J. Photochem. Photobiol. C: Photochem. Rev.,* 2003, vol. 4, no. 2, pp. 145–153. https://doi.org/10.1016/S1389-5567(03)00026-1
2. Elliott, D., Renewable energy and sustainable futures, *Futures,* 2000, vol. 32, nos. 3–4, pp. 261–274. https://doi.org/10.1016/S0016-3287(99)00096-8
3. Gong, J., Liang, J., Sumathy, K., Review on dye-sensitized solar cells (DSSCs): fundamental concepts and novel materials, *Renewable Sustainable Energy Rev.,* 2012, vol. 16, no. 8, pp. 5848–5860. https://doi.org/10.1016/j.rser.2012.04.044
4. Blakers, A., Zin, N., McIntosh, K.R., and Fong, K., High-efficiency silicon solar cells, *Energy Procedia,* 2013, vol. 33, pp. 1–10. https://doi.org/10.1016/j.egypro.2013.05.033
5. McConnell, R.D., Assessment of the dye-sensitized solar cell, *Renewable Sustainable Energy Rev.,* 2002, vol. 6, no. 3, pp. 271–293. https://doi.org/10.1016/S1364-0321(01)00012-0
6. Sharma, K., Sharma, V., and Sharma, S.S., Dye-sensitized solar cells: fundamentals and current status, *Nanoscale Res. Lett.,* 2018, vol. 13, no. 1, art. no. 381. https://doi.org/10.1186/s11671-018-2760
7. Al-Alwani, M.A., Mohamad, A.B., Ludin, N.A., et al., Dye-sensitised solar cells: development, structure, operation principles, electron kinetics, characterization, synthesis materials & natural photosensitizers, *Renewable Sustainable Energy Rev.,* 2016, vol. 65, no. 1, pp. 183–213. https://doi.org/10.1016/j.rser.2016.06.045
8. O'Regan, B. and Grätzel, M.A., Low-cost, high-efficiency solar cell based on dye-sensitized colloidal TiO2 films, *Nature,* 1991, vol. 353, no. 6346, pp. 737–740. https://doi.org/10.1038/353737a0
9. Leung, D.Y., Fu, X., Wang, C., et al., Hydrogen production over titania-based photocatalysts, *ChemSusChem,* 2010, vol. 3, no. 6, pp. 681–694. https://doi.org/10.1002/cssc.201000014
10. Liu, G., Gong, J., Kong, L., et al., Isothermal pressure-derived metastable states in 2D hybrid perovskites showing enduring bandgap narrowing, *Proc. National Academy of Sciences,* 2018, vol. 115, no. 32, pp. 8076–8081. https://doi.org/10.1073/pnas.1809167115
11. Liu, G., Kong, L., Guo, P., et al., Two regimes of bandgap redshift and partial ambient retention in pressure-treated two-dimensional perovskites, *ACS Energy Lett.,* 2017, vol. 2, no. 11, pp. 2518–2524. https://doi.org/10.1021/acsenergylett.7b00807
12. Wang, X., Li, Z., Shi, J., and Yu, Y., One-dimensional titanium dioxide nanomaterials: nanowires, nanorods, and nanobelts, *Chem. Rev.,* 2014, vol. 114, no. 19, pp. 9346–9384. https://doi.org/10.1021/cr400633s
13. Biswas, R. and Chatterjee, S., Effect of surface modification via sol-gel spin coating of ZnO nanoparticles on the performance of WO3 photoanode-based dye-sensitized solar cells, *Optik,* 2020, vol. 212, art. id. 164142. https://doi.org/10.1016/j.ijleo.2019.164142
14. Lee, J.H., Park, N.G., and Shin, Y.J., Nano-grain SnO2 electrodes for high conversion efficiency SnO2–DSSC, *Sol. Energy Mater. Sol. Cells,* 2011, vol. 95, no. 1, pp. 179–183. https://doi.org/10.1016/j.solmat.2010.04.027
15. Zheng, H., Tachibana, Y., and Kalantar-Zadeh, K., Dye-sensitized solar cells based on WO3, *Langmuir,* 2010, vol. 26, no. 24, pp. 19148–19152. https://doi.org/10.1021/la103692y
16. Karki, I.B., Nakarmi, J.J., Mandal, P.K., and Chatterjee, S., Effect of organic dyes on the performance of ZnO based dye-sensitized solar cells, *Appl. Sol. Energy,* 2013, vol. 49, no. 1, pp. 40–45. https://doi.org/10.3103/S0003701X13010052
17. Ayalew, W.A. and Ayele, D.W., Dye-sensitized solar cells using natural dye as light-harvesting materials extracted from *Acanthus sennii chiovenda* flower and *Euphorbia cotinifolia* leaf, *J. Sci.: Adv. Mater. Devices,* 2016, vol. 1, no. 4, pp. 488–494. https://doi.org/10.1016/j.jsamd.2016.10.003
18. Kabir, F., Bhuiyan, M.M., Manir, M.S., et al., Development of dye-sensitized solar cell based on a combination of natural dyes extracted from Malabar spinach and red spinach, *Results Phys.,* 2019, vol. 14, no. 1, art. id. 102474. https://doi.org/10.1016/j.rinp.2019.102474

19. Narayan, M.R., Dye-sensitized solar cells based on natural photosensitizers, *Renewable Sustainable Energy Rev.,* 2012, vol. 16, no. 1, pp. 208–215. https://doi.org/10.1016/j.rser.2011.07.148
20. Biswas, R., Roy, T., and Chatterjee, S., Study of electro-optical performance and interfacial charge transfer dynamics of dye-sensitized solar cells based on ZnO nanostructures and natural dyes, *J. Nanoelectron. Optoelectron.,* 2019, vol. 14, no. 1, pp. 99–108. https://doi.org/10.1166/jno.2019.2445
21. Wu, J., Lan, Z., Hao, S., et al., Progress on the electrolytes for dye-sensitized solar cells, *Pure Appl. Chem.,* 2008, vol. 80, no. 11, pp. 2241–2258. https://doi.org/10.1351/pac200880112241
22. Vasei, M., Tajabadi, F., Jabbari, A., and Taghavinia, N., Stable dye-sensitized solar cells based on a gel electrolyte with ethyl cellulose as the gelator, *Appl. Phys. A,* 2015, vol. 120, pp. 869–874. https://doi.org/10.1007/s00339-015-9332-8
23. Richter, A., Hermle, M., and Glunz, S.W., Reassessment of the limiting efficiency for crystalline silicon solar cells, *IEEE J. Photovoltaics,* 2013, vol. 3, no. 4, pp. 1184–1191. https://doi.org/10.1109/JPHOTOV.2013.2270351
24. Mahmood, A., Recent research progress on quasi-solid-state electrolytes for dye-sensitized solar cells, *J. Energy Chem.,* 2015, vol. 24, no. 6, pp. 686–692. https://doi.org/10.1016/j.jechem.2015.10.018
25. Shi, L.Y., Chen, T.L., Chen, C.H., and Cho, K.C., Synthesis and characterization of a gel-type electrolyte with ionic liquid added for dye-sensitized solar cells, *Int. J. Photoenergy,* 2013, vol. 2013, art. id. 834184. https://doi.org/10.1155/2013/834184
26. An, H., Xue, B., Li, D., et al., Environmentally friendly LiI/ethanol-based gel electrolyte for dye-sensitized solar cells, *Electrochem. Commun.,* 2006, vol. 8, no. 1, pp. 170–172. https://doi.org/10.1016/j.elecom.2005.11.012
27. Pathak, C., Surana, K., Kumar Shukla, V., and Singh, P.K., Fabrication and characterization of a dye-sensitized solar cell using natural dyes, *Mater. Today: Proc.,* 2019, vol. 12, no. 3, pp. 665–670. https://doi.org/10.1016/j.matpr.2019.03.111
28. Trihutomo, P., Soeparman, S., Widhiyanuriyawan, D., and Yuliati, L., Performance improvement of dye-sensitized solar cell- (DSSC-) based natural dyes by clathrin protein, *Int. J. Photoenergy,* 2019, vol. 2019, art. id. 4384728. https://doi.org/10.1155/2019/4384728
29. Umale, S.V., Tambat, S.N., Sudhakar, V., et al., Fabrication, characterization, and comparison of DSSC using anatase TiO2 synthesized by various methods, *Adv. Powder Technol.,* 2017, vol. 28, no. 11, pp. 2859–2864. https://doi.org/10.1016/j.apt.2017.08.012
30. Wang, Q., Moser, J.E., and Grätzel, M., Electrochemical impedance spectroscopic analysis of dye-sensitized solar cells, *J. Phys. Chem. B,* 2005, vol. 109, no. 31, pp. 14945–14953. https://doi.org/10.1021/jp052768h
31. Sarker, S., Ahammad, A., Seo, H.W., and Kim, D.M., Electrochemical impedance spectra of dye-sensitized solar cells: fundamentals and spreadsheet calculation, *Int. J. Photoenergy,* 2014, vol. 2014, art. id. 851705. https://doi.org/10.1155/2014/851705
32. Fabregat-Santiago, F., Bisquert, J., Palomares, E., et al., Correlation between photovoltaic performance and impedance spectroscopy of dye-sensitized solar cells based on ionic liquids, *J. Phys. Chem. C,* 2007, vol. 111, no. 17, pp. 6550–6560. https://doi.org/10.1021/jp066178a
33. Sonai, G.G., Tiihonen, A., Miettunen, K., et al., Long-term stability of dye-sensitized solar cells assembled with cobalt polymer gel electrolyte, *J. Phys. Chem. C,* 2017, vol. 121, no. 33, pp. 17577–17585. https://doi.org/10.1021/acs.jpcc.7b03865

SPELL: 1. OK

Journal of
Nanoelectronics and Optoelectronics
Vol. 14, pp. 99–108, 2019
www.aspbs.com/jno

ARTICLE

Study of Electro-Optical Performance and Interfacial Charge Transfer Dynamics of Dye Sensitized Solar Cells Based on ZnO Nanostructures and Natural Dyes

Rajat Biswas, Trinakhi Roy, and Suman Chatterjee*

The present work reports comparative assessment of optical and electrical properties of DSSCs fabricated using vertically aligned ZnO nanorods synthesized using low cost Sol–Gel spin coating technique on ITO coated glass substrate and ZnO nanopowder and their application in the fabrication of natural dye based Dye Sensitized Solar Cells. Natural dyes extracted from pomegranate and turmeric are used sensitizers. The surface morphology and crystal structure have been investigated by scanning electron microscopy and X-ray diffraction techniques. Optical absorption properties of the dyes were studied using UV-VIS spectroscopy. Photovoltaic parameters like Open Circuit voltage (V_{OC}), Short Circuit current (I_{SC}), fill factor (FF), Energy Conversion efficiency (η) were calculated to study the performances of the cells. Cell parameters like series resistance (R_s) and shunt Resistance (R_{sh}) were calculated from the I–V curve. Electrochemical impedance spectroscopy (EIS) was employed for detail investigation of the charge carrier recombination properties and the charge transfer mechanism at different interfaces of the DSSC devices. Various cell parameters were determined by fitting the experimental EIS curves with the appropriate equivalent circuit. The electron lifetimes were determined using bode plot of EIS measurement for the ZnO nanorod and ZnO nanoparticle photo electrodes sensitized using curcumin dye from turmeric and anthocyanin dye from pomegranate juice. The ZnO nanorod sensitized with curcumin cell emerged out as the best performing cell among the four cells which can be attributed to the highest electron lifetime, higher recombination resistance resulting in lower charge carrier recombination in the ZnO/Dye/Electrolyte interface. Many researchers have studied sensitizing effect of curcumin dye with different nanostructures of ZnO but we are the first to study the sensitizing effect of curcumin dye on ZnO nanorod like structure.

Keywords: Dye-Sensitized Solar Cells, Zinc Oxide Nanorod, Sol–Gel Hydrothermal Growth, Natural Dyes, Electrochemical Impedance Spectroscopy, Carrier Lifetime.

1. INTRODUCTION

With the increasing world population, spreading urbanization and technological advancement, matching the energy supply with the energy demand is the major challenging issue world is facing these days. The environmental consequences related to extensive use of fossil fuels, safety related issues of nuclear power, ever-growing energy demand and depleting the stock of fossil fuels have motivated the researchers to search for alternative economically and environmentally sustainable renewable energy sources.[1] In such a context of global energy requirement, among all the non-polluting and renewable energy sources, the photovoltaic technology utilizing solar energy has emerged as the most assuring candidate.[2] Though conventional photovoltaic devices (silicon-based solar cells) are promising for the direct conversion of photons into electrons, the prohibitive cost of these cells is noncompetitive with conventional power generating methods.[3,4] On the contrary, dye-sensitized solar cells (DSSCs), invented by O'Regan and Grätzel in 1991, are non-conventional

Department of Physics, University of North Bengal, Raja Rammohunpur, Siliguri 734013, India
*Author to whom correspondence should be addressed.
Email: suman_chatterjee@hotmail.com
Received: 14 June 2018
Accepted: 3 September 2018

photovoltaic technology based solar cells that have attracted significant attention because of its novel fabrication concept derived from nature's principle (photosynthesis), easy fabrication procedure using abundant materials, cost-effectiveness, suitability for wide variety of end-user products and can be made flexible. DSSC is a device which converts the solar energy into electrical energy, based on the principle of sensitization of wide bandgap semiconductors.[5] The photoelectrochemical performance of a DSSC mainly depends on the selected Photoanode material including its surface morphology and the sensitizing dye used.[6–9] Although a large number of different DSSCs have been investigated, most of them are not commercially popular until now because of its issues with low conversion efficiency, higher production cost, lower stability and durability.[10, 11]

Different inorganic, organic and hybrid dyes were employed as sensitizers in DSSCs. But among all of them, the ruthenium complexes are the most popular sensitizers because of their intense charge transfer absorption across the complete visible range and immensely efficient metal-to-ligand charge transfer mechanism.[12] But the major downsides of Ruthenium dyes are its rareness, high cost and complicated synthesis process.[13] Also, ruthenium polypyridyl complexes contain heavy metal, which is harmful to the environment.[14] In order to find out low cost and environment-friendly alternative to these expensive ruthenium compounds, researchers are focusing on easily available natural dyes extracted from various natural resources. Many researchers have studied sensitizing effects of several natural dyes derived from various fruits, flowers and leaves.[15] Most of them are used with TiO_2 nanostructures as photoanode.[16–20] However, recently ZnO has been emerging out as a great potential alternative to TiO_2 due to some its fascinating electrical and optical properties. ZnO is a wide band gap semiconductor having a direct band gap of 3.37 eV making it suitable as a photoanode material for DSSC.[21, 22] Apart from this, ZnO is very easy to synthesis, abundant, inexpensive and poses higher electron mobility (200–300 $cm^2V^{-1}S^{-1}$ for bulk material and 1000 $cm^2V^{-1}S^{-1}$ for nanowire) than that of TiO_2 nanoparticles (0.1–4 $cm^2V^{-1}S^{-1}$).[23–25] Moreover, the 1-D single crystalline rod-like structure of ZnO nanorods provide a higher surface to volume ratio enabling better dye loading.[26] These qualities of ZnO make it a potential alternative to TiO_2 for fabrication of DSSCs.

In this study, we aimed to combine natural sensitizers with two types of nanostructured ZnO to get both the advantages of ZnO and also the benefits of natural organic dyes targeting lower fabrication cost, echo friendly devices along with good cell performance and wanted to find out the best suitable ZnO nanostructure-Natural dye combination. In this regard, we fabricated four DSSCs using two types of natural dyes, anthocyanin extracted from pomegranate (*Punica granatum*) and curcumin extracted from fresh turmeric (*Curcuma longa*) and studied their electro-optical responses to investigate their usefulness as natural sensitizers when adsorbed onto ZnO nanorod (NR) and ZnO nanoparticle (NP) films in DSSCs. Hydroxyl and Carbonyl groups existing the natural sensitizers bound them easily to the surface of the ZnO nanorods which facilitates very easy electron injection from LUMO of dye molecule to the conduction band of ZnO.[27]

2. EXPERIMENTAL DETAILS

2.1. Structure and Working Principle of DSSC

A typical DSSC consists of four elements: a photoanode with a thin layer of mesoporous wide band gap semiconductor oxide layer (usually TiO_2, ZnO, SnO_2 or Nb_2O_5) over a transparent conducting substrate (ITO or FTO), a monolayer of the sensitizing dye adsorbed on the semiconductor oxide surface to facilitate light absorption, an redox mediator electrolyte solution (typically I^-/I^{3-}) in an organic solvent and a counter electrode made up of a catalyst (platinized ITO or FTO) to facilitate charge collection. The schematic of device architecture and working principle of a typical DSSC is shown in Figures 1(a) and (b).

Upon exposure to the sunlight, dye molecule absorbs photon energy and goes through an electronic state change, the electron jumps from ground state (HOMO) to the excited state (LUMO). As a result, electron injection into the conduction band of the semiconductor oxide (ZnO) film takes place whereby the dye molecule gets oxidized. This oxidized dye molecule is regenerated by taking an electron from the redox species of the electrolyte (I^-). Subsequently, I^- is regenerated by reduction of I^{3-} with electrons migrated from photo anode via external load and collected at the counter electrode, completing the cycle.[5, 6]

2.2. Materials

Transparent ITO coated glass (10 Ω/square) was purchased from Techinstro, India. The liquidplatinum paint (Platisol T) purchased from Solaronix, Switzerland was used to prepare the platinum coated transparent counter electrode. Commercial ZnO nanopowder (<50 nm,), Zinc acetate dehydrate and Hexamethylenetetramine all were purchased from Sigma Aldrich. Ethylene Glycol (Sigma Aldrich) was used as a solvent for the electrolyte preparation using KI (S D Fine-Chemical Ltd., India) and I_2 (RANKEM, India). Meltonix 1170-60 (60 μm) purchased from Solaronix was used as a spacer between the electrodes to avoid short-circuiting between them.

2.3. Extraction and Preparation of Natural Dye Sensitizers

In the fabrication of Dye Sensitized solar cells, selection of the dyes is one the crucial task as it significantly affects the performance and production cost the cells. By choosing abundant natural dyes instead of expensive synthetic

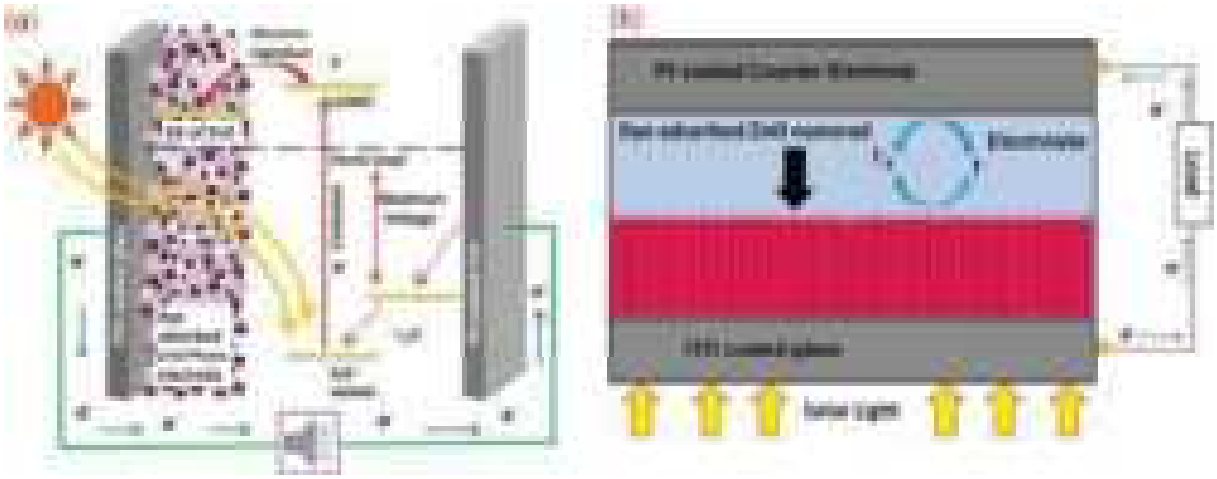

Fig. 1. Schematic diagram and basic working mechanism of DSSCs based on (a) ZnO nanoparticle (b) ZnO nanorod.

ruthenium dyes we can reduce the production cost by a large amount. In this work, we have chosen extracts of Curcumin and pomegranate juice as sensitizers. Curcumin was extracted by grinding turmeric root in an iron mortar and then mixing in 100 ml ethanol. After extraction, solid residues were filtered out to obtain a clear natural dye solution.

For pomegranate extraction of pomegranate juice, afresh pomegranate was squeezed and then mixed with 100 ml deionized water. This solution is also filtered to obtain pure dye. The dye solutions were properly stored protecting from direct sunlight for further use. Studies have shown that Curcumin dyes have two forms and they are identified as Keto and Enol.[28] On the other hand, it was found that pomegranate juice mostly contains six type anthocyanins. These are cyanidin 3-glucoside, cyanidin 3,5-diglucoside, delphinidin 3-glucoside, delphinidin 3,5-diglucoside, pelargonidin 3-glucoside and pelargonidin 3,5-diglucoside.[29] The chemical structures of these dyes are shown in Figure 2.

2.4. Sol–Gel Synthesis of ZnO Nanorods: Preparation of Working Electrodes

To prepare the working electrode, first, the ITO coated glass was cut into 2×2 cm square shaped pieces. Cleaning of this substrate is very important as it removes any organic or inorganic contaminant present on its surface which can significantly affect the performances of the cells. Furthermore, cleaning enhances the adhesion of the subsequent layers to be deposited over it. The ITO substrates were cleaned using dilute HCl for 15 minutes in an ultrasonic cleaner to remove oxide impurities. Then they were rinsed extensively with deionized water to remove the HCl residues. The substrates were then subjected to cleaning in acetone, ethanol and deionized water for 15 minutes each using an ultrasonic bath. Finally, the substrates were dried using a hairdryer. The cleaned substrates were masked using scotch tape on four sides leaving the central area empty for semiconductor material deposition.

ZnO nanorods were grown on the ITO coated glass substrate by following a simple two-step Sol–Gel spin coating protocol followed by hydrothermal growth.[30] In the first step, a thin ZnO seed layer was formed on the ITO glass substrates using 5 mM Zinc acetate dehydrate $CH_3COO)_2Zn$, $2H_2O$, (98% Merck) in acetone as precursor solution. The solution was well mixed using an ultrasonic bath for 2 hours at room temperature and then spun onto cleaned and masked ITO coated glass substrates using a programmable spin coater (Apex Technologies, Model SCU-2008C) at 1000 rpm for 30 seconds. The coated substrates were then annealed at 350 °C temperature for 30 minutes. After evaporation of the solvent, a thin ZnO film was formed whose thickness can be controlled by repeating the above process. In this way, the seed layer is formed. The thickness of the film can also be controlled by varying solution concentration and the spinning speed of the spin coater.[31] In the second step, vertically aligned ZnO nanorods were grown over the seed layer-coated ITO glass substrate by hydrothermal method. In this method, the seed layer coated substrate was immersed in a solution containing an equal proportion of 5 mM Zinc acetate dehydrate, $(CH_3COO)_2Zn$, $2H_2O$ and 5 mM Hexamethylenetetramine, $(C_6H_{12}N_4)$ at 90 °C temperature in a Pyrex vessel for 2 hours. This creates an array of vertically aligned ZnO nanorods on the substrate. It was then taken out from the solution and rinsed immediately with ethanol and deionized water in order to remove any left-over residues from the film surface and allowed to air dry at room temperature. Finally, the ZnO nanorod formation was completed by annealing the film at 450 °C for 30 min. This ZnO nanorod array coated substrates were then immersed in the dye solutions to allow adsorption of the dye molecules onto the semiconductor nanorod surface for 24 hours. Then the electrodes were taken out from the

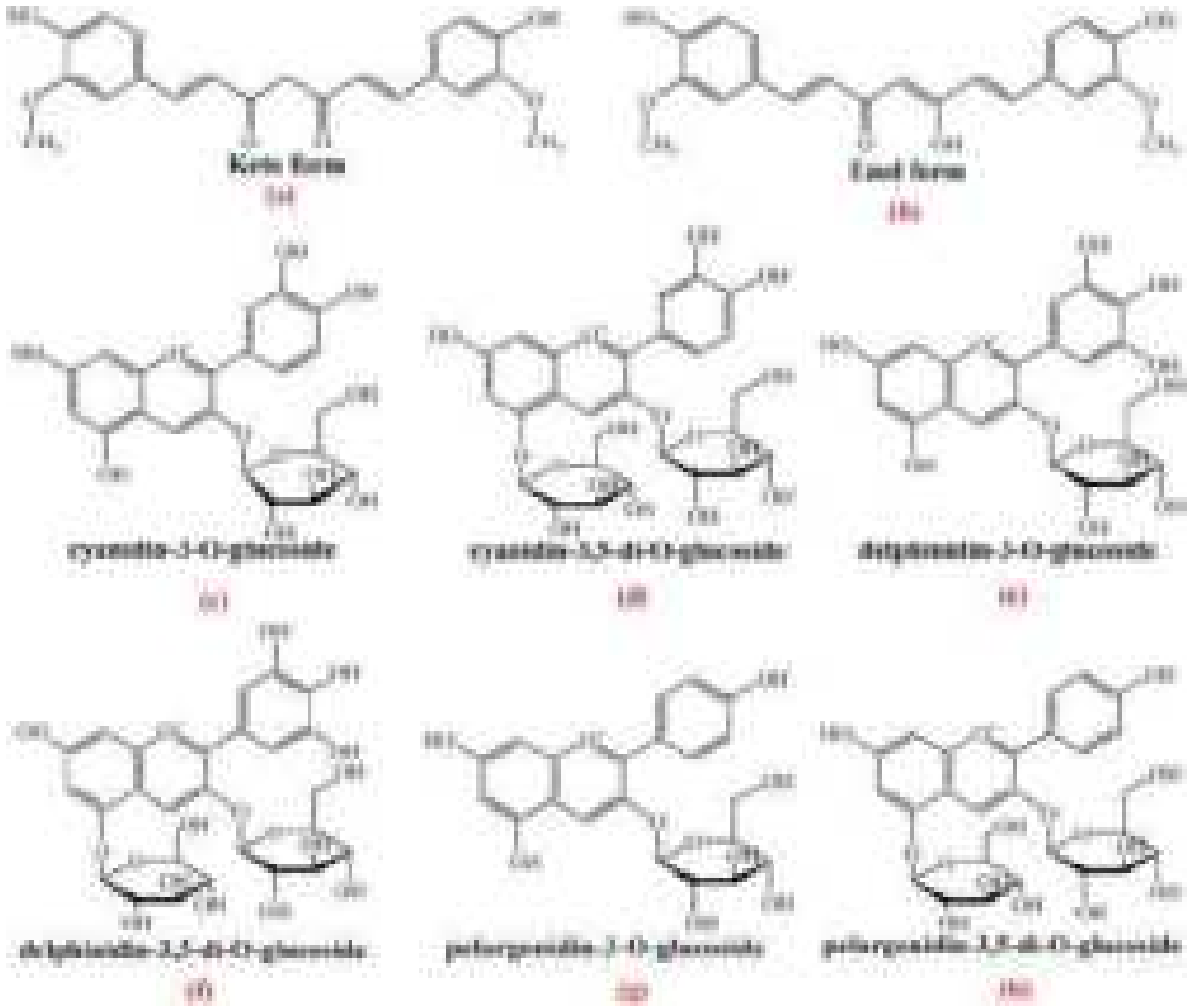

Fig. 2. Chemical structures of curcumin (a and b) present in turmeric and six major anthocyanins (c–h) present in pomegranate fruit extracts.

solutions and rinsed with ethanol and deionized water to remove the excess dye from the surface of the films and air dried at room temperature. The platinum counter electrode was prepared by spin coating the platinum precursor solution (platisol T–solaronix) at 1000 rpm for 30 seconds onto a drilled ITO substrate and giving heat treatment at 450 °C for 15 minutes.

2.5. DSSC Assembling

To assemble the solar cell, the conductive side of the platinum coated counter electrode was placed over the dye adsorbed ZnO nanorod photoanode so that the platinized side of the counter electrode faces the ZnO film. Surlyn spacer (Meltonix 1170-25 μm) was placed in between them to prevent the uncoated areas of the electrodes from short-circuiting. Two binder clips were used to firmly clamp the two electrodes together in a sandwich manner. The redox electrolyte was prepared by mixing 0.5 M KI and 0.05 M I_2 in Ethylene Glycol solvent in a proportionate amount. This electrolyte solution was injected into the cell through the drilled hole on the counter electrode. The hole was then sealed using a hot melt sealant. The effective cell area was 1 cm^2.

2.6. Device Characterization and Measurements

The absorption spectra of the dyes were studied using a Perkin Elmer Lambda–35 UV-VIS spectrophotometer in the wavelength range of 200–600 nm range. The crystalline structure of the ZnO films was studied using PANalytical X'Pert PRO X-ray diffractometer with CuKα (30 mA, 40 kV, $\lambda = 1.5406$ Å). The surface morphologies of the ZnO films were characterized by using scanning electron microscopy (JEOL). The current–voltage (I–V) characteristics of the fabricated cells under illumination of 100 mW/cm^2 (Oriel Xenon lamp 450 W) were recorded by employing a Keithley 2400 source meter connected to a PC. The desired intensity of incident light was obtained

with the help of a reference cell by adjusting the distance between the light source and the cell.

The performance of the solar cell is determined by the overall photoconversion efficiency of the cell which is defined as the ratio of maximum electrical output power of the cell to the incident optical power and is given by the equation

$$\eta = \frac{P_{out}}{P_{in}} = \frac{I_{sc} V_{oc} \mathrm{FF}}{P_{in}} \quad (1)$$

where P_{in} is the power of the incident light, I_{max} and V_{max} are the current and voltage corresponding to the maximum output power from the solar cell and I_{SC} and V_{OC} represents the short circuit current and open circuit voltage respectively. The term FF is known as Fill factor of the cell. It is determined from the I–V characteristics and calculated as

$$\mathrm{FF} = \frac{I_{max} V_{max}}{I_{sc} V_{oc}} \quad (2)$$

The efficiency is generally expressed in percentage.

3. RESULTS AND DISCUSSION

3.1. UV-VIS Absorption Spectral Analysis of the Dyes

UV-VIS absorption spectra of the Curcumin and pomegranate dye in are shown in Figure 3. A clear difference the absorption peaks of the two dyes can be seen. Curcumin exhibits absorption peak at 422 nm whereas pomegranate fruit extract solution at 517 nm. The difference in the absorption peaks is due to the different types of colors and chromophores present in Curcumin and pomegranate extracts.

3.2. X-ray Diffraction Analysis of the ZnO Film

The structural and crystalline quality information of the synthesized ZnO nanorods and purchased ZnO nanopowder were studied using X-ray diffraction pattern of the samples which is shown in Figure 4. The consistency of the obtained diffraction peak was confirmed by comparing them with the standard JCPS card no. 36-1451. A remarkably enhanced diffraction peak for (002) plane at 34.4595°

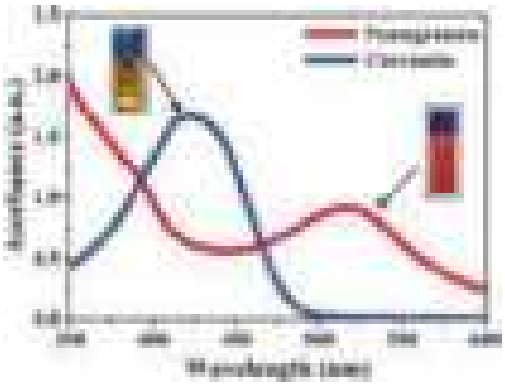

Fig. 3. Absorption spectra of the natural sensitizers.

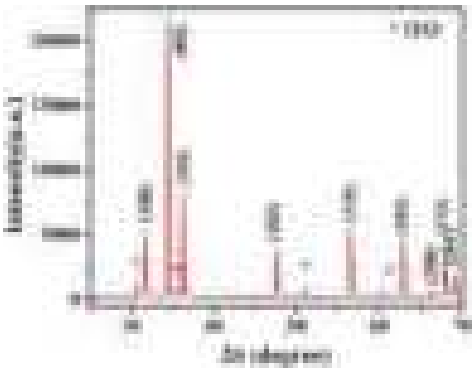

Fig. 4. XRD pattern of ZnO nanorods.

can be clearly observed for the ZNO nanorods. It indicates strong preferential growth of ZnO nanorods along c-axis and vertical alignment on the ITO substrate and also the hexagonal wurtzite structure. XRD of ZnO nanoparticles was not performed since the powder was commercially purchased.

The average crystalline size of the ZnO films were estimated from the width of the (002) peak for ZnO nanorod and (101) peak for ZnO nanoparticle using Debye-Scherrer formula for X-ray diffraction,

$$\text{Crystalline Size } (D) = \frac{0.9\lambda}{\beta \mathrm{Cos}\theta} \text{ Å} \quad (3)$$

where β, θ and λ are FWHM of the peak, Bragg angle and wavelength of X-ray used. The dislocation density (δ), representing the amount of defects in the crystal and the strain (ε) of the film were determined using following formulae respectively:[32]

$$\delta = \frac{1}{D^2} \quad (4)$$

$$\varepsilon = \frac{\beta \cos\theta}{4} \quad (5)$$

The values of different parameters calculated from the structural analysis of the XRD pattern are given in Table I.

Crystalline size estimated from X-ray analysis is generally found to be less than the particle size found from SEM images. The reason behind this is that generally a particle may be formed by combination of several crystallites or just one crystallite.

3.3. Scanning Electron Microscope Studies

Scanning electron microscopy (SEM) was carried out to study the morphological properties of the sample film.

Table I. Structure parameters of the ZnO nanorod thin film.

ZnO particle type	Plane	FWHM (β)°	2θ°	D (nm)	δ nm^{-2}	ε
Nanorod	002	0.20567	34.4595	40.43	6.11×10^{-4}	4.91×10^{-2}

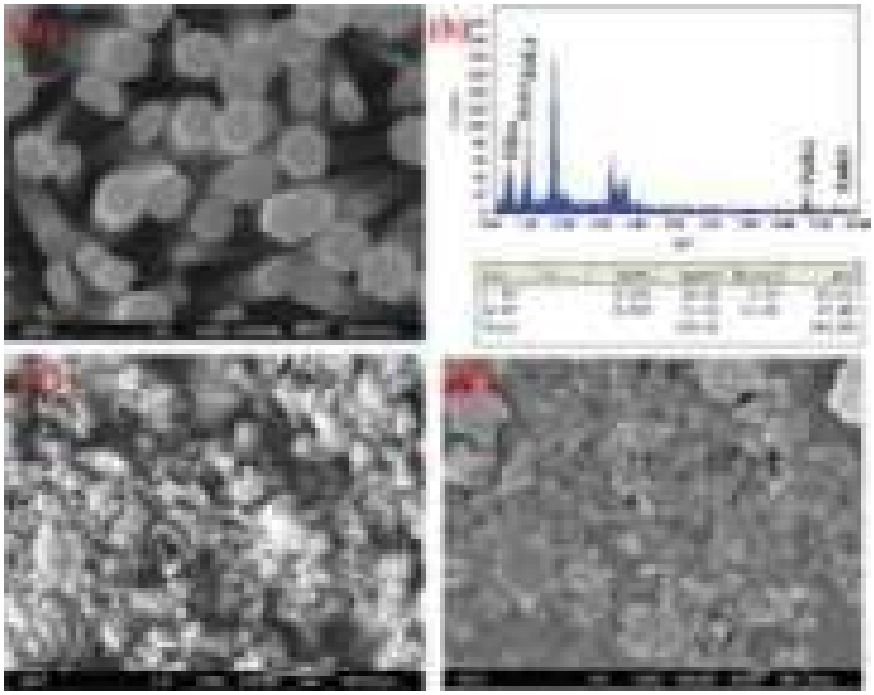

Fig. 5. SEM image of (a) ZnO nanorods grown on ITO substrate (b) EDX spectra of the nanorod sample showing elemental composition (c and d) ZnO nanoparticle deposited sample at lower and higher magnification respectively.

Figure 5(a) is the SEM image of the ZnO nanorod arrays on ITO substrate. The SEM observation reveals that most the most of the nanorods have grown vertical to the seed layer on the ITO substrate and have hexagonal wurtzite.

The nanorods have diameters ranging from 100–200 nm with an average length of 300 to 400 nm and in case of nanoparticles; the average particle size was around 50 nm. To investigate the chemical composition of the nanorods, EDX analysis was performed which is shown in Figure 5(b), which confirms the presence of Zn and O. The unidentified peaks are due to the presence of indium (In) and tin (Sn) in ITO substrate.

3.4. Current–Voltage Characteristics Study of Cells/Solar Cell Efficiency Measurements

The current–voltage characteristic of a Solar cell allows us to determine the photovoltaic performance of the cell. The J–V curves of the fabricated cells under illumination of 100 mW/cm^2 are shown in Figure 6(a). The Power–Voltage plot to calculate the maximum power point (P_{max}), I_{max} and V_{max} are represented in Figure 6(b). Table II shows various parameters extracted from the I–V curves of the ZnO nanorod based DSSCs fabricated using natural dyes Curcumin and Pomegranate. The solar cell fabricated using Curcumin extract exhibits higher shortcircuit photocurrent density (J_{SC}), open-circuit voltage (V_{OC}) and

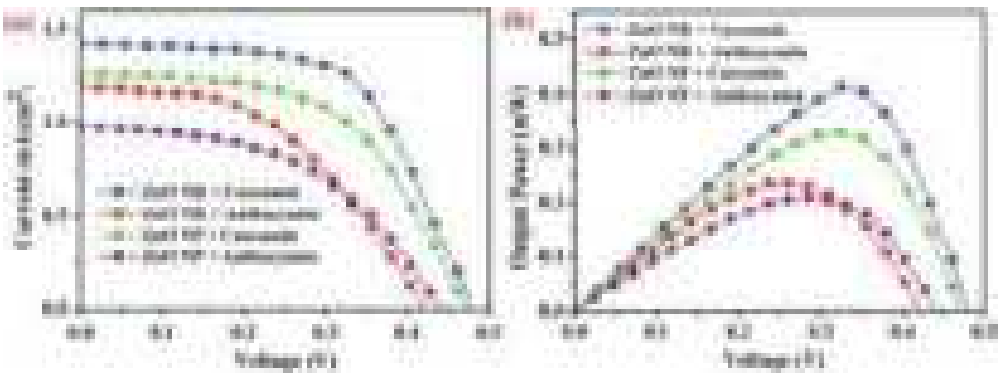

Fig. 6. (a) Current density–voltage characteristics of the cells under illumination (b) power–voltage curve to obtain maximum power point.

Table II. Solar cell parameters of fabricated DSSC's.

Cell No.	Dye used and ZnO microstructure	J_{sc} (mA/cm^2)	V_{oc} (V)	R_s (Ω cm^2)	R_{sh} (Ω cm^2)	FF	Efficiency (η %)
1	Curcumin and ZnO NR	1.43	0.49	86.28	7866.28	0.59	0.41
2	Anthocyanin and ZnO NR	1.20	0.43	116.67	2722.90	0.46	0.24
3	Curcumin and ZnO NP	1.27	0.46	101.19	6629.31	0.56	0.33
4	Anthocyanin and ZnO NP	0.98	0.45	146.87	4659.92	0.48	0.21

fill factor (FF) compared to the DSSC fabricated using pomegranate extract as a dye. The Curcumin dye cell shows an improved overall photoelectric conversion efficiency (η) over the anthocyanin dye cell. The efficiency of these natural dye based cells may be low compared to the synthetic dye based DSSCs but these values are comparable to the efficiencies obtained for natural dye based DSSCs reported by other researchers.[33]

Equivalent circuit modeling is a very important tool required for better understanding and explanation of the solar cell performance and analysis of the electrical processes occurring inside the cell. The functioning of a solar cell generally modeled by a single diode with a constant photo-generated current source, a series (R_s) and shunt resistance (R_{sh}) as shown in Figure 7. The current–voltage relation is given by the equation

$$I = I_{ph} - I_o\left[\exp\left\{\frac{q(V+IR_s)}{Ak_BT}\right\} - 1\right] - \frac{V+IR_s}{R_{sh}} \quad (6)$$

where I_{ph}, I_o, R_s, R_{sh}, q, A, k_B and T are the photocurrent, the saturation current of the diode, the series resistance, the shunt resistance, the electron charge, the ideality factor, the Boltzmann constant, and absolute temperature, respectively.[34]

The circuit parameters like R_s and R_{sh} are not directly measurable. They are calculated by fitting the experimental J–V curve with the Eq. (6). Values of these parameters obtained for the fabricated cells are also represented in Table II.

Cell-1 shows lowest series resistance (R_s) compared to other cells. This indicates improved electrical contacts, lower junction resistances and better ZnO nanorod morphology in case of cell-1. Higher series resistance means greater voltage drop inside the cell resulting in lower terminal voltage and sagging of current controlled part of the J–V curve towards the origin which can be correlated with Table II and Figure 6(a). In addition, from single diode equivalent circuit of the solar cell (Fig. 7), it can be clearly seen that R_{sh} provides an alternative path to the photocurrent which causes power losses in the solar cell. Lower R_{sh} results in partial shorting between the two electrodes of the solar cell giving rise to leakage current. So, the highest value of R_{sh} of cell-1 attributes to lowest leakage current which results in improved cell performance. Also, from Table II it can be confirmed that higher shunt resistance results in higher fill factor and consequently better photoconversion efficiency.

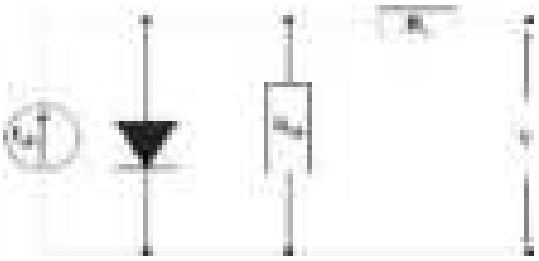

Fig. 7. The equivalent circuit (single diode model) of a solar cell.

3.5. Electrochemical Impedance Spectroscopy Study of the Cells

The electrochemical impedance spectroscopy is a very useful diagnostic technique which has often been performed to investigate the interfacial charge transfer dynamics and recombination mechanisms occurring inside a DSSC.[35] These are generally modelled using appropriate equivalent circuit in terms of resistors and capacitors. The EIS measurements were performed using HIOKI Impedance Analyser in the frequency range 0.1 Hz to 190 kHz under dark condition with employing an AC sinusoidal signal having amplitude of 10 mV under influence of V_{oc} bias voltage. EIS findings as Nyquist plot of the DSSCs are shown in Figure 8(a). Physical interpretation of the different electrochemical operations across the interfacial regions of the DSSCs can be done by fitting the EIS spectra with the equivalent circuit shown in Figure 8(b). Generally a typical Nyquist plot exhibits three semicircles. However, only two semicircles are present in our study due to low frequency limitation of our instrument. The first smaller semicircle (in the high frequency range) attributes to the charge transfer resistance at the Pt counter electrode/Electrolyte interface (R_{CE}) and the second semicircle (mid frequency range) having higher diameter corresponds to the resistance of charge transfer and recombination process at the ZnO photoelectrode/dye/electrolyte interface (R_{ct}). The intercept of the first semicircle in the high frequency range on real axis of the Nyquist plot is associated with the contact resistances and external ohmic series resistance (R_{SER}) of the assembled cell.[36] The experimental Nyquist plot is fitted with the equivalent circuit shown in inset of Figure 8(a) using MEISP software by Kumho Chemical Laboratories, on the basis of algorithm developed by Professor J. R. Macdonald (LEVM v7.0) for non-linear complex least square fitting, and the obtained parameters are represented in Table III. The chemical capacitance (C_μ) is very useful in illustrating the underlying mechanism through which photoelectrons store free energy and generates current and voltage in the outer circuit.[37] Also, the

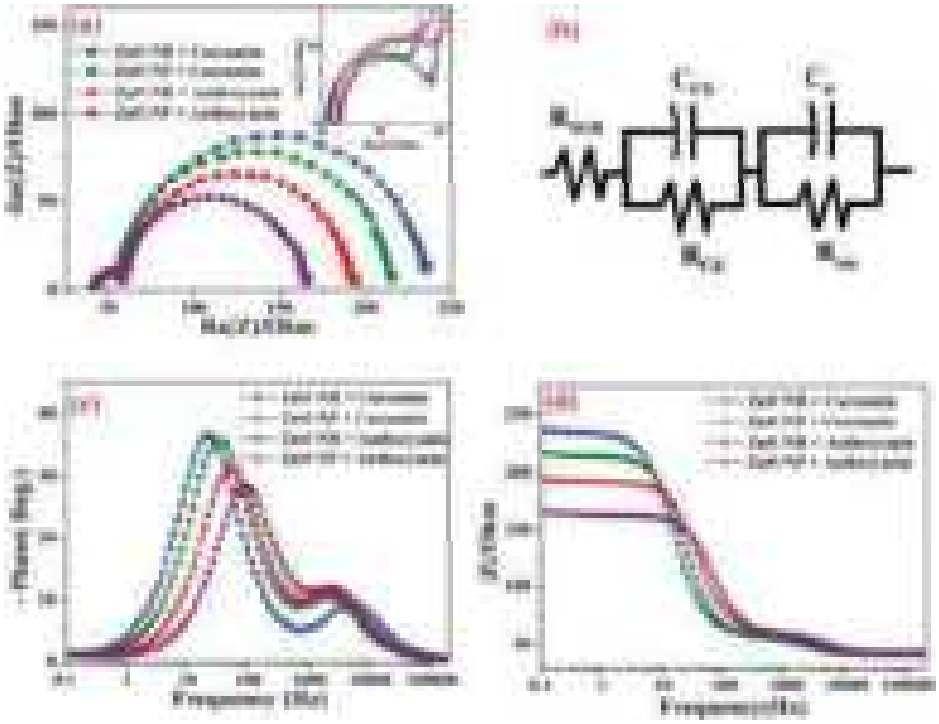

Fig. 8. EIS spectra of DSSCs (a) nyquist plot (b) equivalent circuit for fitting (c) bode phase plot and (d) bode magnitude plot for impedance.

chemical capacitance (C_μ) reflects charge carrier accumulation on the ZnO film and the density of states in the band-gap region.[38] From Table III, it can be seen that Cell-1 exhibits much higher C_μ value than the other cells, which indicates conversion of higher amount of photon energy into chemical energy resulting in higher amount of energy storage by virtue of carrier injection into the conduction band of ZnO. Reduced C_μ values for cell-2, 3 and 4 also suggest poor dye loading.[39,40] It can also be clearly observed from the Nyquist plot that the recombination resistance (R_{rec}) at the ZnO NR-Dye/Electrolyte interface is highest for cell-1 compared to the other three cells. This shows that cell-1 has better resistance to the charge recombination between the photo-generated electrons and the electron acceptors in the red-ox electrolyte attributing lower recombination current.[41]

Table III. EIS parameters of the DSSCs determined by fitting experimental data.

Cell No.	Dye used and ZnO microstructure	R_{SER} (Ω)	R_{rec} (Ω)	R_{CE} (Ω)	C_μ (μF)	Peak freq. (Hz)	Electron lifetime (τ_e) (ms)
1	Curcumin and ZnO NR	42.85	173.21	16.28	83.16	22	7.24
2	Anthocyanin and ZnO NR	40.93	156.37	15.17	59.41	33.29	4.78
3	Curcumin and ZnO NP	43.25	129.74	17.56	42.52	51	3.12
4	Anthocyanin and ZnO NP	41.63	103.56	16.85	29.40	88.48	1.80

Since counter electrodes of all the cells were prepared using same procedure, the values of R_{CE} are almost same for all the four cells. Another important representation of the EIS data is Phase and Magnitude bode plots representing Phase ($-\theta$) versus Frequency (f) and Magnitude of Impedance ($|Z|$) versus Frequency curve. Unlike Nyquist plot, the very important aspect of this plot is that frequency information is not lost. The average carrier lifetime can be estimated from phase bode plots (shown in EIS Fig. 8(b)) using the formula

$$\tau_e = \frac{1}{2\pi f_{max}}$$

where f_{max} represents peak frequency in the mid-frequency range.[42] ZnO NR loaded with Curcumin dye shows lowest characteristic peak frequency attributing to highest electron lifetime in the LUMO of the Curcumin dye molecule. It shifts towards higher frequency values for the other cells which results in decreased electron lifetime (refer to Table III). The lowest value of τ_e in ZnO NP cell loaded with anthocyanin (cell-4) extracted from pomegranate juice attributes to fastest electron recombination leading to degraded overall cell performance.

On the other hand, bode magnitude plots depicted in Figure 8(d) represents the variation of magnitude of impedance with frequency. It may be noted from bode magnitude plot shown in Figure 8(d) that at low frequencies the magnitude of impedance is high, which indicates

higher recombination resistance. But with increase in frequency the impedance starts falling which is due to the faster electron recombination at higher frequencies. In the lower frequency region, the ZnO NR cell sensitized with Curcumin is showing highest magnitude of impedance implying slowest recombination rate, giving rise to highest short circuit current (I_{SC}). In contrary, ZnO NP cell sensitized with anthocyanin extracted from pomegranate fruit shows the lowest impedance in the low frequency region implying fastest recombination process which is reflected in Table III. The possible reason behind these behaviours may be the better adsorption of Curcumin dye molecules over the hexagonal rod shaped ZnO nanostructures in comparison to the other cells. It also can be seen that the value of characteristic frequency shifts towards lower side for increasing value of either R_{rec} or C_{μ}. One more thing can be noted from the impedance plots that the maximum value of phase angle is also decreases with the decrease in value of R_{rec}.

4. CONCLUSIONS

In this study, hexagonal shaped ZnO nanorods with preferential growth along (002) plane were successfully grown on ITO substrates using low cost sol–gel hydrothermal technique. The nanorods have diameters ranging from 100–200 nm. XRD study revealed remarkably high crystalline quality of the nanorods. These ZnO nanorod based substrates were used as photoanodes to prepare DSSCs using natural dyes extracted from pomegranate and turmeric. On the other hand, commercial ZnO nano powder is also used to fabricate DSSCs using the same natural dyes. Photo electrochemical performances of all the four cells were recorded. From the J–V measurements, a clear enhanced overall cell performance was noticed for the cell constructed using ZnO nanorods and sensitized using Curcumin dye compared to the other three cells. One of the reasons for this could be the higher amount of Curcumin dye molecule adsorption by the ZnO film due to the better interaction between the carbonyl and hydroxyl groups of Curcumin molecule and the ZnO nanorod film than that of Pomegranate extract. For deeper understanding of the performances obtained from the cells, the different interfacial mechanisms of the cells were investigated using EIS technique. It is found that the shape of ZnO nanostructures and different dye molecules present in the extracts affected the electrochemical parameters of the cells. Best performance of the cell prepared with ZnO nanorod with Curcumin dye is found to be due to highest chemical capacitance (C_{μ}) along with lowest electron recombination rate and fast charge transport along the ZnO nanorod. Therefore, the Curcumin dye should be an alternative to anthocyanin source for natural dye sensitized solar cells. These results also show that the performances of the natural extract based DSSCs can be enhanced significantly by combining proper natural dye with appropriate shape of semiconductor nanostructures and they can become potential alternative to the synthetic sensitizers based DSSCs. In fact, such combination may result in environment friendly, remarkably low cost and easily manufacturable dye sensitized solar cells.

Acknowledgment: Authors gratefully acknowledge the Dept. of Physics, University of North Bengal for providing financial support and laboratory facilities for carrying out the research work.

References and Notes

1. A. Horvath and E. Rachlew, Nuclear power in the 21st century: Challenges and possibilities. *Ambio* 45(Suppl. 1), S38 **(2016)**.
2. S. Chu and A. Majumdar, Opportunities and challenges for a sustainable energy future. *Nature* 488, 294 **(2012)**.
3. N. L. Chang, Y. Ho-Baillie, A. Wing, P. A. Basore, T. L. Young, R. Evans, and R. J. Egan, A manufacturing cost estimation method with uncertainty analysis and its application to perovskite on glass photovoltaic modules. *Progress in Photovoltaics: Research and Applications* 25, 390 **(2017)**.
4. A. Kumar, M. Bieri, T. Reindl, and A. G. Aberle, Economic viability analysis of silicon solar cell manufacturing: Al-BSF versus PERC. *Energy Procedia* 130, 43 **(2017)**.
5. M. Grätzel, Dye-sensitized solar cells. *Journal of Photochemistry and Photobiology C: Photochemistry Reviews* 4, 145 **(2003)**.
6. B. O'regan and M. Grätzel, A low-cost, high-efficiency solar cell based on dye-sensitized colloidal TiO_2 films. *Nature* 353, 737 **(1991)**.
7. Y.-T. Kim, J. Park, S. Kim, D. W. Park, and J. Choi, Fabrication of hierarchical ZnO nanostructures for dye-sensitized solar cells. *Electrochim. Acta* 78, 417 **(2012)**.
8. C. Jiang, X. Sun, G. Lo, D. Kwong, and J. Wang, Improved dye-sensitized solar cells with a ZnO-nanoflower photoanode. *Appl. Phys. Lett.* 90, 263501 **(2007)**.
9. J. B. Baxter and E. S. Aydil, Nanowire-based dye-sensitized solar cells. *Appl. Phys. Lett.* 86, 053114 **(2005)**.
10. A. Jena, S. P. Mohanty, P. Kumar, J. Naduvath, V. Gondane, P. Lekha, J. Das, H. K. Narula, S. Mallick, and P. Bhargava, Dye sensitized solar cells: A review. *Transactions of the Indian Ceramic Society* 71, 1 **(2012)**.
11. J. Gong, J. Liang, and K. Sumathy, Review on dye-sensitized solar cells (DSSCs): Fundamental concepts and novel materials. *Renewable and Sustainable Energy Reviews* 16, 5848 **(2012)**.
12. S. Hao, J. Wu, Y. Huang, and J. Lin, Natural dyes as photosensitizers for dye-sensitized solar cell. *Solar Energy* 80, 209 **(2006)**.
13. H. Zhu, H. Zeng, V. Subramanian, C. Masarapu, K.-H. Hung, and B. Wei, Anthocyanin-sensitized solar cells using carbon nanotube films as counter electrodes. *Nanotechnology* 19, 465204 **(2008)**.
14. Y. Amao and T. Komori, Bio-photovoltaic conversion device using chlorine-e6 derived from chlorophyll from spirulina adsorbed on a nanocrystalline TiO_2 film electrode. *Biosens. Bioelectron.* 19, 843 **(2004)**.
15. K.-H. Park, T.-Y. Kim, S. Han, H.-S. Ko, S.-H. Lee, Y.-M. Song, J.-H. Kim, and J.-W. Lee, Light harvesting over a wide range of wavelength using natural dyes of gardenia and cochineal for dye-sensitized solar cells. *Spectrochimica Acta Part A: Molecular and Biomolecular Spectroscopy* 128, 868 **(2014)**.

16. F. Shao, J. Sun, L. Gao, S. Yang, and J. Luo, Growth of various TiO_2 nanostructures for dye-sensitized solar cells. *The Journal of Physical Chemistry C* 115, 1819 **(2010)**.
17. X. Mao, R. Zhou, S. Zhang, L. Ding, L. Wan, S. Qin, Z. Chen, J. Xu, and S. Miao, High efficiency dye-sensitized solar cells constructed with composites of TiO_2 and the hot-bubbling synthesized ultra-small SnO_2 nanocrystals. *Scientific Reports* 6, 19390 **(2016)**.
18. D. Maheswari and D. Sreenivasan, Review of TiO_2 nanowires in dye sensitized solar cell. *Applied Solar Energy* 51, 112 **(2015)**.
19. B. Roose, S. Pathak, and U. Steiner, Doping of TiO_2 for sensitized solar cells. *Chem. Soc. Rev.* 44, 8326 **(2015)**.
20. M. S. Ahmad, A. Pandey, and N. A. Rahim, Advancements in the development of TiO_2 photoanodes and its fabrication methods for dye sensitized solar cell (DSSC) applications. A review. *Renewable and Sustainable Energy Reviews* 77, 89 **(2017)**.
21. K. Tennakone, G. Kumara, A. Kumarasinghe, P. Sirimanne, and K. Wijayantha, Efficient photosensitization of nanocrystalline TiO_2 films by tannins and related phenolic substances. *Journal of Photochemistry and Photobiology A: Chemistry* 94, 217 **(1996)**.
22. J. A. Anta, E. Guillen, and R. Tena-Zaera, ZnO-based dye-sensitized solar cells. *The Journal of Physical Chemistry C* 116, 11413 **(2012)**.
23. Ü. Özgür, Y. I. Alivov, C. Liu, A. Teke, M. Reshchikov, S. Doğan, V. Avrutin, S.-J. Cho, and H. Morkoc, A comprehensive review of ZnO materials and devices. *J. Appl. Phys.* 98, 11 **(2005)**.
24. H. Bae, M. Yoon, J. Kim, and S. Im, Photodetecting properties of ZnO-based thin-film transistors. *Appl. Phys. Lett.* 83, 5313 **(2003)**.
25. Q. Zhang, C. S. Dandeneau, X. Zhou, and G. Cao, ZnO nanostructures for dye-sensitized solar cells. *Adv. Mater.* 21, 4087 **(2009)**.
26. Y. Zhang, M. K. Ram, E. K. Stefanakos, and D. Y. Goswami, Synthesis, characterization, and applications of ZnO nanowires. *Journal of Nanomaterials* 2012, 20 **(2012)**.
27. T. Senthil, N. Muthukumarasamy, and M. Kang, ZnO nanorods based dye sensitized solar cells sensitized using natural dyes extracted from beetroot, rose and strawberry. *Bull. Korean Chem. Soc.* 35, 1050 **(2014)**.
28. S.-I. Kawano, Y. Inohana, Y. Hashi, and J.-M. Lin, Analysis of keto-enol tautomers of curcumin by liquid chromatography/mass spectrometry. *Chin. Chem. Lett.* 24, 685 **(2013)**.
29. M. Viuda-Martos, J. Fernández-López, and J. Pérez-Álvarez, Pomegranate and its many functional components as related to human health: A review. *Comprehensive Reviews in Food Science and Food Safety* 9, 635 **(2010)**.
30. B. Pradhan, S. K. Batabyal, and A. J. Pal, Vertically aligned ZnO nanowire arrays in Rose Bengal-based dye-sensitized solar cells. *Sol. Energy Mater. Sol. Cells* 91, 769 **(2007)**.
31. F. Zhang, C. A. Di, N. Berdunov, Y. Hu, Y. Hu, X. Gao, Q. Meng, H. Sirringhaus, and D. Zhu, Ultrathin film organic transistors: Precise control of semiconductor thickness via spin-coating. *Adv. Mater.* 25, 1401 **(2013)**.
32. A. H. Kurda, Y. M. Hassan, and N. M. Ahmed, Controlling diameter, length and characterization of ZnO nanorods by simple hydrothermal method for solar cells. *World Journal of Nano Science and Engineering* 5, 34 **(2015)**.
33. H. Zhou, L. Wu, Y. Gao, and T. Ma, Dye-sensitized solar cells using 20 natural dyes as sensitizers. *Journal of Photochemistry and Photobiology A: Chemistry* 219, 188 **(2011)**.
34. M. Murayama and T. Mori, Equivalent circuit analysis of dye-sensitized solar cell by using one-diode model: Effect of carboxylic acid treatment of TiO_2 electrode. *Japanese Journal of Applied Physics* 45, 542 **(2006)**.
35. M. Wang, A. M. Anghel, B. Marsan, N.-L. C. Ha, N. Pootrakulchote, S. M. Zakeeruddin, and M. Grätzel, CoS supersedes Pt as efficient electrocatalyst for triiodide reduction in dye-sensitized solar cells. *J. Am. Chem. Soc.* 131, 15976 **(2009)**.
36. L. Tao, Z. Huo, Y. Ding, Y. Li, S. Dai, L. Wang, J. Zhu, X. Pan, B. Zhang, and J. Yao, High-efficiency and stable quasi-solid-state dye-sensitized solar cell based on low molecular mass organogelator electrolyte. *Journal of Materials Chemistry A* 3, 2344 **(2015)**.
37. S. S. Negi, Integrated electronic, optical, and structural features in pseudo-3D mesoporous TiO_2–X delivering enhanced dye-sensitized solar cell performance. *ACS Omega* 3, 1645 **(2018)**.
38. G. Di Carlo, A. O. Biroli, M. Pizzotti, F. Tessore, V. Trifiletti, R. Ruffo, A. Abbotto, A. Amat, F. De Angelis, and P. R. Mussini, Tetraaryl ZnII porphyrinates substituted at β-pyrrolic positions as sensitizers in dye-sensitized solar cells: A comparison with meso-disubstituted push–pull znii porphyrinates. *Chem. Eur. J.* 19, 10723 **(2013)**.
39. J. Bisquert, Chemical capacitance of nanostructured semiconductors: Its origin and significance for nanocomposite solar cells. *PCCP* 5, 5360 **(2003)**.
40. F. Fabregat-Santiago, E. M. Barea, J. Bisquert, G. K. Mor, K. Shankar, and C. A. Grimes, High carrier density and capacitance in TiO_2 nanotube arrays induced by electrochemical doping. *J. Am. Chem. Soc.* 130, 11312 **(2008)**.
41. J. Akilavasan, K. Wijeratne, H. Moutinho, M. Al-Jassim, A. Alamoud, R. Rajapakse, and J. Bandara, Hydrothermally synthesized titania nanotubes as a promising electron transport medium in dye sensitized solar cells exhibiting a record efficiency of 7.6% for 1-D based devices. *Journal of Materials Chemistry A* 1, 5377 **(2013)**.
42. P. Bhatt, K. Pandey, P. Yadav, B. Tripathi, and M. Kumar, Impedance spectroscopic investigation of the degraded dye-sensitized solar cell due to ageing. *International Journal of Photoenergy* Article ID 8523150 **(2016)**, DOI: 10.1155/2016/8523150.

Sl. No: NTMS-2015/PPC/23

National Conference
on
Modern Trends in Materials Science - 2015
(NTMS – 2015)

Organized by

Department of Physics, University of North Bengal, West Bengal, India

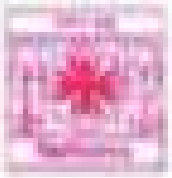

Paper Presentation Certificate

This is to certify that Prof./Dr./Mr./Mrs./Ms. Rajat Biswas

of Dept. of Physics, N.B.U. Siliguri, P. 734013

has presented a paper (~~Oral~~/Poster) entitled ZnO Nanorod Based Dye Sensitized Solar cells Sensitized Using Natural Dyes Extracted from Pomegranate and Curcumin

in the National Conference on Modern Trends in Materials Science – 2015 (NTMS – 2015) held at Department of Physics, University of North Bengal, West Bengal, India during 5 – 6 February, 2015.

Dr. N. K. Das Chairman	Dr. S. Chatterjee Organizing Secretary	Dr. S. Sarkar Convener

UGC SPONSORED

NATIONAL SEMINAR ON

CONDENSED MATTER, LASER AND COMMUNICATION (NSCMLC 2015)

February 27-28, 2015

Organized by

Department of Physics

(UGC-Centre of Advanced Study)

The University of Burdwan, Golapbag, Burdwan

Certificate of Participation

This is to certify that Prof. / Dr. / Mr. / Mrs. Rajat Biswas

of University of North Bengal

has participated and ~~delivered an invited talk~~/presented a paper (~~contributed~~) in National Seminar on Condensed Matter, Laser and Communication (NSCMLC 2015).

A. Bose & A. Dutta
Secretaries

S. Mukhopadhyay & P. Mitra
Conveners